THE UNIVERSITY OF CHICAGO

OBSERVATIONAL CONSEQUENCES OF HAWKING RADIATION FROM PRIMORDIAL BLACK HOLES

A DISSERTATION SUBMITTED TO
THE FACULTY OF THE DIVISION OF THE PHYSICAL SCIENCES
IN CANDIDACY FOR THE DEGREE OF
DOCTOR OF PHILOSOPHY

DEPARTMENT OF ASTRONOMY AND ASTROPHYSICS

BY
CELESTE SUMMER KEITH

CHICAGO, ILLINOIS
JUNE 2023

To me. This was hard.

Weird but fucking beautiful. -Taylor Swift

TABLE OF CONTENTS

LIST OF FIGURES

ACKNOWLEDGMENTS

So many people have made a meteoric impact on my life to make this possible. My friends, both old and new, kept me sane and working during the pandemic. Megan Barnett and Adina Feinstein, thank you for making me feel less alone, playing board games with me and Elly, and for letting me pet your cats. Thank you to Darryl Seligman and Blake Sanders for being such good sports, playing board games, and helping the graduate school experience to be a lot more fun. Ben Reeve, Kevin Gayley, and Diane Gayley, thank you for being a near constant presence online, even though we no longer live in the same city. I love talking with you about our dreams for the future and how much we hate Boat Game, while still constantly playing it. Thank you Naa Ashitey for being the hardest working person I know who also still found time to be the best friend and photographer an amateur instagram model could ask for. Thank you to Jamie Dietrich for being an amazing astronomer, friend, hostess, and for going through so much and still always up to chatting. Thank you to Trevor Keith for being the best brother, I'm so proud of you.

Thank you to my family, Mom, Dad, and Aunt Barb. Thank you to my advisor, Dan Hooper, for giving me exactly what I've needed for the past 5 years, whether I knew I needed it or not.

Thank you to World of Warships, RuneScape, the Lakefront Trail, lululemon, Twilight, Taylor Swift, Harry Styles, Kirby, Behind the Bastards, Panic at the Disco, Squishmallows, C2E2, central air conditioning, Nike, sunscreen, non-in-ear headphones, Lactaid, the color pink, Glossier, baseball caps, Dungeons and Dragons, Stranger Things, Stardew Valley, cactuses, Pokemon, board games, liquid eyeliner, roller blades, rock climbing, running, ThredUp, that bird that flew into my head twice, and Trader Joe's chocolate chip ice cream for making the last five years the most fun and fulfilling years of my life so far.

Saving the best for last, thank you to Elyssa Brooks. You are the light of my life and I love you more than I ever thought it was possible to love another human being. I'm so proud of what we have accomplished both together and separately over the past 8 years and

I am so excited to share whatever comes next with you.

ABSTRACT

Black holes that were formed in the early universe, known as primordial black holes, are promising candidates for dark matter. They evaporate in a process known as Hawking radiation, the rate of which is dependant of the black holes' mass and leads to observable effects on the universe around them. These effects can be especially impactful during the minutes after the Big Bang for light PBHs, and near the center of the Milky Way for black holes evaporating today. The existence and evaporation of PBHs in the very early universe could affect the light element abundances that are measured today. We utilize modern measurements of the light element abundances to update the constraints on PBHs from Big Bang nucleosynthesis. Additionally, we use our own black hole model and template analysis to show that PBHs can explain the excess of 511 keV photons originating from the center of the Milky Way. Finally, we assess the ability of future gamma ray telescopes to detect Hawking radiation from PBHs emanating from the Inner Galaxy. We find that these telescopes will be able to precisely measure the abundance and mass distribution of PBHs, if they exist, within a mass range of $m_{\rm BH} \sim (0.6 - 20) \times 10^{16}$ g if the black holes make up one part in $10^6 - 10^7$ of the total dark matter. These constraints will improve upon current constraints by at least two orders of magnitude.

CHAPTER 1

INTRODUCTION

Black holes have long been a colossal source of curiosity and confusion, in both the scientific community and beyond. They are well known in both astrophysics and popular culture as objects that have a gravitational pull so strong that not even light can escape. Additionally, black holes are known emit Hawking radiation, which allows them to evaporate over time, and slowly lose mass. The theoretical exploration and study of black holes has led to numerous advances in the understanding of our universe. Because of this, black holes are called upon in high energy astrophysics and astronomy to potentially solve a large number of scientific problems. One particularly exciting class of black holes are primordial black hole, which are defined as black holes that are formed in the moments following the Big Bang, through large density perturbations or phase transitions in the early universe. Primordial black holes are generally thought to be less massive than those formed via stellar evolution and stellar collapse, though it is not required. These black holes have garnered specific interest in the field because they are a good candidate for dark matter, or they could be a source of dark matter in the universe. Their observational consequences have been invoked to help constrain their possible existence as dark matter.

This thesis will present a comprehensive examination of primordial black holes, their history as a topic of study, their theoretical formation mechanisms, the consequences of their existence on both the early and present universe, and current constraints on their abundance. We will then discuss the specific work that we have completed for this thesis. This includes the updated constraints on primordial black holes as derived from Big Bang nucleosynthesis, which is informed by the current measurements of the primordial light element abundances. Next, we will discuss primordial black holes in the Galactic Center, that have survived until the present day. We first discuss the sensitivity of future gamma-ray telescopes to these primordial black holes, as the Hawking radiation from an evaporating black hole may be able to be detected by gamma-ray telescopes. Finally, we focus on the specific signal of the 511 keV excess from the direction of the Galactic Center. We propose an explanation for this signal via the annihilation of positrons and electrons, where the positrons originated

from evaporating black holes.

The extensive work described in this thesis represents a step forward in the study of primordial black holes, their observational consequences, and their candidacy for dark matter.

CHAPTER 2

PRIMORDIAL BLACK HOLES AND HAWKING RADIATION

Black hole masses are hypothesized to span a large range, from many times larger than the Sun, to asteroid mass, to tiny black holes that are only relevant on quantum mechanical scales. It is known that a supermassive black hole lies at the center of our own Milky Way; and in fact it is thought that most massive galaxies harbor black holes with masses above 10^6 $M_\odot$ in their centers [265]. These SMBHs are mostly quiescent, like the black hole recently photographed at the center of M87, and a few are AGN [14]. Black holes around a few solar masses are predicted to originate from core collapse supernovae. Black holes with masses in the tens of solar masses have been detected by gravitational waves that are produced when a black hole merges with another black hole or a neutron star [2]. Even smaller mass black holes that are called primordial black holes, are hypothesized to have formed in the early universe. Such black holes do not have observational evidence as of yet to conclusively prove their existence. Nevertheless, black holes in mass ranges significantly smaller than a solar mass may be utilized in many astrophysical theories, such as being a candidate for dark matter, or the progenitor of the 511 keV we see from the center of the Milky Way. Black holes in a mass range of $10^{20} - 10^{24}$g may be detected with tools such as microlensing within our own galaxy. Even lower mass black holes may exist. In the range of masses from approximately 10^{14}g to 10^{17}g, black holes are small enough to be significantly affected by Hawking evaporation, which is the ability of a black hole to lose mass over time by emitting particles. All black holes produce Hawking radiation, but smaller black holes emit this radiation at a much faster rate than high mass black holes. In this chapter, the large mass range of black holes will be discussed, as well as the possibility of primordial black holes as a dark matter candidate. Finally, we will discuss the current constraints on the existence of primordial black holes.

2.1 History of Black Holes

The thought experiment of an object so massive that not even light can escape is not new. The natural philosopher and clergyman John Michell from Yorkshire, England, proposed

the existence of so-called "dark stars" in 1783. He accepted Newton's theory of light, in which light is made up of tiny particles which Newton called "light corpuscles". Michell knew that as particles, light would be affected by gravity, and therefore could be slowed by large gravitational fields [241]. In 1676 the speed of light was approximately determined by Danish astronomer Ole Rømer by measuring the eclipses of Io. Michell used this calculation in his paper printed in *Philosophical Transactions*, predicting that light would be slowed as it escaped from a source, and showing that the amount of light emitted from a star is related to its mass. Therefore, the utilization of brightness as a way to measure distance to a star could be instead replaced by an estimate of the star's mass. Since the concept of escape velocity had already been worked out by Newton a century prior, the mass of the star could be determined by measuring how much the light coming from a star was slowed by the star's gravitational pull. Michell calculated that the escape velocity from the Sun was 497 times smaller than the velocity of light. This lead to the logical conclusion that any object with the same density as the Sun, but with a radius 497 times larger, would be sufficient to prevent the escape of light. He points out that a particle with a velocity of the speed of light trying to escape this massive sun would be forever unobservable. Michell then went even further, suggesting that these objects, though invisible, could be detected via their gravitational interactions with visible objects, which would of course prove to be true.

Michell's theories inspired others to continue thinking about "dark stars." William Herschel had already corresponded with Michell about the construction of lenses and telescopes. Because of Michell's aforementioned paper, Herschel slightly modified his own method to measure the slowing of light from stars, but was unable to himself detect any decrease in light's speed. Michell had suggested this was because no star was sufficiently massive to slow light enough to be measurable. In 1791 Herschel wrote a paper where he discussed the idea of slowing light in more detail, agreeing with Michell by suggesting that the particulate theory of light required a conclusion where light will be susceptible to gravity. He went on to

suggest that as light is travelling throughout space, there will be innumerable gravitational obstacles, all of which will be exerting a force on the light itself. This hypothesis that light, like matter, was affected by gravity, was a novel and extremely relevant idea.

Pierre-Simon Laplace may have also independently come to the same conclusions as Herschel and Michell [210]. Considered one of France's greatest scientists, he mentions his idea for "dark stars" almost in passing in the sixth chapter of *Exposition du Système du Monde* published in 1796. While describing the solar system, he makes the conjecture that the gravitational pull from a star approximately 250 times more massive than the sun and comparable in density to the Earth would be so great that no light could escape from its surface. He then went on to suggest that the largest bodies in the universe may very well be invisible due to this theory. He offered no technical mathematical proof for this claim, however. When asked for one in 1799, he provided a simple proof. It is remarkable to note that both Laplace and Michell made only passing references to what we now call black holes. It is also interesting to note that both Michell and Laplace opted to think of black holes as huge objects, rather than the compact objects that we know them to be today.

Other scientists at the time were expectedly excited at these ideas, and as the dawn of the 20th century loomed, the theory of the wavelike nature of light became substantiated. This caused scientists to briefly move away from the "dark star" theory, as it was unclear what sort of impact gravity would have on wavelike light [210]. The wavelike theory of light had been floating around since the 1600s, when Robert Hooke developed a "pulse theory". About a half century later, Christiaan Huygens worked out a mathematical theory of light as a wave. He predicted that light travels in a medium called the "luminiferous aether" where it was assumed light will slow down when in a denser medium. The existence of this aether was called into extreme doubt by the Michelson–Morley experiment in 1887.

Of course, we know today that light have both wavelike and particle-like characteristics. In 1915, Einstein developed and published his theory of general relativity. This geometric theory of gravitation emphasizes that gravity does in fact influence the motion of light.

General relativity universalizes Newton's often sufficient but imperially inaccurate theory of gravity. It describes gravity in three spatial dimensions and one time dimension. While Newton's law of gravitation is considered extremely accurate for classical physics problems that have flat spacetime geometry, it will not be accurate for any curved geometry and at velocities nearing the speed of light. General relativity must be used for things like gravitational waves, gravitational lensing, redshift, time dilation, and of course, to describe black holes [110].

In Newtonian mechanics, the source of gravity is mass. In general relativity, gravity is the consequence of the curvature of spacetime, which is determined by the distribution of all forms of energy within it, including mass. Mass and energy are described by the more generalized energy-momentum tensor, $T_{\mu\nu}$. This tensor describes mass and the energy and momentum densities, as well as other quantities like pressure and shear. In short, the curvature of spacetime is determined by the energy and momentum present. The curvature is described by the metric tensor, $g_{\mu\nu}$. The metric tensor is a generalization of the gravitational potential of Newtonian gravitation. This metric encapsulates both the geometric and causal structure of spacetime. Once you have defined some space with an arbitrary coordinate system, $g_{\mu\nu}$ allows you to define fundamental quantities such as lengths and time in a consistent manner, no matter which coordinate system is being utilized.

The curvature of spacetime is related to the energy-momentum tensor according to the Einstein equations:

$$G_{\mu\nu} + \Lambda g_{\mu\nu} = \frac{8\pi \mathrm{G}}{c^4} T_{\mu\nu}, \tag{2.1}$$

where $G_{\mu\nu}$ is the Einstein tensor, which is a function of the metric and encodes the curvature of spacetime. c is the speed of light, Λ is the cosmological constant, and G is the Newtonian gravitational constant. Equation 2.1 is generalized to curved spacetime, which is inherent to understanding black holes. The left hand side of the equation describes curvature, and the right hand side is energy. This allows us to move between a mass telling spacetime how

to warp, and spacetime telling mass how to move, to paraphrase the classic John Wheeler quote. This geometric theory of spacetime is the theory we still use today, and has held up to scrutiny for over a century and counting. The implications that come out of the theory of general relativity are vast and include but are not limited to predicting gravitational lensing, gravitational waves, and led to the quantifying and closer theoretical study of what we now know as black holes.

2.2 The Schwarzchild Solution

Only a few months after Einstein published the theory of general relativity, German physicist and astronomer Karl Schwarzchild developed the Schwarzchild solution, or the Schwarzchild metric. The main principle of general relativity is that physics is irrelevant from the coordinates chosen. Coordinates are simply labels to make calculations easier [122]. The choice of coordinates can be extremely critical when trying to solve Einstein's equations. For example, in linearized general relativity, coordinates defined by the Lorenz gauge will give the simple wave equation. The oldest and most relevant solution to the Einstein equations is the Schwarzchild metric. His coordinate choice permitted him to find the solution in a straightforward way, very soon after Einstein published his theory of general relativity [245]. This coordinate choice is called a coordinate chart, which is defined in the theory of Lorentzian manifolds. The Schwarzschild chart is a kind of polar spherical coordinate chart on a static and spherically symmetric spacetime. Schwarzchild considered a solution to the Einstein field equations where the Ricci tensor as described in equation 2.1 was zero [122]. In a Schwarzchild chart, with Schwarzchild coordinates of t, r, θ, ϕ, the line element is defined to be

$$g = -c^2\, d\tau^2 = -\left(1 - \frac{r_\mathrm{s}}{r}\right) c^2\, dt^2 + \left(1 - \frac{r_\mathrm{s}}{r}\right)^{-1} dr^2 + r^2 g_\Omega \tag{2.2}$$

$$r_s = \frac{2GM}{c^2} \tag{2.3}$$

where G is the gravitational constant.

His exact solutions to the Einstein equations for a non rotating, spherically symmetric body of mass M were found to be $1 - r_{\mathrm{s}}/r$ and $\frac{1}{1-r_{\mathrm{s}}/r}$. These solutions become singular where $r_s = r$ and $r = 0$. Both of these solutions create a singularity, though the solution at $r_s = r$ is a coordinate singularity, meaning that it is an artifact of the particular system of coordinates that was used. However, the solution of $r = 0$ is a spacetime singularity, and cannot be removed even with a change of coordinates. At this solution, some of the terms in the Einstein equations become infinite [61]. This is strange and unexpected. Einstein's equations have been observationally confirmed and have held up for over 100 years. However, certain solutions to Einstein's equations create out-of-control geometry. The behavior of a body where $r < 2GM$ is nonconsequential to everyday life. For example, the Sun has a Schwarzchild radius of 2.9 km. The true radius of the sun is about $7{\times}10^6$ km, approximately three orders of magnitude larger than its r_s. However, it has been theorized that there are objects that do meet the qualifications of equation 2.3, which we will from now on refer to as black holes.

After the publication of this metric, and the singularity solution that followed, the hunt was on to discover, or rule out, the existence or possible creation mechanisms of objects like this. Overly large densities for stars that are visible in the night sky have been ruled out. For example, in 1924 astronomer Arthur Eddington commented on the star Betelgeuse, saying that [109]

> *A star of 250 million km radius could not possibly have so high a density as the Sun. Firstly, the force of gravitation would be so great that light would be unable to escape from it, the rays falling back to the star like a stone to the earth. Secondly, the red shift of the spectral lines would be so great that the*

spectrum would be shifted out of existence. Thirdly, the mass would produce so much curvature of the spacetime metric that space would close up around the star, leaving us outside (i.e., nowhere).

It would be another decade before the first potential mechanism for creating a black hole would be discussed. But the golden age of black hole study was upon us.

2.3 Modern Study of Black Holes

In 1958, an american Professor of Physics named David Finkelstein identified that the Schwarzchild surface (black hole) was an event horizon [118]. He stated that the gravitational field of a spherical point particle is not to be invariant under time reversal for any admissible choice of time coordinate. Therefore the Schwarzchild surface is not a singularity but acts as a perfect unidirectional membrane in which that causal influences can cross it but only in one direction. This work strongly influenced scientists John Wheeler and Roger Penrose, the former of whom coined the term "black hole", to finally accept the concept and existence of black holes and event horizons, [221]. Finkelstein's paper sent the study of black holes mainstream, along with the discovery of pulsars by Jocelyn Bell Burnell in 1967, which were shown within a few years to be rapidly rotating neutron stars [144].

Further black hole solutions continued to be found. In 1963 Roy Kerr, a New Zealand mathematician, discovered what would come to be known as Kerr geometry, another solution to the Einstein field equations. His solution was a model for the gravitational field around a rotating, uncharged massive object, like a black hole [184]. This work predicted the existence of rotating black holes prior to their discovery. Since all black holes spin, this discovery has been invaluable to black hole studies since. In 1918 theorists showed that a rotating mass will also distort spacetime via frame dragging. A perfect solution to the Einstein equations for a rotating mass would have the symmetry of a cylinder, but because this is not a spherical solution, it will make the calculation very difficult. Kerr found his exact solution with two

free parameters, one that corresponded to the mass parameter from the Schwarzschild metric, and the other parameter represented angular momentum, or the amount of spin, the mass has. The Kerr metric is a description of spacetime curvature around a spinning mass. The Schwarzchild metric is used for a non-rotating black hole, whereas the Kerr metric is used to describe a rotating black hole. The Kerr metric, in spherical coordinates, is

$$\begin{aligned} ds^2 &= -c^2 d\tau^2 \\ &= -\left(1 - \frac{r_{\mathrm{s}} r}{\Sigma}\right) c^2 dt^2 + \frac{\Sigma}{\Delta} dr^2 + \Sigma d\theta^2 \\ &\quad + \left(r^2 + a^2 + \frac{r_{\mathrm{s}} r a^2}{\Sigma} \sin^2\theta\right) \sin^2\theta \; d\phi^2 - \frac{2 r_{\mathrm{s}} r a \sin^2\theta}{\Sigma} c dt \, d\phi \end{aligned} \tag{2.4}$$

where r, θ, and ϕ are the standard oblate spherical coordinates [263].

A few years later, the solution for a rotating and charged black hole was discovered by american physicist Ezra Newmann [214]. Eventually, the no-hair theorem emerged from this groundbreaking era. Simply put, the no-hair theorem states that a black hole can be described by three different parameters, and these three parameters can completely characterize a black hole: mass, spin, and charge. All other information, ie the "hair", disappears into the black hole and will be permanently inaccessible to any observer.

For example, imagine there are two black holes of the same mass, charge, and spin. However, the first black hole is made of collapsing matter, and the other collapsing antimatter. The no-hair theorem states that from an outside observer, both black holes will look identical and will be indistinguishable. A study by Stephen Hawking, Malcolm Perry and Andrew Strominger postulates that black holes might contain "soft hair" that gives a black hole more degrees of freedom than previously thought. This "hair" permeates at a very low energy state, which explains why it didn't come up in previous calculations of the no-hair theorem [143], though this idea is very controversial. In the later 1970s, work by Stephen Hawking and his collaborators led to the description of black hole thermodynamics. These laws describe the laws of thermodynamics in regards to a black hole by relating mass

to energy, area to entropy, and surface gravity to temperature [29]. This discovery lead to Stephen Hawking's work on quantum field theory that states that black holes will in fact radiate like a black body. This idea is now widely known as Hawking radiation.

2.4 Hawking Radiation

In 1971, Stephen Hawking proposed what is known today as the area theorem, which set off a series of fundamental insights about black hole mechanics [139]. This theorem predicts that the total area of any black hole's event horizon should never decrease, although it can increase if black holes merge, as was observationally confirmed using LIGO data in 2021 [162]. This theorem is a parallel to the second law of thermodynamics, which states that the entropy of a black hole should also never decrease.

The similarity between the second law of thermodynamics and the area theorem suggests that black holes could behave as thermal, heat-emitting objects. This was an odd and controversial idea, as it was thought that nothing could escape from a black hole's event horizon. However, in 1974 Stephen Hawking published a paper showing that quantum field theory requires black holes to radiate as a black body with temperature proportional to that of the inverse mass of the black hole [140]. This radiation will over time reduce the total mass of the black hole, if the black hole is not also accreting mass faster than it can evaporate away. This also implies that after a certain amount of time, a black hole may radiate away all of its mass and cease to exist. For most black holes, the time scale on which it would evaporate completely is many orders of magnitude greater than the age of the universe. However, lower mass black holes may evaporate on timescales that can be astronomically relevant. For example, a black hole of mass on the order of 10^{14} g will evaporate completely in about the age of the universe. Black holes lighter than this will evaporate even faster, and may have significant observational consequences because of it.

To derive the requirement that black holes will emit particles, Hawking looked to quantum mechanics. He first examined the space around the black hole using quantum field theory.

Hawking used this knowledge to examine what occurs when a field is quantized in the spacetime outside of a black hole. Black holes are not magical, they are bound by the law of conservation of energy, and cannot create mass out of nothing. However, quantum field theory does not describe space as "nothing". Rather, it has a vacuum energy and can be described as teeming with virtual particles and antiparticles popping in and out of existence. One may naively think that the creation of these particles violates the law of conservation of energy. However, we can think about this in the language of quantum mechanics by using the analogy of the energy-time form of the Heisenberg uncertainty principle

$$\frac{\hbar}{2} \leq \Delta E \Delta t. \tag{2.5}$$

This equation tells us that the product of the uncertainty on energy and the uncertainty on time is greater than or equal to $\frac{\hbar}{2}$. If we are working with very small timescales, our change in energy can actually be quite high. These virtual particles are created and annihilate on such a short timescale that the Heisenberg uncertainty principle takes over, and the law of conservation of energy is not violated.

The next logical thought, then, is what happens if a particle-antiparticle pair is allowed to pop into existence through equation 2.5, but one particle is produced on one side of the black hole's event horizon, and its paired particle on the other? From the perspective of an outside viewer onto the black hole, it appears the black hole has created mass, and radiated a particle. To conserve energy, the black hole must lose the mass associated with the radiated particle. It gets even more complicated when you consider that this means that the particle that fell into the black hole then must have had negative energy. Nonetheless, this is the process by which black holes radiate, and is commonly referred to today as Hawking radiation.

Black holes radiate all particle species lighter than or comparable to their temperature,

which is related to the mass of the black hole:

$$\begin{aligned} T_{\rm BH} &= \frac{M_{\rm Pl}^2}{8\pi m_{\rm BH}} \\ &\approx 1.05\,{\rm MeV} \times \left(\frac{10^{16}\,{\rm g}}{m_{\rm BH}}\right). \end{aligned} \tag{2.6}$$

Note that the temperature of a black hole is inversely proportional to its mass. This radiation causes a black hole to lose mass at the following rate:

$$\begin{aligned} \frac{dm_{\rm BH}}{dt} &= -\frac{\mathcal{G} g_{*,H}(m_{\rm BH}) M_{\rm Pl}^2}{30720\pi m_{\rm BH}^2} \\ &\approx -8.2 \times 10^{-7}\,{\rm g/s} \times \left(\frac{g_{*,H}}{10.92}\right)\left(\frac{10^{16}{\rm g}}{m_{\rm BH}}\right)^2, \end{aligned} \tag{2.7}$$

where $\mathcal{G} \approx 3.8$ is the appropriate greybody factor, and $M_{\rm Pl}$ is the Planck mass. The quantity $g_{\star,H}(T_{\rm BH})$ counts the number of particle degrees-of-freedom with masses below $\sim T_{\rm BH}$, weighted by factors of approximately 1.82, 1.0, 0.41 or 0.05 for particles of spin 0, 1/2, 1 or 2, respectively [206, 205]. For $T_{\rm BH} \gg 100$ GeV ($M_{\rm BH} \ll 10^{11}$ g), the particle content of the Standard Model corresponds to $g_{\star,H} \simeq 108$. For Kerr black holes (black holes with appreciable angular momentum), the values of $g_{\star,H}$ are somewhat higher, and favor the radiation of high-spin particles [218, 258, 151]. In this thesis, we will limit ourselves to the case of non-rotating (Schwarzschild) black holes.

Black holes will, without bias, emit any and all types of particles available to it, based on its temperature, regardless of the couplings or interations of the particles. For example, a solar mass black hole will not be able to emit particles like electrons, quarks, or muons and will only have access to particles like photons and gravitons. As the black hole gets hotter it will eventually gain access to all particles in existence.

As a black hole loses mass, it emits Hawking radiation at a greater rate, causing it to

evaporate over the following timescale:

$$t_{\rm evap} = \frac{30720\pi}{\mathcal{G}M_{\rm Pl}^4}\int_0^{M_i}\frac{dM_{\rm BH}M_{\rm BH}^2}{g_{\star,H}(T_{\rm BH})} \approx 4.0\times10^2\,{\rm s}\times\left(\frac{M_i}{10^{10}\,{\rm g}}\right)^3\left(\frac{108}{\langle g_{\star,H}\rangle}\right), \tag{2.8}$$

where M_i is the initial mass of the black hole and $\langle g_{\star,H}\rangle^{-1} \equiv (3/M_i^3)\int_0^{M_i} dMM^2/g_{\star,H}(T_{\rm BH})$ is the value of $g_{\star,H}$ appropriately averaged over the course of the black hole's evaporation.

Black hole evaporation has many consequences. First, their evaporation leads to a better understanding of how black holes interact thermodynamically with the rest of the universe. Second, because a black hole's temperature increases as its mass decreases, it will be able to emit both heavier and more energetic particles as it gets lighter. This implies as a black hole approaches the Planck mass, it will emit a high amount of gamma rays and high energy particles. Additionally, the evaporation of black holes leads to the black hole information paradox. The information content of a black hole appears to be lost when it dissolves at the end of its life, as under common models, emission from Hawking radiation will be random. This means that the information the black hole releases will have no relation to the original information captured.

There have been a few experimental searches, specifically the Fermi telescope in 2008, to look for the gamma ray flashes as a black hole finishes evaporating. Additionally, the Large Hadron Collider at CERN has attempted to create micro black holes in a collider environment [199]. Unfortunately, no evaporating black holes have been confirmed to have been found. It is additionally impossible to search for direct Hawking radiation evidence around massive black holes, as they do not emit anything bright enough or significant enough to be picked out from things like cosmic rays and other light.

2.5 Formation Mechanisms

When Schwarzchild and his peers began writing about black hole solutions, there were no known mechanisms for how a black hole might form. Additionally, little was known about

stellar evolution and death. Luckily, the latter field of study was moving forward, and as physicists learned about stellar evolution, new hypothesis about black hole formation also emerged.

To discuss the formation mechanisms of black holes, we need to go back to the 1930s. In 1931, an Indian-American theoretical physicist named Subrahmanyan Chandrasekhar calculated the maximum mass of a type of star called a white dwarf. At the time white dwarf stars were thought to be the final product of stellar evolution.

We know that normal, main sequence stars, do not collapse. During a star's regular lifetime it burns hydrogen in its core to produce radiation pressure that will keep the star from collapsing against its own gravity. This balance between radiation pressure and gravity is called hydrostatic equilibrium, and a star maintains it throughout its life on the main sequence. However, once it has exhausted its hydrogen, it can no longer hold itself up under the force of its own gravity. This causes the star to contract, which leads to an increased temperature and pressure in the core, which allows the core to begin to burn helium. The point at which a star starts to burn helium is called the helium flash.

At this point, the core of the star is made up of mostly helium, with some other elements like carbon and nitrogen. These cores are not supported by radiation pressure, but by electron degeneracy pressure. Electron degeneracy pressure is a physical manifestation of the Pauli exclusion principle [28]. The Pauli exclusion principle states that in a system of identical fermions, two or more particles cannot occupy the same state. For electrons, which have a fundamental property called spin, described as either spin up or spin down. Electrons of course surround non-ionized atoms, like the ones in the cores of stars. Because of the Pauli exclusion principle, electrons resist being compressed and forced close to other electrons of the same spin. The two electrons that occupy the lowest energy state, cannot share the same spin state. In the helium cores of these stars, the pressure these electrons exert acts as a resistance to being further compressed, which keeps the core from collapsing further.

Fusion of other elements will continue in shells around this helium core. Elements like

oxygen and carbon continue to be synthesized in the outer shells, and helium continues to be burned at the core. Eventually, however, these shells will run out of fuel to burn and the layers of the star will be ejected to form what is known as a planetary nebula. When the outer shells have dissipated, all that is left is the helium core of the star, which is known as a white dwarf.

The material of a white dwarf cannot fuse. It is being held up by electron degeneracy pressure as its mass attempts to force it to contract again. As expected, in order for a star to be held up against electron degeneracy pressure it must become extremely dense. The rough average density of a white dwarf star is 1×10^6 g/cm^3 [67]. Comparatively, the mean density of the entire Sun is about 1.4 g/cm^3.

Chandrasekhar used special relativity to determine that a non-rotating body with a mass above a certain limit that is being held up by electron degeneracy pressure has no stable solutions. The energy of the electrons will be increased the more the electrons are compressed. With sufficient pressure the electrons will be forced into the nuclei through electron capture. Chandrasekhar found that as the mass of an electron degenerate white dwarf star increases, its radius will decrease. Eventually, the radius becomes zero. This is the Chandrasekhar limit. Combining both the relativistic and non-relativistic regimes, Chandrasekhar found that the maximum mass of a white dwarf is approximately 1.4M$\odot$, or written explicitly as

$$M_{\text{limit}} = \frac{\omega_3^0\sqrt{3\pi}}{2}\left(\frac{\hbar c}{G}\right)^{\frac{3}{2}}\frac{1}{(\mu_{\text{e}}m_{\text{H}})^2}, \tag{2.9}$$

where ω_3^0 is a constant connected with the solution to the Lane–Emden equation (a dimensionless form of Poisson's equation for the gravitational potential of a Newtonian self-gravitating, spherically symmetric, polytropic fluid), $\hbar$ is the reduced Plancks constant, c is the speed of light, G is the gravitational constant, μ_{e} is the average molecular weight per electron, which will depend on the chemical composition of the star, and m_{H} is the mass of a hydrogen atom. This is the mass limit above which electron degeneracy pressure can no longer support the star against its own gravity.

It is now known that a white dwarf star slightly above the Chandrasekhar mass can in fact be stable, but it becomes a new type of star, a neutron star. Neutron stars are partially held up by neutron degeneracy pressure, which is a phenomenon also explained by the Pauli exclusion principle [28]. Neutron degeneracy is analogous to electron degeneracy pressure, but in the case of a neutron star, the electrons have been forced into the nuclei due to the extreme pressure, and the collapse of the star is halted by the physical neutron nuclei smashed against each other. Neutron stars are sometimes referred to as a star sized nucleus because of this fact. Neutron stars are additionally held up by other nuclear forces [106]. Just as white dwarfs, neutron stars are also extremely dense.

Neutron stars may be stable, but they are not necessarily the end of the star's journey. In 1939, Robert Oppenheimer and his co-authors described the Tolman–Oppenheimer–Volkoff limit [217]. The Tolman–Oppenheimer–Volkoff limit is the upper limit on the mass of a neutron star. Beyond this, the star will continue to collapse into a black hole.

However, this is not the way we theorize that black holes form from stars today. For one, white dwarf stars are usually left behind by lower mass stars, and do not continue to collapse. As an example, the Sun will eventually become a white dwarf, and continue to cool over the billions of years after it burns through all of its hydrogen. It takes a massive star to continue this collapse past the white dwarf stage and the neutron star stage to become a black hole.

Massive stars, or stars above approximately 8 $M\odot$, behave similarly to lower mass stars during their main sequence lifetime, burning hydrogen to helium in their core (though the fusion processes through which this occurs will be different). As a massive star ages, it will eventually run out of hydrogen to burn in its core. It will then move on to fusing heavier and heavier elements, like helium, carbon, neon, oxygen, nickel, and then iron, among others. Like a smaller star this fusion will occur in shells around the core, though higher mass stars will be able to fuse many more elements and by consequence produce many more shells. Once the star runs out of one element to fuse, it falls out of hydrostatic equilibrium and

will collapse further, and a heavier element will be able to be burned due to the increased pressure and heat generated from the collapse. However, this cannot continue in perpetuity. Eventually, when the star has exhausted all of its fusion options it now has two paths it may take. Stars in this phase between about 8-22 M$\odot$ are theorized to explode in what is called a type II supernova [209]. It is theorized that these explosions are neutrino powered [274, 275]. The iron core of the massive star will collapse to a neutron star. The binding energy of the neutron star is released as neutrinos, some of which will deposit their energy in the material above the iron core. The sheer amount of these neutrinos may cause the outer material to expand, and therefore explode. If the mass of the neutron star remnant is still too high to prevent further collapse, the core will become a black hole. Extremely massive stars, like ones above a mass of about 22 M$\odot$ will not explode, rather they will collapse into a black hole directly.

Because of the consistent expulsion of material before and during a type II supernova, the black hole remnant is not the same mass as the star that died. A black hole of mass 5 M$\odot$ was probably formed from a star that had a mass of at least 20 M$\odot$. This means that most black holes formed from dying massive stars will have masses on the order of 1 M$\odot$. The existence of black holes of stellar mass has been confirmed by the LIGO collaboration [3]. In 2021 they confirmed the detection of two neutron star–black hole mergers. The black holes were approximately 9 M$\odot$ and 6 M$\odot$, respectively. These black holes were very likely core collapse black holes, formed from dying massive stars up to 50 M$\odot$.

In the early universe, stars could form that were even more massive than the massive stars we see today. Extremely massive stars do not live very long, so they would quickly explode on the order of millions of years [234]. These massive stars could have produced black holes of masses up to 1×10^3 M$\odot$. These black holes may have merged over the following billions of years, and eventually became even more massive. Black holes above the mass of about 1×10^6 M$\odot$ are considered supermassive, and are most commonly cited for their existence at the center of massive galaxies.

So far we have discussed formation mechanisms for two types of black holes; stellar mass and supermassive black holes. Both of these types have been observationally confirmed to exist, and in the case of the latter, photographed. However, the black holes that will be the focus of this thesis are so-called primordial black holes, which are not formed from a collapsing star.

Primordial black holes (PBHs) are theoretical black holes that formed not from a collapsing star, but rather formed a short time after the Big Bang, approximately 13.8 billion years ago. They were first suggested in 1967 by Yakov Borisovich Zel'dovich and Igor Dmitriyevich Novikov, and by Stephen Hawking in 1971 [280, 138]. In his paper, Hawking discussed the theory that in order to produce the structure in the universe we see today, there were initially small random fluctuations in density on all length scales. However, there may have been some fluctuations where the gravitational energy of the fluctuation exceeded the energy of the expansion of the universe. These regions would not have continued to expand, but would have collapsed into a sort of black hole. Hawking also suggested that these objects would have a lower bound on mass of approximately 10^{-5} g (which is approximately the Plank mass).

In more modern times, there are two prevailing theories for how primordial black holes may have formed. First, black holes could have formed through phase transitions, which are a common but not necessarily universal feature of gauge field theories [145]. Phase transitions can give rise to large density pertubations, which can give rise to primordial black holes.

Another natural source of density perturbations are the quantum fluctuations that arise during inflation. An inflationary period needs to be invoked in order to explain a few cosmological problems, namely why the universe is homogeneous and isotropic, why the universe is spatially flat, and why we don't see any magnetic monopoles or other massive relics from the high energy early universe. During the inflationary phase, the universe underwent exponential expansion followed by an era of reheating. This phase occurred approximately 10^{-35}s after the Big Bang.

Black holes from inflation would form when density pertubations of a given size enter the horizon. At early times, the horizon size will be smaller, and not causally connected to higher densities elsewhere. However, as horizon sizes grow, they will eventually be able to encompass an entire density pertubation, and that can form a black hole.

The mass of a black hole which collapsed in the early Universe depends on its formation time. We know that a black hole can be characterized by an extremely dense amount of matter in a very compact region, which we have characterized as the Schwarzchild radius. The mean density inside that region can be characterized as

$$\rho_S = M_{\rm PBH}/(4\pi R_S^3/3) \sim 10^{18}(M/M_\odot)^{-2}{\rm g\ cm}^{-3} \tag{2.10}$$

Additionally, the mean density of the universe in the radiation era scales with time, as

$$\rho_c \sim 10^6(t/{\rm s})^{-2}{\rm g\ cm}^{-3} \tag{2.11}$$

In order to form a black hole, we want densities at least on the order of the mean inside the black hole horizon, where $\rho_c \sim \rho_S$. Therefore, the mass of the PBHs that result, should be on the order of the horizon mass at that time, which will be the Hubble horizon, $M_{\rm PBH} \sim M_{\rm H}$. The total mass within the Hubble horizon at the black hole's formation time is defined, in a radiation dominated era, as

$$M_{\rm hor} = \frac{M_{\rm Pl}^2}{2H} \sim 10^{10}\,{\rm g} \times \left(\frac{10^{11}\,{\rm GeV}}{T}\right)^2 \left(\frac{106.75}{g_\star(T)}\right)^{1/2}, \tag{2.12}$$

where $M_{\rm Pl} = 1.22 \times 10^{19}$ GeV is the Planck mass, H is the Hubble rate, T is the temperature of radiation, and $g_\star(T)$ is effective number of relativistic degrees-of-freedom [125, 177, 79, 170, 180, 46, 277, 279, 77, 156, 195, 194, 196, 269, 251, 5, 146, 142, 186]. $g_\star(T)$ can generally be straightforward to calculate. For example, in the very early universe (T $\gg$ 100 GeV), all of the particle species described by the Standard Model were present and maintained at

a common temperature. When we add up the total number of bosonic degrees-of-freedom, plus 7/8 times the total number of fermionic degrees-of-freedom contained in the Standard Model, we get $g_\star(T) = 28 + (7/8) \times 90 = 106.75$ (For a more detailed discussion, see [149], chapter 4).

With this calculation, we can move from the mass of the PBHs, to the time at which they were formed. A more detailed calculation shows that $M_{\rm PBH} = \gamma M_{\rm H}$, where the proportionality factor γ depends on the details of gravitational collapse, and gets values lower than 1 [57]. Since PBHs are formed when fluctuations cross the horizon by the time of formation, t_f, their mass can be related to the wavelength of perturbations. When the mode of wavenumber k crosses the horizon, the condition $a(t_f)\, H(t_f) = k$ holds. Since the mass of PBHs is proportional to the horizon mass at the moment of formation, $M_{\rm PBH} \propto \gamma H^{-1}$, at the radiation dominated era [239],

$$M_{\rm PBH} \simeq 30\ M_\odot\ \left(\frac{\gamma}{0.2}\right) \left(\frac{2.9 \times 10^5 {\rm Mpc}}{k}\right)^2 \ . \tag{2.13}$$

Therefore, probing a given scale k could constrain a PBH population of its corresponding mass [261]. For example, PBHs with masses of $\sim M_\odot \simeq 2 \times 10^{33}$ g would have been formed at around the QCD (quantum chromodynamic) phase transition, at $t \sim 10^{-6}$ s [261]. Since the PBH mass is approximately given by the mass within the horizon, it means that fluctuations entering the horizon can collapse into PBHs.

Although the mass of the black holes that may have formed in the early universe is model dependent, we expect this mass to be comparable to the total energy enclosed within the horizon at the time of their formation. This provides us with motivation to consider a wide range of masses, extending from very small black holes (which evaporate well before the onset of BBN), to black holes with masses as large as $M \sim 10^2 M_\odot$, which may have formed shortly before the BBN era. If there existed even a very small abundance of black holes in the early universe, they would make up an increasingly large fraction of the total energy density

as the universe expands, with the ratio $\rho_{\rm BH}/\rho_{\rm rad}$ growing proportionally to the scale factor during the era of radiation domination [203, 211, 152]. If the black holes are very massive and long-lived, they could make up all or some of the dark matter in the universe today [37, 54]. Alternatively, there may have been an era prior to BBN in which much smaller black holes dominated the total energy density, up to the point of their evaporation and the subsequent reheating of the radiation bath through Hawking radiation.

After inflation, the universe continued to expand, but at a slower rate. Although any PBHs formed before the end of inflation (with masses around 1 g) would be diluted exponentially, the inflationary fluctuations themselves could generate PBHs on scales larger than this [52]. The spectrum of the mass of any produced black holes will depend on the shape of the inflationary potential and other model dependant feature. In the most simplistic scenario, the inflationary fluctuations would depend on the inflation potential V(ϕ), and would have a power law form. Additional theories about PBH formation include collapse from scale-invariant fluctuations, collapse in a matter-dominated era, quantum diffusion, critical collapse, collapse of cosmic loops, and collapse of domain walls, among others [56].

As discussed previously, primordial black holes under a mass of about 10^{14} g would have evaporated already. However, there is nothing in their theorized formation mechanism that prevents them from having a large range of masses. Primordial black holes are non-baryonic, collisionless, stable, and non-relativistic, so they are a good candidate for dark matter. They may have formed in the early universe, prior to Big Bang nucleosynthesis, and therefore their possible existence as dark matter wouldn't conflict with the measured value for Ω_b (the energy density in the universe from baryons). Primordial black holes are under the larger dark matter candidate umbrella of "MACHOs", or massive compact halo objects. PBH formation may also be the source of so-called "intermediate mass black holes', which are black holes with masses in the range 10^2–10^5 solar masses. In general, however, the existence of PBHs remains theoretical, though their possible existence remains a promising area of study.

2.6 Constraints on Primordial Black Holes

Black holes, specifically black holes as dark matter, have been a major point of study in astrophysics. Since black holes as dark matter can theoretically span a large mass range that may span many orders of magnitude, many different types of experimental searches must be utilized to provide constraints on their existence.

The abundance and mass spectrum of primordial black holes is strongly constrained by several types of observations, which are listed and briefly explained below.

- *Lifetime of PBHs*: Due to Hawking radiation, black holes will evaporate on a timescale $t_{\rm evap} \approx 4.0 \times 10^2\,{\rm s} \times \left(\frac{M_i}{10^{10}\,{\rm g}}\right)^3 \left(\frac{108}{\langle g_{\star,H}\rangle}\right)$. As discussed previously, black holes that formed shortly after the Big Bang with masses on the order of 10^{14} g would be completely evaporated by today, and therefore cannot contribute to the dark matter abundance we currently measure [59, 58]. Additionally, black holes evaporating right now should dissipate in a large explosion of particles. However, no such explosions have been confirmed to be detected, and are unlikely to be detected in the future [247, 208].

- *Constraints on Light Elements from BBN*: If PBHs are formed shortly after the Big Bang, and have masses around or slightly below 10^{10} g, they will evaporate during Big Bang nucleosynthesis. The particles they produce will affect the light element abundances through the hadro-dissociation and photo-dissociation processes. The energy density of the black holes may also affect the Hubble rate during BBN.

- *Constraints from Gamma Rays*: Slightly more massive PBHs that are still present today would be evaporating currently, producing observable extragalactic gamma-ray radiation. This radiation spectrum can be calculated, and would have been detected by EGRET and Fermi Large Area telescopes. Additionally, PBHs are expected to be clustered around galactic halos, and therefore so should be their emission. Therefore, there should be a galactic background of gamma radiation. This radiation should be anisotropic and separable from extragalactic emission.

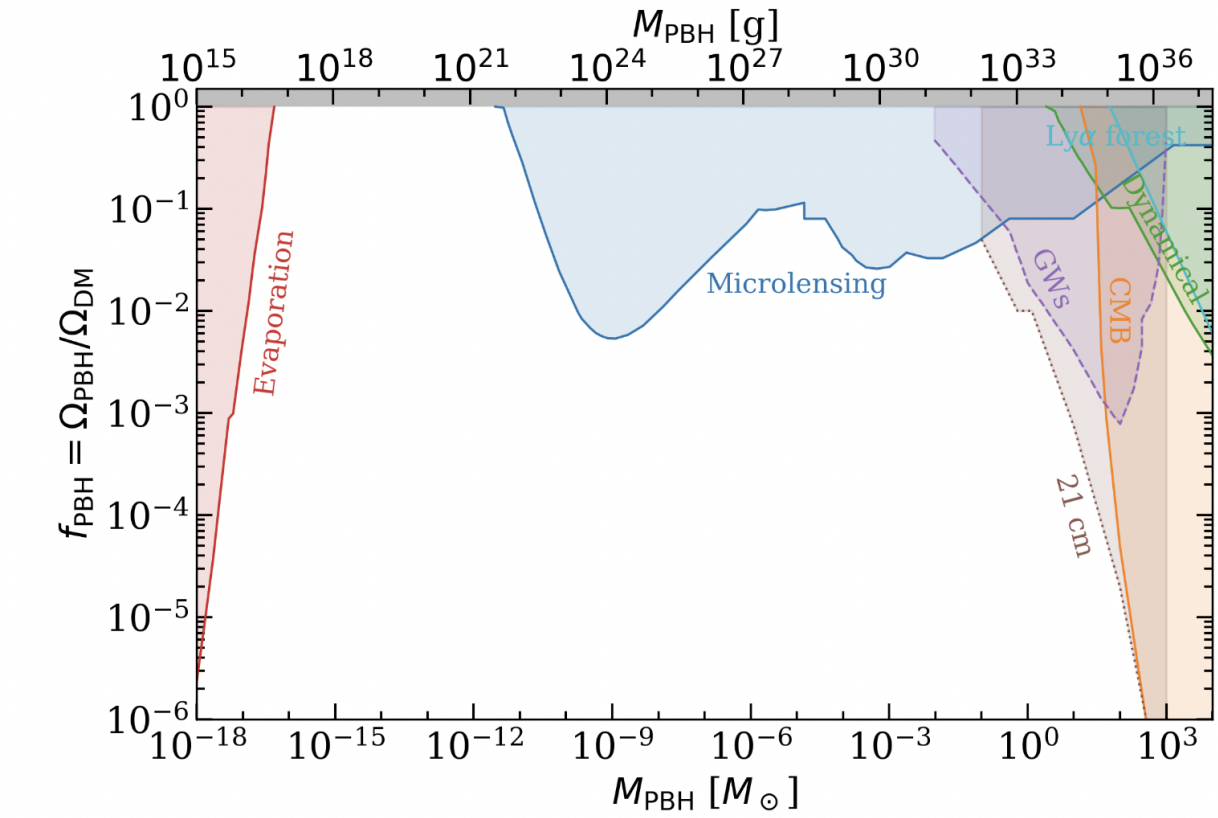

Figure 2.1: Compilation of contraints on the PBH fraction (with respect to DM) as a function of the PBH mass, assuming a monochromatic mass function. The different probes considered are: impact of PBH evaporation (red) on the extragalactic γ-ray background and on the CMB spectrum; non-observation of microlensing events (blue) from the MACHO, EROS, Kepler, Icarus, OGLE and Subaru-HSC collaborations; PBH accretion signatures on the CMB (orange), assuming spherical accretion of PBHs within halos; dynamical constraints, such as disruption of stellar systems by the presence of PBHs (green), on wide binaries and on ultra-faint dwarf galaxies; power spectrum from the Lyα forest (cyan); merger rates from gravitational waves (purple), either from individual mergers or from searches of stochastic gravitational wave background. Gravitational waves limits are denoted by dashed lines, since they could be invalidated. Dotted brown line corresponds to forecasts from the 21 cm power spectrum with SKA sensitivities and from 21 cm forest prospects. This figure, its caption, and its components were compiled by [261].

- *Femtolensing of gamma-ray bursts*: MACHOs can induce gravitational femtolensing of gamma ray bursts. The Fermi Gamma-ray Burst Monitor has not detected PBHs in the mass range $5\times10^{17} - 10^{20}$ g, implying that PBHs cannot make up the majority of the dark matter in that mass range [30].

- *Star Formation*: Star formation can occur in spaces dominated by dark matter, whether partially or totally PBHs. If this occurs, the black holes will eventually inherit the stellar remnant, and destroy it. The constraints that result from the observation of neutron stars and white dwarves in globular clusters does not allow PBH to constitute totally the dark matter in the PBH mass range $10^{16} - 10^{22}$ g [50]. There have been doubts about the robustness of these constraints.

- *Gravitational microlensing*: Microlensing is analogous to gravitational lensing, but on a smaller scale. When a massive object comes between the line of sight of an observer and a point source, the point source is observed to brighten. PBHs are theorized to do this; if they exist in the galaxy as black holes they should slightly brighten background stars. If the dark matter galactic halo is mostly composed of PBH, one expects gravitational microlensing events of stars in the Magellanic clouds. The EROS microlensing survey, and the MACHO collaboration have not observed any microlensing events, and have put limits on PBHs as dark matter around $10^{25} - 10^{34}$ g [259, 15]. Additionally, the Subaru Hyper Suprime-Cam (HSC) has searched for PBHs around M31, placing constraints on PBHs from their results. [215]

- *CMB spectral distortions*: More massive PBHs can have a substantial accretion disk, that can emit X rays. This emission can modify recombination history, which generates CMB spectral distortions and CMB temperature anisotropies. These distortions are strongly constrainted by CMB measurements from COBE/FIRAS. It is found that PBH of M_{PBH} >10 M$\odot$ cannot comprise of more than ≈1% of dark matter, and solar mass PBHs cannot comprise of more than 10% of dark matter.

- *Gravitational waves*: The observations by LIGO and Virgo can constrain the existence of primordial black holes. If we insist that the predicted merger rates of PBH binaries cannot exceed the ones that we have measured via gravitational waves, we find upper bounds of $f_{\rm PBH}$ <0.01, for black hole masses between 1 and 300 M$\odot$ [16, 172].

- *Lyα forest*: Because PBHs are discrete, they will lead to a shot-noise contribution to the matter-power spectrum. This will enhance small scale fluctuations. We can observe the Lyα forest and put bounds on the maximum allowed fraction of PBHs [12]. This method is very model dependant.

- *21 cm cosmology*: The 21 cm line signal emitted from the hyperfine structure of hydrogen is very sensitive to the thermal state of the intergalactic medium and therefore any energy injection from PBH accretion or evaporation may leave an observable signature. Additionally, future detection of the cosmological 21 cm power spectrum could improve the bounds placed on PBHs even more significantly.

This list is not comprehensive, but does capture the current main constraints on a wide mass range of primordial black holes as a dark matter candidate. In the future, additional experiments will be conducted to provide even more comprehensive constraints on PBH existence. The Square Kilometer Array (SKA) radio telescope will observe the possible effects of PBHs on reionization. LIGO/VIRGO will detect new black hole merging events, from which one could reconstruct the mass distribution of possible primordial black holes. This may also lead to the distinction of black holes originating from stellar events, versus primordial black holes [78]. Other gravitational wave detectors like the Laser Interferometer Space Antenna (LISA) will probe the stochastic background of gravitational waves emitted by primordial black hole binaries, when they are still orbiting relatively far from each other, prior to merging [80]. Observations of faint dwarf galaxies, specifically their central cluster, could be used to test whether these dark matter dominated objects are also dominated by PBHs as the dark matter. One could also monitor the movement of stars in the galaxy, to

test for kinematic influence by a possible PBH. Just because a PBH has not been explicitly detected yet, does not mean they are ruled out as dark matter.

Black holes have long been both controversial and extensively studied. They are theorized to form both from an explosion of a star too massive to hold itself up, and density fluctuations in the early universe. PBHs specifically are a very promising dark matter candidate, and have had constraints over large mass ranges placed on them. Keeping these constraints in mind, we move on to discuss updating the constraints that come from BBN.

CHAPTER 3

CONSTRAINTS ON PRIMORDIAL BLACK HOLES FROM BIG BANG NUCELOSYNTHESIS

In this chapter, we revisit the constraints on primordial black holes that can be derived from measurements of the primordial light element abundances [182]. For black holes with evaporation times between $t_{\rm evap} \sim 10^{-1}$ s and $\sim 10^{13}$ s (corresponding to $M \sim 6 \times 10^8$ g to $\sim 2 \times 10^{13}$ g, assuming Standard Model particle content), measurements of the light element abundances typically provide us with the most stringent constraints on their abundance. For longer evaporation times, measurements of the CMB are generally more restrictive [53]. In particular, we use modern measurements of primordial hydrogen, deuterium and helium to derive upper limits on the initial abundances of $M \sim 10^8 - 10^{13}\,{\rm g}$ black holes. For black holes heavier than $\sim 10^{10}\,{\rm g}$, the strongest constraints result from the photodissociation or hadrodissociation of helium nuclei and the corresponding production of antideuterons.

Lighter black holes are constrained by their impact on the Hubble rate, which can alter the time at which the weak interactions effectively freeze-out, as well as the Hawking radiation of hadrons and mesons, each of which can alter the neutron-to-proton ratio and enhance the resulting helium abundance. We also consider how these constraints can change in the presence of particle content beyond the Standard Model. The existence of additional particle species can increase the rate at which black holes evaporate, typically weakening the resulting constraints. Furthermore, in scenarios that feature large numbers of decoupled degrees-of-freedom, the fraction of a black hole's mass that goes into particles that can break up helium can be significantly reduced. If stable, such Hawking evaporation products can act as dark radiation or dark matter.

3.1 Measurements of the Primordial Light Element Abundances

In this chapter, we make use of two sets of measurements of the primordial light element abundances:

- We use the deuterium-to-hydrogen measurement of $({\rm D/H})_p = (2.53 \pm 0.04) \times 10^{-5}$, based on the observation of four damped Lyman-alpha systems [88, 235]. Note that the

uncertainties quoted for this result are significantly smaller than those associated with previous measurements, allowing us to place constraints that are significantly more stringent than previous constraints. [60, 190].

- For the helium mass fraction, we adopt $Y_p \equiv \rho(^4\mathrm{He})/\rho_b = 0.2449 \pm 0.0040$, based on the measurements of recombination lines emitted from 45 extragalactic HII regions that have been statistically analyzed [163, 25]. While other recent determinations are not in total agreement (including $Y_p = 0.2446 \pm 0.0029$ and $Y_p = 0.2551 \pm 0.0022$), the measurement adopted in this chapter is consistent with (and has slightly larger error bars than) that recommended in the Particle Data Group's BBN review [220, 163, 257].

For two reasons, we do not explicitly make use of ^{3}He measurements in this chapter. First, measurements of primordial ^{3}He are complicated by the fact that stellar nucleosynthesis models for ^{3}He are in conflict with observations [216]. In light of this, it may be unwise to treat ^{3}He as a reliable probe of the early universe [257]. Second, in light of recent improvements in the precision of primordial deuterium measurements, the constraints one might derive from ^{3}He are most stringent only in small corners of parameter space (for example, in a scenario in which black holes evaporate $\sim 10^6 - 10^8$ s after the Big Bang to a large number of electromagnetically-charged degrees-of-freedom, beyond those of the Standard Model). On similar grounds, we do not make use of primordial lithium measurements in our analysis [257].

3.2 The Impact of Evaporating Black Holes on Big Bang Nucleosynthesis

A great deal of effort has been invested in developing sophisticated codes which can make detailed and accurate predictions for the primordial element abundances. These predictions have been found to be in excellent agreement with the measured abundances of primordial D, ^{3}He and ^{4}He, demonstrating that our universe was radiation dominated and generally

well-described by the standard ΛCDM cosmological model during the era of primordial nucleosynthesis [244, 250, 161, 96, 223, 116]. The measured lithium abundance is somewhat higher than predicted by standard BBN models [115]. At this time, it is not clear whether this is a consequence of new physics, or the result of challenges associated with accurately measuring the primordial abundance of this nuclear species. These measurements can be used to place stringent constraints on the expansion history of the universe as early as a few seconds after the Big Bang, as well as on any energy injection that may have occurred during or after this era [238, 168, 225, 158, 157, 119, 159, 102, 60, 176].

The evaporation of primordial black holes could potentially impact the resulting light element abundances in a number of different ways. In this discussion, we will focus on the following four mechanisms, each of which can play a significant role:

- At a temperature near ~ 1 MeV, the rate of weak interactions (which can convert neutrons into protons and vice versa) falls below the rate of Hubble expansion, freezing-in the value of the neutron-to-proton ratio. The presence of black holes and their evaporation products can increase the expansion rate during this era, causing these interactions to freeze-out earlier, enhancing the neutron-to-proton ratio during BBN, and increasing the amount of helium that is ultimately produced.

- Hadrons and mesons radiated from black holes can alter the neutron-to-proton ratio after the weak interactions have frozen out through processes such as $n + \pi^+ \leftrightarrow p + \pi^0$ and $p + \pi^- \leftrightarrow n + \pi^0$. This can enhance the neutron-to-proton ratio during BBN and increase the resulting helium abundance.

- Energetic photons from black holes can break up helium nuclei through photodissociation, reducing the resulting helium abundance and (more importantly) increasing the abundance of primordial deuterium. This process is effective, however, only if the temperature of the background radiation is too low to absorb the dissociating photons through e^+e^- pair production, $T \lesssim m_e^2/22E_{\rm He} \sim 0.4$ keV (where $E_{\rm He} \simeq 28.3$ MeV is

the nuclear binding energy of helium) [179].

- At earlier times ($T \gtrsim 0.4\,\mathrm{keV}$), energetic photons are typically absorbed before they can break up any helium nuclei. During this era, helium nuclei are most efficiently broken up by the energetic mesons that are radiated from black holes (hadrodissociation).

These and other processes have been modeled in detail by a number of modern BBN codes, and the impact of evaporating black holes on these processes has been studied in the past [21, 20, 224, 222, 83, 85, 60, 190, 6]. In particular, Carr *et al.* (2010) used primordial measurements of Y_p, D/H, ^{3}He/D and ^{6}Li/^{7}Li to constrain the abundance of primordial black holes with evaporation times in the range of $t_{\rm evap} \sim 1 - 10^{13}\,\mathrm{s}$ [60, 53]. Although that study considered a wide range of hadronic and electromagnetic interactions, significant progress has been made in the past decade in improving these measurements, as well as in refining the codes that calculate the resulting light element abundances. Furthermore, these previous studies did not consider how the existence of particle content beyond the Standard Model could potentially alter these constraints.

In this chapter, we revisit the impact of evaporating black holes on the formation of primordial nuclei, making use of the recent study by Kawasaki *et al.* (2018), who have used a sophisticated code to study the effects of long-lived particles on BBN [176].[1] In many respects, evaporating black holes alter the predicted light element abundances in ways that are similar to decaying particles. That being said, decaying particles and evaporating black holes typically produce particles in different ratios (branching fractions), with a different distribution of energies, and with a different time profile. In what follows, we will describe our procedure for adapting constraints on long-lived decaying particles to the case of evaporating black holes.

In Kawasaki *et al.*, the authors present their results in terms of the decaying particle mass multiplied by the number of such particles per unit entropy, MY, as evaluated at $t \ll \tau_X$

1. For earlier work studying the impact of long-lived decaying particles on BBN, see Refs. [119, 228, 94, 193, 167, 189, 166, 174, 175, 174, 174, 95, 188, 173, 147, 178].

[176]. In contrast, Carr *et al.* present their constraints on evaporating black holes in terms of the quantity β', which is closely related to $\beta \equiv \rho_{\rm BH}/\rho$ evaluated at the time of black hole formation, $t_{\rm form}$ [60, 53]. Through the following, β can be directly related to the quantity constrained in Kawasaki *et al.*, MY:

$$\beta \equiv \frac{\rho_{\rm BH}(t_{\rm form})}{\rho(t_{\rm form})} = \frac{M n_{\rm BH}(t_{\rm form})}{\pi^2 g_\star(T_{\rm form}) T_{\rm form}^4/30} = \frac{4}{3}\frac{M}{T_{\rm form}}\left(\frac{n_{\rm BH}}{s}\right) \equiv \frac{4}{3}\frac{MY}{T_{\rm form}}, \tag{3.1}$$

where $T_{\rm form}$ is the temperature at the time of formation for a black hole of mass M [176]. Carr *et al.* further introduced the quantity γ, which is the mass of the black hole divided by the mass enclosed within the horizon (see Eq. 2.12) at the time of formation. This allows us to write the formation temperature as $T_{\rm form} = (45\gamma^2 M_{\rm Pl}^6/16\pi^3 g_\star(T_{\rm form})M^2)^{1/4}$, and to express β as follows:

$$\beta = \frac{4}{3}\left(\frac{16\pi^3 g_\star(T_{\rm form})M^2}{45\gamma^2 M_{\rm Pl}^6}\right)^{1/4} MY. \tag{3.2}$$

For convenience, Carr *et al.* introduces the quantity β', which is β multiplied by the following powers of γ and $g_\star$:

$$\beta' \equiv \gamma^{1/2}\left(\frac{106.75}{g_\star}\right)^{1/4}\beta = \frac{4}{3}\left(\frac{16\pi^3 M^2 \times 106.75}{45 M_{\rm Pl}^6}\right)^{1/4} MY. \tag{3.3}$$

This expression directly relates the ways in which Carr *et al.* and Kawasaki *et al.* characterize the magnitude of energy injection, allowing us to convert between these quantities. To put this in terms that the reader may find more intuitive, we can also relate β' to $\Omega_{\rm BH}$, which we define as the value of $\rho_{\rm BH}/\rho_{\rm crit}$ that would be the case today if the black holes had not evaporated:

$$\beta' \simeq 2.2 \times 10^{-20} \times \left(\frac{\Omega_{\rm BH}}{1}\right)\left(\frac{M}{10^{10}\,{\rm g}}\right)^{0.5}. \tag{3.4}$$

Alternatively, we can write β' in terms of the ratio of densities in black holes and matter (at

$t \ll t_{\rm evap}$):

$$\beta' \simeq 7.0 \times 10^{-21} \times \left(\frac{M}{10^{10}\,{\rm g}}\right)^{0.5} \left.\frac{\rho_{\rm BH}}{\rho_M}\right|_{t \ll t_{\rm evap}}. \tag{3.5}$$

While the branching fractions for the decays of a generic long-lived particle are entirely model dependent, Hawking evaporation produces various particle species with a calculable ratio, proportional to $g_{\star,H}$ (as introduced in Eq. 2.8). In contrast to decaying particles, Hawking evaporation is a purely gravitational phenomenon, and thus does not depend on the charges or interactions of the particles being radiated. For the case of Standard Model particle content, and for black holes in the mass range under consideration in this chapter, approximately 73% of the total energy radiated from a black hole is in the form of quarks and gluons (and 94.5% of the energy goes into particles other than neutrinos). When translating limits for decaying particles, we thus reduce the total decay rate by these factors (depending on whether we are in the hadrodissociation or photodissociation limit, respectively).

A second way in which evaporating black holes impact BBN differently from long-lived particles follows from the fact that the temperature of a black hole (and thus the average energy of the injected particles) increases as a black hole loses mass. For example, when a particle decays into a pair of quarks, $X \to q\bar{q}$, those quarks each have an energy of $E_q = m_X/2$. Hawking radiation, in contrast, produces an approximately thermal spectrum of particles, with a temperature that steadily increases as the black hole radiates. Throughout this chapter, we adopt a thermal (Fermi-Dirac or Bose-Einstein) distribution for the spectral shape of the products of Hawking evaporation. Although this is not precisely true, it is an adequate approximation for the purposes of this chapter [219, 206, 205]. Averaged over the course of a black hole's evaporation, the mean energy of a radiated quark (or other fermion) is given by:

$$\langle E_q \rangle = \frac{\int_{M_i}^{0} 3.15\, T_{\rm BH}(M)\, \frac{dN}{dM}(M)\, dM}{\int_{M_i}^{0} \frac{dN}{dM}(M)\, dM} = 6.3\, T_i, \tag{3.6}$$

where M_i (T_i) is the initial mass (temperature) of the black hole, $dN/dM \propto T_{\rm BH}^{-1}$ is the number of particles radiated per unit mass loss, and we have made use of the fact that the

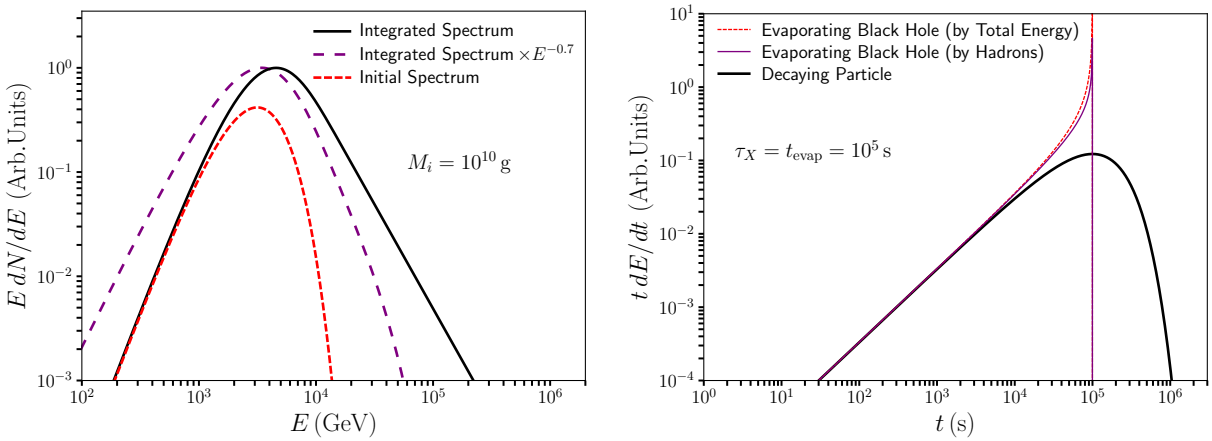

Figure 3.1: Left Frame: The spectrum of particles radiated from a black hole with an initial mass of 10^{10} grams. We show the initial spectrum (when $M = 10^{10}$ g), the spectrum integrated over the lifetime of the black hole, and the integrated spectrum weighted by an additional factor of $E^{-0.7}$ (as appropriate for considering the production of hadrons). Right frame: The time profile for energy injection from particle decay or black hole evaporation, for the case of a lifetime or evaporation time of 10^5 seconds. In the case of black hole evaporation, we show profiles corresponding to the total injected energy and to the number of injected hadrons.

average energy of a relativistic fermion in a thermal distribution is approximately 3.15 times the temperature of that distribution. Based on this result, we approximate the spectrum of the emission from an evaporating black hole with that from the (two-body) decays of a particle with a mass equal to $m_X \simeq 12.6\,T_i$. In the left frame of Fig. 3.1, we plot the spectrum of Hawking radiation injected from a black hole with an initial mass of $M_i = 10^{10}$ g, both at that moment, and as integrated over the course of its evaporation.

The prescription described in the previous paragraph is appropriate for cases in which the destruction of helium nuclei is dominated by photodissociation (the total quantity of injected electromagnetic energy sets the rate of photodissociation). During the hadrodissociation era ($T \gtrsim 0.4$ keV), however, the number of helium nuclei that are broken up instead scales with the number of energetic hadrons that are injected into the early universe. The average number of hadrons that are produced in the jet from a given quark is roughly proportional to $E_q^{0.3}$, and thus the average number of hadrons produced per unit energy is approximately proportional to $E_q^{-0.7}$ [176]. Due to this scaling, as a black hole loses mass and radiates

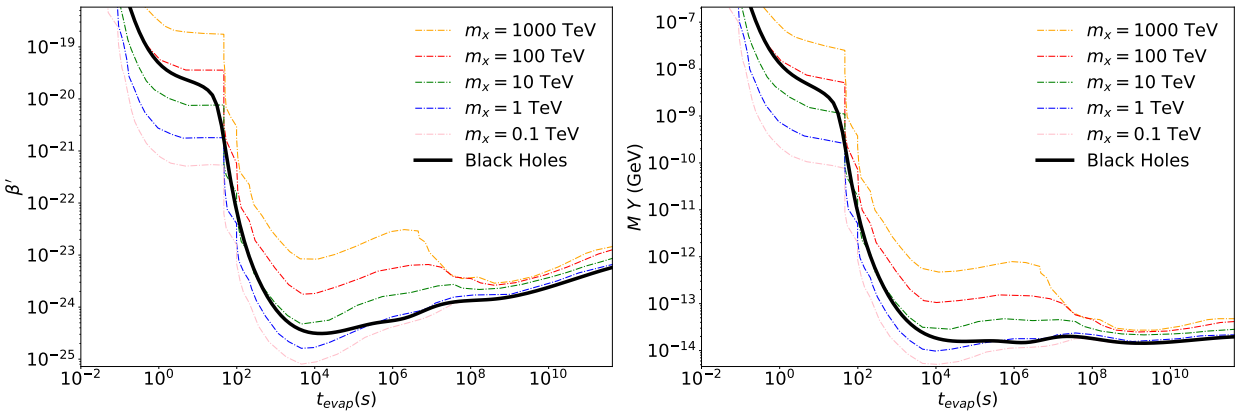

Figure 3.2: Constraints on long-lived particles from Ref. [176], for the case of $X \to q\bar{q}$, for several values of m_X. These constraints are presented both in terms of MY, as used by Kawasaki *et al.*, (right frame) and in terms of β', as used by Carr *et al.* (left frame). The solid black curve in each frame is our constraint on evaporating black holes, based on an interpolation between the long-lived particle constraints, following the relationship between m_X and T_i as described in the text. In this figure, we have assumed that the black holes evaporate only into Standard Model particles.

increasingly high-energy particles, a smaller fraction of the radiated energy takes the form of hadrons. Over the course of a black hole's evaporation, the average hadron is produced by a quark of energy $\langle E_q \rangle \simeq 3.7\,T_i$. Thus in the hadrodissociation era, the spectrum of the emission from an evaporating black hole can be approximately related to that from a (two-body) decaying particle with a mass of $m_X \simeq 7.4\,T_i$. This is illustrated by the fact that purple dashed curve in the left frame of Fig. 3.1 peaks at a lower energy than the solid black curve, by a factor of $7.4/12.6 \approx 0.6$.

A third way in which long-lived particles behave differently from evaporating black holes is in the rates at which they inject energetic particles into the early universe. Unlike a population of decaying particles, the evaporation rate of a black hole increases as it loses mass. In the right frame of Fig. 3.1, we compare the time profiles for these emission mechanisms. Well before the particle's lifetime or black hole's evaporation time, the shape of these time profiles are nearly identical. During the final stages of evaporation and decay, however, they are quite different. In the photodissociation regime, in our translation of the constraints on decaying particles to the case of evaporating black holes, we shift the decaying particle's

lifetime by a factor of 0.79 in order to match the time at which the mean unit of energy was injected into the early universe. In the hadrodissociation era, we instead adjust the lifetime such that the median hadron is injected at the same time. For decaying particles, this occurs at a time, $t_{\rm med} = \ln 2 \times \tau_X = 0.69\,\tau_X$, while for an evaporating black hole, $t_{\rm med} \simeq 0.71\,t_{\rm evap}$. This case, therefore, requires only a small correction factor to translate between the two timescales.

In Fig. 3.2, we plot the constraints on long-lived particles from Ref. [176], for the case of $X \to q\bar{q}$, for several values of m_X. These constraints are shown in terms of the quantities used by Kawasaki *et al.* (right frame), as well as those used by Carr *et al.* (left frame). Also shown as a solid black curve in each frame is our constraint on evaporating black holes, based on an interpolation between the long-lived particle constraints, following the relationship between m_X and T_i as described in the paragraphs above.

The procedure described in this section relies on the validity of two underlying assumptions. First, we have assumed that the overall shape of the spectrum of particles injected into the early universe does not strongly impact the resulting constraints, so long as the average energy is the same. Second, we have assumed that the time profile of the particle injection does not strongly impact the results, so long as the average particle is injected at the same time. We acknowledge that these assumptions are not strictly true, and that these considerations could introduce a systematic error into the constraints that are presented here. In terms of the shape of the spectrum, considering the total integrated emission from a black hole (see Fig. 3.1), approximately 32% of the injected energy is in the form of particles that lie within only a factor of 2 in energy. Similarly, approximately 78% of the injected energy is in particles that lie within an order of magnitude in energy. Combining this with the information shown in Fig. 3.2, we conclude that this could potentially introduce an error in our constraint that is as large as $\sim$30% for $t_{\rm evap} \gtrsim 10^7$ s, and up to a factor of $\sim$2 for shorter-lived black holes. On similar grounds, the more gradual time profile associated with the energy injection from the late stages of long-lived particle decay (see Fig. 3.1) could

potentially impact our constraints. For most values of $t_{\rm evap}$, this effect is quite small. For $t_{\rm evap} \approx 80 - 200\,{\rm s}$, however, the constraints change rapidly with $t_{\rm evap}$, allowing the resulting constraints to be impacted more significantly, potentially shifting the constraints on this part of parameter space by up to a factor of a few to the right (toward larger values of $t_{\rm evap}$).

In Fig. 3.3, we plot our constraints on primordial black holes, assuming that they evaporate entirely into the particle content of the Standard Model (in other words, assuming that there is no particle content beyond the Standard Model). For rapidly evaporating black holes ($t_{\rm evap} \lesssim 80$ s), these constraints are dominated by the measured primordial helium fraction, Y_p, while for longer evaporation times the primordial deuterium abundance provides the most stringent constraint. In each frame, we also plot contours of constant $\Omega_{\rm BH}$, defined as the value of $\rho_{\rm BH}/\rho_{\rm crit}$ that would be the case today if the black holes had not evaporated. In the upper right corner of each frame, we show constraints on evaporating black holes based on derived spectral distortions of the CMB [176, 71, 68, 229, 7, 252, 75]. We note that constraints derived from CMB spectral distortions due to evaporating primordial black holes have recently been revisited in somewhat more detail , resulting in somewhat weaker bounds [7, 70]. Future measurements by PIXIE are expected to improve upon these constraints by a factor of $\sim 10^3$ or more [69, 70]. Primordial black holes with somewhat higher masses, which evaporate slightly after the formation of the CMB, may also be constrained by considering their effects on the CMB power spectrum and the optical depth to reionization [227, 252].

3.3 Constraints on Black Holes in Scenarios Beyond the Standard Model

Unlike particle decays (and most other processes in nature), Hawking evaporation is an entirely gravitational phenomenon, and thus produces all particle species with masses below $\sim T_{\rm BH}$, regardless of their charges or couplings. As a result, the rate at which Hawking evaporation occurs, and the varieties of particles that are produced through this process,

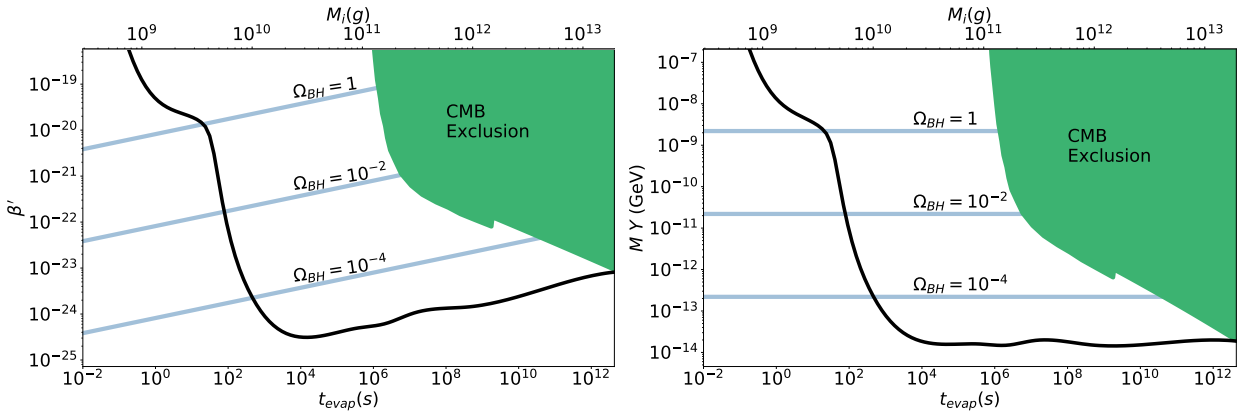

Figure 3.3: Constraints on primordial black holes, assuming that they evaporate entirely into Standard Model particles. Again, we have presented these constraints both in terms of MY, as used by Kawasaki *et al.*, (right frame) and in terms of β', as used by Carr *et al.* (left frame). For rapidly evaporating black holes ($t_{\rm evap} \lesssim 80$ s), the constraints are dominated by the measured primordial helium fraction, Y_p, while for longer evaporation times the primordial deuterium abundance provides the most stringent constraint. In each frame, we also plot contours of constant $\Omega_{\rm BH}$, defined as the value of $\rho_{\rm BH}/\rho_{\rm crit}$ that would be the case today if the black holes had not evaporated. The green regions in the upper-right regions of each frame are excluded by measurements of the CMB (via spectral distortions).

depend on the complete spectrum of particles that exist, including all such species beyond the limits of the Standard Model [152, 151, 203, 204, 207, 211, 17, 137, 123, 148]).

The existence of physics beyond the Standard Model can impact the constraints presented in this paper in three ways. First, additional particle species have the effect of increasing the rate at which black holes evaporate, shifting (and typically weakening) the resulting limits. Second, any particle species without appreciable couplings to the Standard Model will only impact the light element abundances through their influence on the expansion history of the universe. In scenarios that include large numbers of decoupled degrees-of-freedom, the fraction of a black hole's mass that goes into particles that can break up helium and produce deuterium can be significantly reduced, while instead producing substantial abundances of dark matter and/or dark radiation [152, 151, 203, 207, 211, 17, 123, 26]. Third, the presence of black holes and their decoupled evaporation products can impact the expansion history of the early universe, altering the light element abundances that emerge from this era without directly disrupting any nuclei. In the remainder of this section, we will explore several classes

of scenarios beyond the Standard Model and discuss their impact on the resulting constraints on primordial black holes.

A wide range of well-motivated scenarios have been proposed in which the degrees-of-freedom associated with the Standard Model constitute only a small fraction of the particle spectrum of the universe. In particular, self-consistent string compactifications have been shown to generically predict the existence of large numbers of feebly interacting states, including gauge bosons, axion-like particles, and other forms of exotic matter [91, 135, 136, 254, 255, 23, 120, 42, 76, 89, 127, 201, 18, 92]. Frameworks featuring extremely large numbers of massive degrees-of-freedom have also been considered within the context of possible solutions to the electroweak hierarchy problem [107, 108, 22].

Given the gravitational nature of Hawking radiation, as we have discussed before, black holes are expected to radiate all particle species with masses below $\sim T_{\rm BH}$, regardless of their charges or couplings. Thus in scenarios with expansive particle content, black holes could potentially radiate mostly or almost entirely to hidden sector states, which could act as a combination of dark matter and dark radiation [152, 151, 203, 207, 211, 17, 123, 26]. If feebly interacting, such particles would not directly disrupt nuclei during or after BBN, but could still impact the resulting light element abundances through their impact on the universe's expansion rate during this era.

To constrain a black hole population that evaporates dominantly to hidden sector particles, we calculate the combined energy density of the black holes and their evaporation products as a function of redshift, and then use the publicly available program AlterBBN to calculate the resulting light element abundances [20, 21]. In doing so, we follow the procedure described in [34], and use the deuterium-burning rates from [84] and other reaction rates from [19, 93, 276]. These rates correspond to systematic uncertainties of 1.9% on $({\rm D/H})_{\rm p}$ and 0.13% on Y_p, approximately independent of the time evolution of the energy injection [34].

To calculate the evolution of the energy densities in black holes and their evaporation

products, we solve the following system of differential equations:

$$\begin{aligned} \frac{d\rho_{\rm BH}}{dt} &= -3\rho_{\rm BH}H + \rho_{\rm BH}\frac{dM}{dt}\frac{1}{M}, \\ \frac{d\rho_{\rm SM}}{dt} &= -3(w_{\rm SM}+1)\rho_{\rm SM}H - \rho_{\rm BH}\frac{dM}{dt}\frac{(1-f_d)}{M}, \\ \frac{d\rho_d}{dt} &= -3(w_d+1)\rho_d H - \rho_{BH}\frac{dM}{dt}\frac{f_d}{M}, \end{aligned} \tag{3.7}$$

where $\rho_{\rm BH}$, $\rho_{\rm SM}$, ρ_d are the energy densities in black holes, Standard Model fields, and dark matter plus dark radiation, respectively, $H^2 = 8\pi G(\rho_{\rm BH}+\rho_{\rm SM}+\rho_d)/3$ is the rate of Hubble expansion, and dM/dt is the black hole evaporation rate (see Eq. 2.7). The quantities $w_{\rm SM}$ and w_d represent the equation-of-state of the Standard Model and hidden sector particles, with values of 0 and 1/3 corresponding to pure matter and radiation, respectively. Lastly, f_d is the fraction of Hawking radiation that proceeds to hidden sector particles, following from the Standard Model and hidden sector contributions to $g_{\star,H}$. The temperature dependence of $w_{\rm SM}$ is directly related to the values of $g_\star$ and $g_{\star,S}$, where $g_{\star,S}$ is the number of relativistic degrees-of-freedom in entropy [191, 152]). The entropy density can be written in terms of the photon temperature and $g_{\star,S}$.

3.3.1 Light Hidden Sectors

We begin by considering a class of scenarios in which the black holes evaporate almost entirely to light, hidden sector states (corresponding to $w_d = 1/3$ and $f_d \simeq 1$, which implies $g_{\star,H} \gg 10^2$). In Fig. 3.4, we plot the evolution of the energy densities in black holes, Standard Model radiation, matter (including both baryonic and dark matter), and dark radiation, for the case of $t_{\rm evap} = 10\,{\rm s}$ and an initial black hole abundance corresponding to $\Omega_{\rm BH} = 2.6 \times 10^4$ (defined as the value that would be the case today if the black holes had not evaporated). To relate the value of $\Omega_{\rm BH}$ to that of β' or MY, see Eqs. 3.3 and 3.4. In this scenario, the black hole population evaporates almost entirely into dark radiation at $t \sim t_{\rm evap} = 10$. The ultimate energy density of this dark radiation, which we determine

by solving Eq. 3.7, can be written in terms of its contribution to the effective number of neutrino species, $\Delta N_{\rm eff}$ (as evaluated at $t \gg t_{\rm evap}$):

$$\Delta N_{\rm eff} = \frac{\rho_{\rm DR}}{\rho_{\rm R}} \left[N_\nu + \frac{8}{7} \left(\frac{11}{4} \right)^{4/3} \right], \tag{3.8}$$

where $N_\nu = 3.046$, $\rho_{\rm DR}$ is the energy density of dark radiation, and $\rho_{\rm R}$ is the energy density in photons and neutrinos. In the scenario shown in Fig. 3.4, the energy density of dark radiation corresponds to a value of $\Delta N_{\rm eff} = 1.0$. In more generality, the contribution to $\Delta N_{\rm eff}$ from black hole evaporation (in the $w_d = 1/3$ and $f_d \simeq 1$ limit) is given by:

$$\Delta N_{\rm eff} \approx 1.0 \times \left(\frac{\Omega_{\rm BH}}{2.6 \times 10^4} \right) \left(\frac{t_{\rm evap}}{10\,{\rm s}} \right)^{1/2} \left(\frac{10}{g_\star(T_{\rm evap})} \right) \left(\frac{g_{\star,S}(T_{\rm evap})}{10} \right)^{4/3}, \tag{3.9}$$

where $g_\star(T_{\rm evap})$ and $g_{\star,S}(T_{\rm evap})$ are the effective numbers of relativistic degrees-of-freedom and relativistic degrees-of-freedom in entropy, respectively, each evaluated at the temperature at $t_{\rm evap}$.

An observant reader may notice a small bump-like feature in the dark radiation curve near $T \sim 10^{-4}\,{\rm GeV}$ in Fig. 3.4. This feature is due to an entropy dump that occurs among the Standard Model particles in the thermal bath. Whereas the dark radiation energy density simply evolves with four powers of the scale factor, $\rho_{\rm DR} \propto a^{-4}$, the Standard Model "radiation" includes particles with non-negligible mass, and thus the energy density of this component evolves as $\rho_{\rm R} \propto a^{-4}\, g_\star / g_{\star,S}^{4/3}$, where $g_\star$ is effective number of relativistic degrees-of-freedom and $g_{\star,S}$ is the effective number of relativistic degrees-of-freedom in entropy. Essentially, because of the high temperature of the black hole, even the particles with mass that it radiates will contribute to dark radiation, due to their high energy. As the temperature decreases, $g_\star / g_{\star,S}^{4/3}$ increases, reducing the ratio of dark radiation to Standard Model radiation [152]).

In this class of scenarios, the black holes and their dark radiation evaporation products impact the light element abundances almost entirely through their influence on the expansion

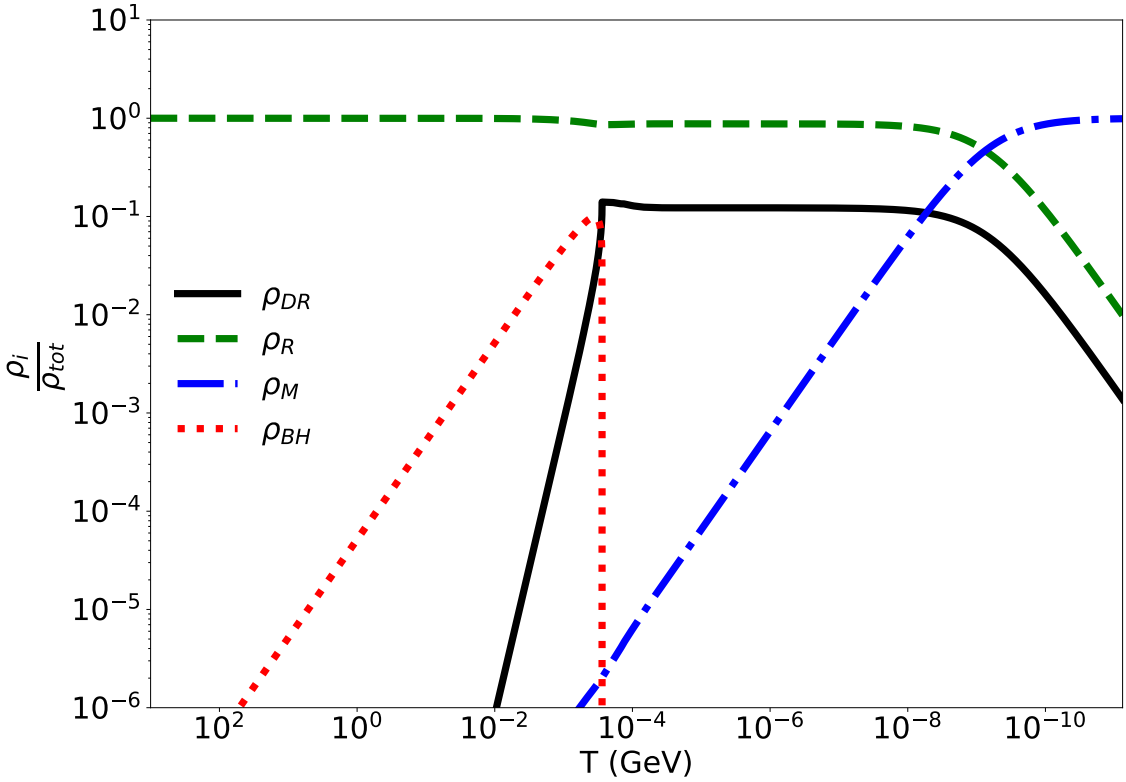

Figure 3.4: The evolution of the energy densities in black holes, Standard Model radiation, matter (including both baryonic and dark matter), and dark radiation, in a scenario in which the black holes evaporate almost entirely to dark radiation (corresponding to $w_d = 1/3$ and $f_d \simeq 1$). We have adopted an evaporation time of $t_{\rm evap} = 10\,{\rm s}$ and an initial black hole abundance corresponding to $\Omega_{\rm BH} = 2.6 \times 10^4$ (defined as the value that would be the case today if the black holes had not evaporated). In this scenario, the final ($t \gg t_{\rm evap}$) energy density of dark radiation corresponds to $\Delta N_{\rm eff} = 1.0$.

history of the early universe. In Fig. 3.5, we illustrate the impact of such black holes on the primordial helium and deuterium abundances, as a function of the final ($t \gg t_{\rm evap}$) energy density in dark radiation, written in terms of $\Delta N_{\rm eff}$. The resulting light element abundances are a function of $t_{\rm evap}$, and those cases with $t_{\rm evap} \lesssim 1\,{\rm s}$ asymptote to the case of a constant $\Delta N_{\rm eff}$, while longer lifetimes impact the expansion history primarily at somewhat later times. For relatively short-lived black holes ($t_{\rm evap} \lesssim 10^2\,{\rm s}$), the measured helium and deuterium abundances rule out scenarios in which the dark radiation contributes more than $\Delta N_{\rm eff} \gtrsim 0.4 - 0.6$ (at the 95% confidence level), similar to the constraints derived from measurements of the CMB [13]. For longer-lived black holes, the constraints on the

resulting contribution to $\Delta N_{\rm eff}$ are weaker (although the constraints derived from the CMB are approximately equally stringent for evaporation times up to $t_{\rm evap} \sim 10^{12}\,{\rm s}$ [43]). Written in terms of β', the measured helium and deuterium abundances provide a constraint of $\beta' \lesssim (0.8 - 6.7) \times 10^{-16} \times (g_{\star,H}/10^5)^{1/6}$ across this entire range of evaporation times considered here. Note that these constraints are much less stringent than those presented in Fig. 3.3 (for the case of Standard Model particle content). From this comparison, we conclude that the constraints based on dark radiation Hawking evaporation products will be more stringent than those resulting from proton-neutron conversion or helium disruption only if $t_{\rm evap} \lesssim 0.1\,{\rm s}$, or if $t_{\rm evap} \lesssim 10^2\,{\rm s}$ and the particle content of the dark sector is very large, corresponding to $g_{\star,H} \gtrsim 10^5$ or greater.

3.3.2 Heavy Hidden Sectors

In this subsection, we will continue to study models which feature a large number of hidden sector states, focusing on Hawking radiation in the form of hidden sector particles with non-negligible masses (which thus contribute to the universe's dark matter abundance). To this end, we follow the same procedure described earlier in this section, but introduce $T_{\rm BH}$-dependent contributions to $g_{\star,H}$, accounting for the inability of a black hole to radiate particles that are much more massive than its temperature.

In the high-temperature limit ($T_{\rm BH} \gg m$), the energy emitted from a black hole in the form of a given particle species is equal to the mass loss rate in Eq. 2.7, for the appropriate choice of $g_{\star,H}$ (for example, $g_{\star,H} = 4$ for a singlet Dirac fermion). Furthermore, the average energy of the radiated particles in this limit is equal to $\langle E \rangle = 3.15\,T_{\rm BH}$ for the case of a fermion, and $\langle E \rangle = 2.70\,T_{\rm BH}$ for a boson [191]. For lower values of $T_{\rm BH}$, the total energy and the total number of particles radiated are each suppressed. This suppression can be quantified by the following expressions for the total energy, and the total number of particles, radiated

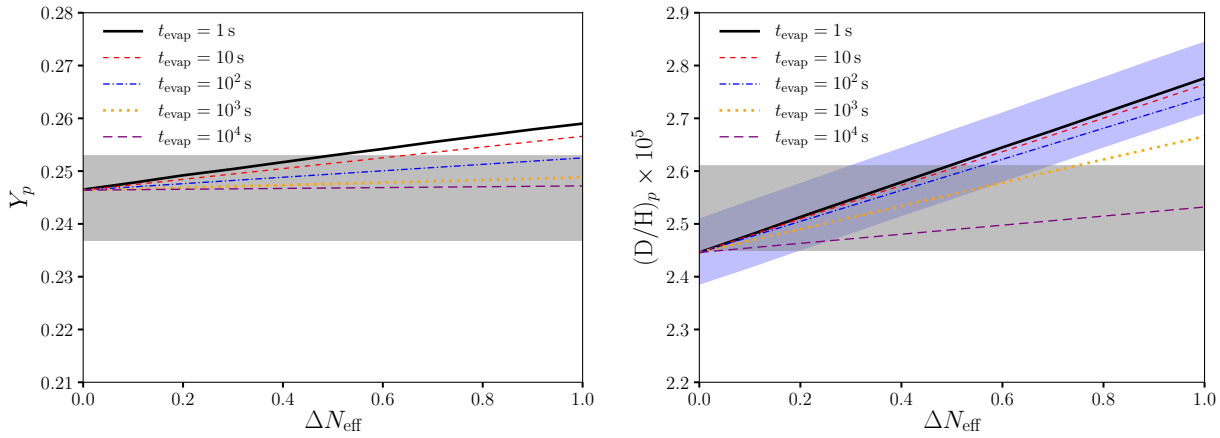

Figure 3.5: The impact on the primordial helium (left) and deuterium (right) abundances of black holes that evaporate overwhelmingly to dark radiation ($f_d \simeq 1$, $w_d \simeq 1/3$). These results are given in terms of the final ($t \gg t_{\rm evap}$) energy density of dark radiation, in terms of $\Delta N_{\rm eff}$. The grey bands represent the measured values (at 2σ), while the blue band in the right frame denotes the systematic uncertainty associated with the nuclear reaction rates (as described in Sec. 3.3). Note that this systematic uncertainty applies to all of the curves shown in the right frame (but for clarity is plotted only for the $t_{\rm evap} = 1\,{\rm s}$ case). For relatively short-lived black holes ($t_{\rm evap} \lesssim 10^2\,{\rm s}$), the measured helium and deuterium abundances rule out scenarios in which this component of dark radiation contributes more than $\Delta N_{\rm eff} \gtrsim 0.4 - 0.6$.

per unit time from a black hole in the form of particles of mass, m:

$$F \propto \int_m^\infty \frac{(E^2 - m^2)^{1/2}}{e^{m/T_{\rm BH}} \pm 1} E^2 dE \qquad (3.10)$$
$$N \propto \int_m^\infty \frac{(E^2 - m^2)^{1/2}}{e^{m/T_{\rm BH}} \pm 1} E dE,$$

where the $\pm$ in the denominators apply to the case of fermions (+) and bosons (-), respectively.

In practice, increasing the mass of the radiated hidden sector particles has the effect of delaying the ability of a given black hole to produce significant quantities of that particle species. In Figs. 3.6 and 3.7, we plot the evolution of the energy densities in Standard Model radiation, baryons, black holes, and dark matter, in a scenario in which the black holes evaporate almost entirely to dark matter. More specifically, we adopt a total value

of $g_{\star,H} = 10^6$ in the $T_{\rm BH} \gg m_{\rm DM}$ limit (of which all but $\simeq 108$ corresponds to Hawking radiation into dark matter particles with a common mass of $m_{\rm DM}$). In these two figures, we adopt $t_{\rm evap} = 10$ and 1000 seconds, respectively, and in each frame we have selected a different value of $m_{\rm DM}$. Although we consider only one value of $m_{\rm DM}$ at a time, one could also consider scenarios in which there is a spectrum of heavy hidden sector states. In each case, we have set the the initial black hole abundance such that the Hawking radiation produces a final dark matter abundance that is equal to the total measured dark matter density. In these figures, we have plotted separately the total energy density of dark matter, $\rho_{\rm DM}$, and the number density of these particles multiplied by their mass, $n_{\rm DM}\, m_{\rm DM}$. This distinction can be non-negligible, as the dark matter particles are not necessarily non-relativistic when they are initially radiated from a black hole. This is most noticeable in the case of $m_{\rm DM} = 1$ TeV, which is not much larger than the initial temperature of the black holes under consideration.

In Fig. 3.8, we show how these scenarios impact the primordial helium and deuterium abundances, focusing on the effects of the black holes and their evaporation products on the expansion rate. Although we show these results in terms of $m_{\rm DM}$, they can be directly translated into values of the black hole abundance, β' or MY. In the $t_{\rm evap} = 10\,{\rm s}$ case, the expansion rate can be significantly altered during the time of proton-neutron freeze-out, enhancing the neutron abundance at early times and leading to constraints based on the measured helium mass fraction, Y_p. For this lifetime, the measured value of Y_p allows us to constrain $\beta' \lesssim 2 \times 10^{-15}$. In the $t_{\rm evap} = 10^3\,{\rm s}$ case, the measured deuterium abundance instead provides the most stringent constraint, allowing us to constrain $\beta' \lesssim 5 \times 10^{-16}$. Additionally in this case, if the black hole abundance is large, the baryon abundance will be enhanced at early times (as can be seen in the lower right frame of Fig. 3.7), impacting the rates of fusion and potentially ruining the successful prediction of Y_p.

When comparing these results to those presented in Fig. 3.3, we reach the following conclusions. First, the black holes and their dark matter Hawking evaporation products only observably impact the expansion history of the universe in regions of parameter space

that are already ruled out as a consequence of Hawking evaporation into Standard Model particles. It is entirely possible, however, that such black holes could generate the entirety of the observed dark matter abundance. For the case of $t_{\rm evap} \sim 10\,{\rm s}$ with $g_{\star,H} \gg 10^2$, this can be self-consistently attained so long as $m_{\rm DM} \lesssim (10^6\,{\rm GeV}) \times (g_{\star,H}/10^4)$. For $g_{\star,H} \sim 10^2$, we instead find that we must require $m_{\rm DM} \lesssim (10^6\,{\rm GeV})/g_{\star,H}^{\rm DM}$ in order to obtain the observed dark matter abundance, where $g_{\star,H}^{\rm DM}$ is the contribution of the dark matter species to $g_{\star,H}$. For heavier dark matter candidates, it is not possible to produce the total measured abundance without violating the constraints presented in this chapter (unless $t_{\rm evap} \lesssim 10\,{\rm s}$). In the case of $t_{\rm evap} \sim 10^3\,{\rm s}$, these requirements are more stringent. In particular, to obtain the full measured dark matter abundance from such black holes, we must require $m_{\rm DM} \lesssim (10\,{\rm GeV}) \times (g_{\star,H}/10^4)$ (for $g_{\star,H} \gg 10^2$) or $m_{\rm DM} \lesssim (10\,{\rm GeV})/g_{\star,H}^{\rm DM}$ (for $g_{\star,H} \sim 10^2$).

Compared to dark matter candidates that are produced as a WIMP-like thermal relic, particles generated through Hawking radiation are much more energetic, raising the question of whether they would behave as cold dark matter (as opposed to warm or hot dark matter) [26]. In the $m_{\rm DM} \gg T_i$ limit, we find the average energy of a radiated dark matter particle by integrating from the time at which $T_{\rm BH} \sim m_{\rm DM}$ to the end of a black hole's evaporation, resulting in $\langle E_{\rm DM} \rangle \sim 6\,m_{\rm DM}$. By then relating $\langle E_{\rm DM} \rangle \sim 3T_{\rm DM}$, we can estimate the approximate free-streaming length [191]:

$$\begin{aligned} \lambda_{\rm fs} &= \int_0^{t_{\rm nr}} \frac{dt}{a(t)} \approx 1\,{\rm Mpc} \times \left(\frac{T_{\rm DM}}{T}\right) \left(\frac{0.3\,{\rm keV}}{m_{\rm DM}}\right) \\ &\sim 6 \times 10^{-4}\,{\rm Mpc} \times \left(\frac{t_{\rm evap}}{\rm s}\right)^{0.5}. \end{aligned} \tag{3.11}$$

From this estimate, it follows that any stable, feebly-interacting particles heavier than T_i that are generated via Hawking radiation will act as cold dark matter ($\lambda_{\rm fs} \lesssim {\rm Mpc}$) so long as $t_{\rm evap} \lesssim 3 \times 10^6\,{\rm s}$.

Considering next the case of $m_{\rm DM} \ll T_i$, we estimate $T_{\rm DM} \sim T_i$, which leads to the

following:

$$\begin{aligned} \lambda_{\rm fs} &= \int_0^{t_{\rm nr}} \frac{dt}{a(t)} \approx 1\,{\rm Mpc} \times \left(\frac{T_{\rm DM}}{T}\right)\left(\frac{0.3\,{\rm keV}}{m_{\rm DM}}\right) \\ &\sim 3 \times 10^{-2}\,{\rm Mpc} \times \left(\frac{T_i/m_{\rm DM}}{100}\right)\left(\frac{t_{\rm evap}}{\rm s}\right)^{0.5}. \end{aligned} \tag{3.12}$$

Thus any stable, feebly-interacting particles lighter than T_i that are generated via Hawking radiation will act as cold dark matter ($\lambda_{\rm fs} \lesssim$ Mpc) so long as $t_{\rm evap} \lesssim 10^7\,{\rm s} \times (m_{\rm DM}/T_i)^2$.

To summarize the results of this subsection, for black holes with $t_{\rm evap} \sim 10\,{\rm s}$, there exist a wide range of scenarios in which the dark matter could be produced through Hawking evaporation, especially if $m_{\rm DM} \sim {\rm GeV} - {\rm PeV}$ (a wider range of $m_{\rm DM}$ are also possible, but only if $g_{\star,H}$ is very large). For black holes with $t_{\rm evap} \sim 10^3\,{\rm s}$, the range of such possibilities are more restricted, but are viable if $m_{\rm DM} \sim 10\,{\rm GeV}$ (or for a wider range of $m_{\rm DM}$ if $g_{\star,H}$ is very large).

3.3.3 TeV-Scale Supersymmetry

As another example, we will consider a scenario in which most of the superpartners of the Standard Model (in particular, the squarks and gluinos) are not much heavier than the current constraints placed by the Large Hadron Collider (LHC), $m_{\rm SUSY} \sim 2$ TeV [1, 248]. In this case, black holes heavier than $M \sim 5 \times 10^9$ g (corresponding to $T_{\rm BH} \sim 2$ TeV) still evaporate almost entirely into Standard Model particles. But as the mass of a black hole falls below this threshold, it will begin to also evaporate into the full spectrum of superpartner particles. Numerically, this has the effect of changing $g_{\star,H}$ from Standard Model value of 108, to approximately 316 (for the case of the Minimal Supersymmetric Standard Model, MSSM). By supersymmetrizing the Standard Model, the value of $g_{\star,H}$ does not merely double, but is further enhanced as a result of the lower spins of most of the sparticle degrees-of-freedom. So whereas a black hole with a mass of $M \sim 5 \times 10^9$ g will evaporate in $t_{\rm evap} \sim 50$ s, assuming Standard Model particle content, this instead occurs in $t_{\rm evap} \sim 17$ s in the presence of low-

energy supersymmetry. This has the effect of relaxing the constraints on black holes in this mass range by a factor of $\sim 2-3$.

Additionally, if R-parity is conserved, each superpartner radiated from a black hole will ultimately decay to a lightest supersymmetric particle (LSP). If the LSP is relatively heavy, such as a neutralino, it could serve as a candidate for dark matter. On the other hand, a very light LSP (perhaps in the form of a gravitino or axino) could act as dark radiation in this context. If $m_{\rm LSP} \ll m_{\rm SUSY}$, this will have little impact on the resulting constraints. If the sparticle spectrum is highly compressed ($m_{\rm LSP} \sim m_{\rm SUSY}$), however, the majority of the energy in the Hawking radiation will be in the form of LSP dark matter, reducing the potential to break up helium (and produce deuterium) by a factor of up to $\sim 2-3$.

The abundance of LSP dark matter that is generated through Hawking radiation in this scenario is given by:

$$\begin{aligned} \Omega_{\rm LSP} &\simeq \Omega_{\rm BH} \times f_{\rm SUSY} \times \frac{m_{\rm LSP}}{m_{\rm SUSY}} \\ &\sim \frac{\beta'}{2.2 \times 10^{-20}} \left(\frac{10^{10}\,{\rm g}}{M}\right)^{0.5} \times f_{\rm SUSY} \times \frac{m_{\rm LSP}}{m_{\rm SUSY}}, \end{aligned} \tag{3.13}$$

where $\Omega_{\rm BH}$ is defined as the value of $\rho_{\rm BH}/\rho_{\rm crit}$ that would be the case today if the black holes had not evaporated (see Eq. 3.4), and $f_{\rm SUSY}$ is the fraction of energy in Hawking radiation that is in the form of superparticles. For $M \lesssim 5 \times 10^9\,{\rm g} \times (2\,{\rm TeV}/m_{\rm SUSY})$, the black hole can efficiently radiate superpartners throughout its evaporation, and this fraction is simply given by: $f_{\rm SUSY} \sim g_{\star,H}^{\rm SUSY}/g_{\star,H}$ where $g_{\star,H}^{\rm SUSY} \simeq 208$. For more massive black holes,

$$f_{\rm SUSY} \sim \left(\frac{5 \times 10^9\,{\rm g}}{M}\right) \left(\frac{2\,{\rm TeV}}{m_{\rm SUSY}}\right) \left(\frac{g_{\star,H}^{\rm SUSY}}{g_{\star,H}}\right). \tag{3.14}$$

For example, for $m_{\rm SUSY} = 2\,{\rm TeV}$, $m_{\rm LSP} = 1\,{\rm TeV}$, and $M = 5 \times 10^9\,{\rm g}$, the value of $\Omega_{\rm LSP}$ is equal to the measured dark matter density for an initial black hole abundance of $\beta' \simeq 10^{-20}$. Given the more rapid rate of evaporation due to superpartner production, such a scenario is

compatible with the measured light element abundances.

Phenomenology similar to that described in this subsection could also arise within the context of other weak-scale extensions of the Standard Model, such as mirror models or Twin Higgs models. Such models are motivated by the little hierarchy problem [66, 65], and generally include a copy of some or all of the Standard Model particle content, with masses rescaled by the larger vacuum expectation value of the mirror Higgs boson. In these models, the lightest mirror-charged state is typically stable, opening up the possibility that a stable population of such particles could be generated through the process of Hawking evaporation [64, 65].

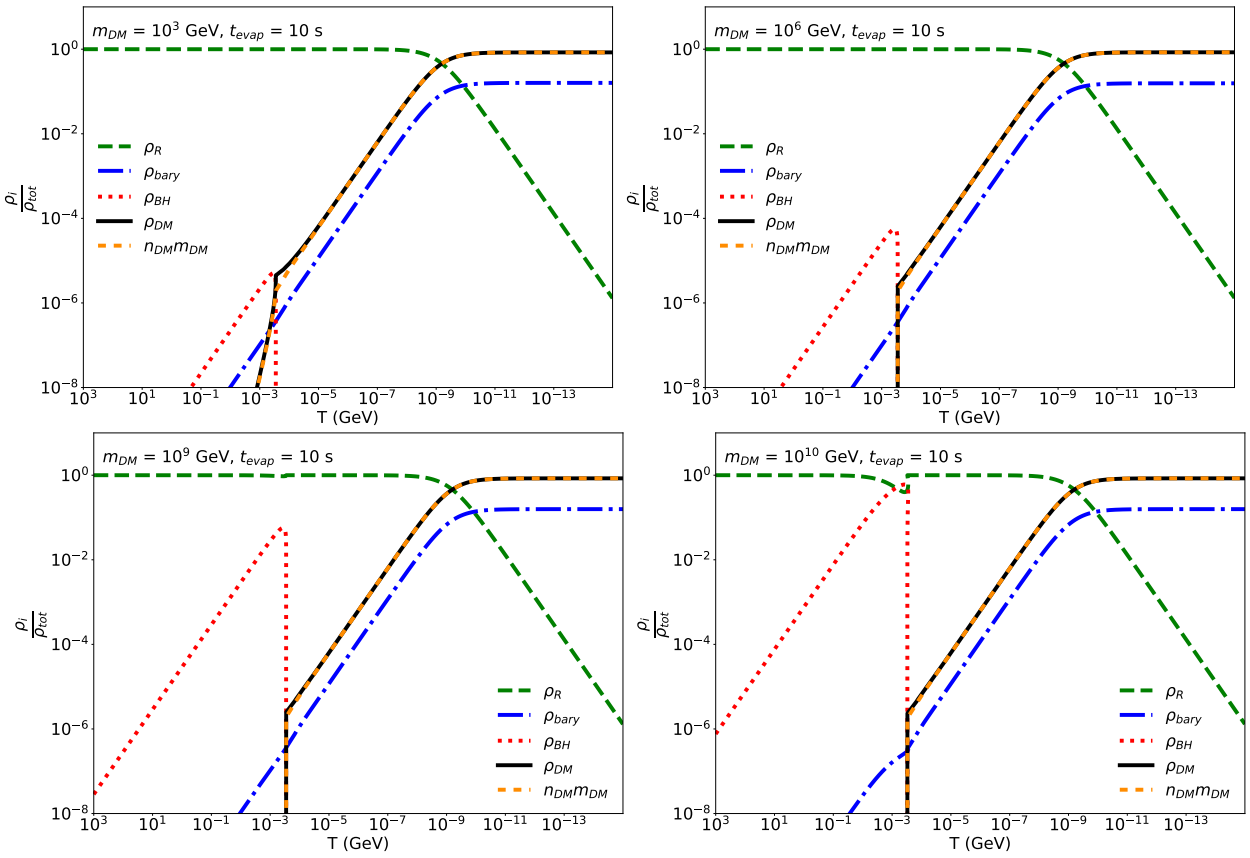

Figure 3.6: The evolution of the energy densities in Standard Model radiation, baryons, black holes, and dark matter, in a scenario in which the black holes evaporate with a lifetime of 10 seconds almost entirely to dark matter particles (corresponding to $g_{\star,H} = 10^6$ for $T_{\rm BH} \gg m_{\rm DM}$). In each frame, the initial black hole abundance was chosen such that the Hawking radiation produces the entirety of the measured dark matter density. This corresponds to $\Omega_{\rm BH} = 6.8$ (upper left), 88 (upper right), 8.6×10^4 (lower left) and 8.6×10^5 (lower right). As we have throughout this paper, we define $\Omega_{\rm BH}$ as the value that would be the case today if the black holes had not evaporated.

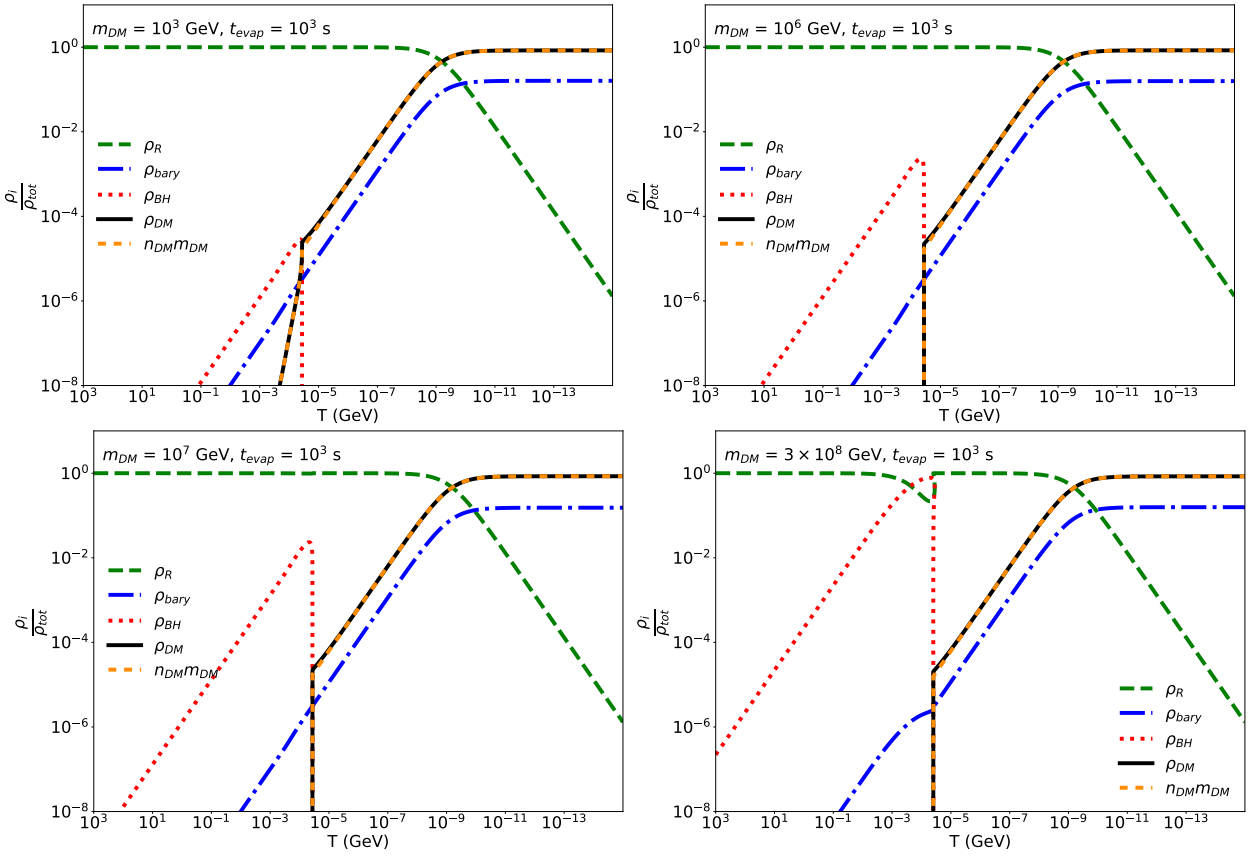

Figure 3.7: The evolution of the energy densities in Standard Model radiation, baryons, black holes, and dark matter, in a scenario in which the black holes evaporate with a lifetime of 1000 seconds almost entirely to dark matter particles (corresponding to $g_{\star,H} = 10^6$ for $T_{\rm BH} \gg m_{\rm DM}$). In each frame, the initial black hole abundance was chosen such that the Hawking radiation produces the entirety of the measured dark matter density. This corresponds to $\Omega_{\rm BH} = 3.7$ (upper left), 4.0×10^2 (upper right), 4.0×10^3 (lower left) and 1.2×10^5 (lower right). As we have throughout this paper, we define $\Omega_{\rm BH}$ as the value that would be the case today if the black holes had not evaporated.

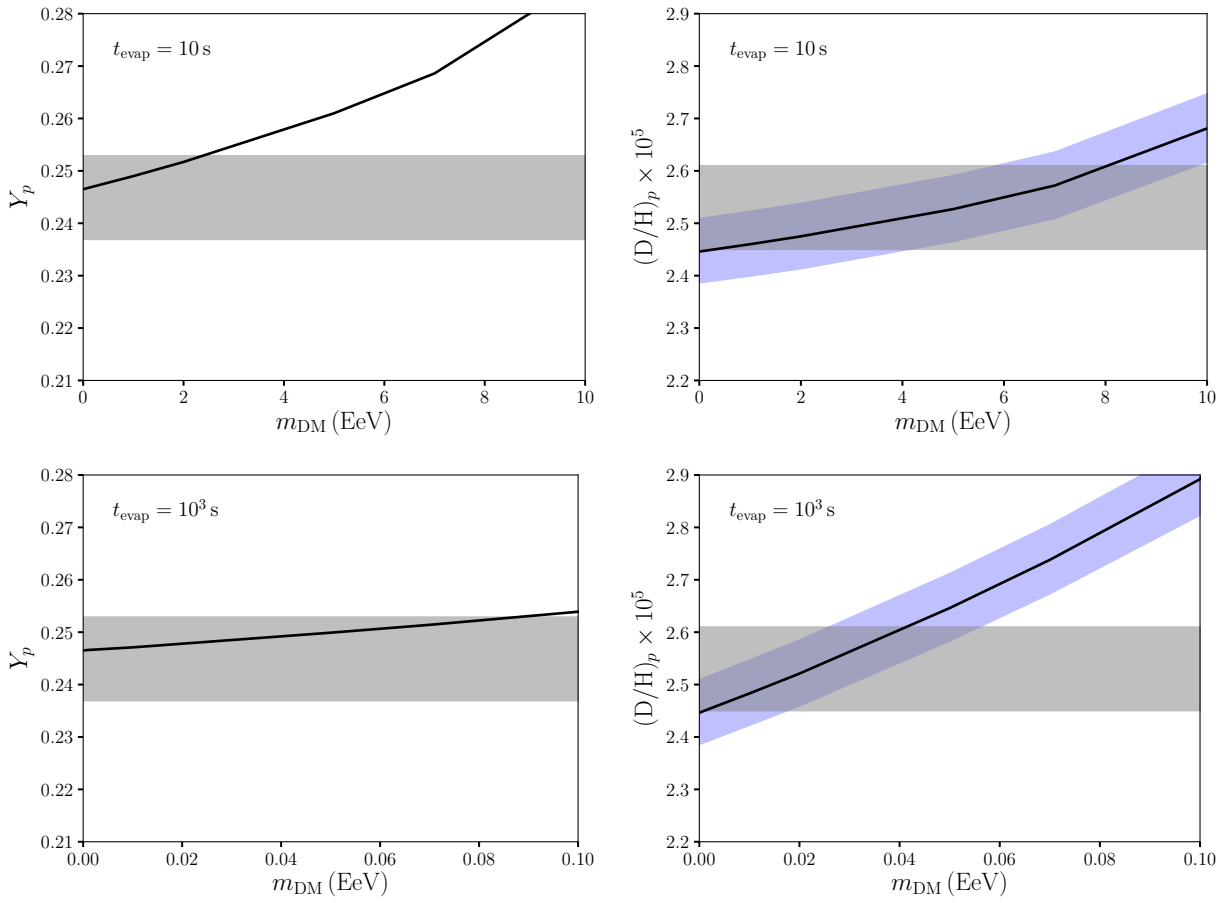

Figure 3.8: The impact on the primordial helium (left) and deuterium (right) abundances of black holes that evaporate largely to dark matter (corresponding to $g_{\star,H} = 10^6$ for $T_{\rm BH} \gg m_{\rm DM}$). These results are given in terms of the dark matter particles' mass $m_{\rm DM}$, and in each case, the initial black hole abundance was chosen such that the Hawking radiation produces the entirety of the measured dark matter density. The grey bands represent the measured values (at 2σ), while the blue band in the right frame denotes the systematic uncertainty associated with the nuclear reaction rates (as described in Sec. 3.3).

CHAPTER 4

PRIMORDIAL BLACK HOLES IN THE GALACTIC CENTER

4.1 The Sensitivity of Future Gamma-ray Telescopes to Primordial Black Holes

It has long been appreciated that black holes radiate an approximately thermal spectrum of particles via Hawking radiation, as has been discussed extensively in this thesis. Searches for Hawking radiation in the form of gamma rays and positrons have been used to derive powerful constraints on primordial black holes [141, 126, 181, 87, 198, 41, 97]. More specifically, local measurements of the cosmic-ray electron (plus positron) flux by the Voyager 1 satellite currently provide the strongest constraint on black holes lighter than $m_{\rm BH} \sim (1-2) \times 10^{16}\,{\rm g}$, while MeV-scale gamma-ray observations of the Inner Galaxy by COMPTEL and INTEGRAL provide the leading constraints in the mass range of $m_{\rm BH} \sim 10^{16} - 10^{17}\,{\rm g}$ [41, 181, 87, 198, 87]. While GeV-scale telescopes such as EGRET and Fermi can be used to search for the Hawking radiation from lower mass black holes, the constraints provided by such instruments are less stringent than those derived from Voyager 1's measurements of the local electron-positron flux [202, 10, 41]. Constraints from the global 21-cm signal have also been explored, as well as constraints that will be provided by future CMB anisotrophy probes [49, 48].

While the data provided by the COMPTEL and INTEGRAL satellites have made it possible to derive interesting bounds on the abundance of primordial black holes, the sensitivity of such instruments is limited. Fortunately, a new generation of satellite-based MeV-scale gamma-ray telescopes have been proposed, including the designs currently known as AMEGO (All-sky Medium Energy Gamma-ray Observatory) and e-ASTROGAM ("enhanced ASTROGAM") [253, 40, 51, 101]. Such instruments would be capable of detecting photons through both pair conversion (as Fermi, for example, does) and Compton scattering, enabling them to have much greater sensitivity to photons in the 1-100 MeV range. While COMPTEL and INTEGRAL are able to detect MeV-scale photons, the projected sensitivity of AMEGO and e-ASTROGAM to such gamma rays exceeds that of these earlier

instruments by roughly two orders of magnitude.

Here, we will consider the sensitivity of next-generation MeV-scale gamma-ray telescopes to the Hawking radiation from a population of primordial black holes [87]). To this end, we have calculated the energy spectrum and angular distribution of the Hawking radiation from a $40^\circ \times 40^\circ$ region around the Galactic Center, including contributions from inflight electron-positron annihilation and final state radiation. We then performed an analysis of simulated e-ASTROGAM data, utilizing spatial templates, allowing us to fully exploit the morphological and spectral information provided by such an instrument (we expect to obtain similar sensitivity for an instrument such as AMEGO). Through this analysis, we have been able to derive projected constraints on the abundance of primordial black holes in the mass range of $m_{\rm BH} \sim (0.3 - 30) \times 10^{16}\,{\rm g}$, and for a wide range of halo profiles. For black holes in the mass range of $m_{\rm BH} \sim 10^{16} - 10^{17}\,{\rm g}$, we find that such a telescope would be able to improve upon current constraints by approximately a factor of ~ 100, potentially excluding scenarios in which the black holes make up more than $f_{\rm BH} \sim 10^{-4} - 10^{-6}$ of the total dark matter density. We also consider scenarios in which primordial black holes are responsible for the excess of 511 keV photons observed from the Inner Galaxy, as reported by the INTEGRAL Collaboration [181, 73, 165, 230]. We find that in such a scenario, an instrument such as AMEGO or e-ASTROGAM would not only be able to detect the gamma rays radiated from the black holes, but would be able to quite precisely measure the abundance and mass distribution of the responsible black hole population.

4.1.1 Hawking Radiation From Primordial Black Holes

Throughout this study, we will focus our attention on the case of Schwarzschild black holes, and not Kerr black holes, as discussed in Chapter 2. The temperature and Schwarzschild radius of a black hole are related to its mass, as described in equation 2.6. Due to the gravitational nature of Hawking evaporation, the radiation from a black hole includes all species of particles that are lighter than or comparable in mass to the black hole's temperature,

leading to the rate of mass loss as described in equation 2.7. Integrating this expression, we find that a black hole with an initial mass of $m_{\rm BH} \sim 4 \times 10^{14}\,{\rm g}$ will evaporate in a length of time equal to the age of the universe.

The spectrum of Hawking radiation from an individual black hole can be written as follows [219]:

$$\frac{dN^{\rm dir}}{dE}(m_{\rm BH}, E) = \frac{1}{2\pi^2} \frac{E^2 \sigma(m_{\rm BH}, E)}{e^{E/T} \pm 1}, \tag{4.1}$$

where for fermions (bosons), the sign in the denominator is positive (negative). The absorption cross section, σ, also depends on the spin of the particles being radiated. In the $E \gg T$ limit, the absorption cross section approaches $\sigma \simeq 27\pi m_{\rm BH}^2/M_{\rm Pl}^4$, regardless of the particle species. At lower energies, σ is a function of energy, and depends on the particle species under consideration. Throughout our calculations, we implement the full spectrum of Hawking radiation from an individual black hole [219].

Black holes can produce gamma rays not only as the direct products of Hawking evaporation (as described by Eq. 4.1), but also through the inflight annihilation of positrons, and as final state radiation. The spectrum of gamma rays from the inflight annihilation of positrons is given by [32, 33]

$$\begin{aligned} \frac{dN_\gamma^{\rm IA}}{dE_\gamma} = \frac{\pi \alpha^2 n_H}{m_e} \int_{m_e}^{\infty} dE_{e^+} \frac{dN_{e^+}}{dE_{e^+}} \int_{E_{\rm min}}^{E_{e^+}} \frac{dE}{dE/dx} \frac{P_{E_{e^+} \to E}}{(E^2 - m_e^2)} \\ \times \left(-2 - \frac{(E+m_e)(m_e^2(E+m_e) + E_\gamma^2(E+3m_e) - E_\gamma(E+m_e)(E+3m_e))}{E_\gamma^2 (E - E_\gamma + m_e)^2} \right), \end{aligned} \tag{4.2}$$

where $\alpha \approx 1/137.037$ is the fine structure constant, n_H is the number density of neutral hydrogen atoms, and dN_{e^+}/dE_{e^+} is the spectrum of positrons radiated from the black hole, as described by Eq. 4.1. The energy loss rate for a positron due to ionization in the presence of neutral hydrogen, dE/dx, is given by the standard Bethe-Bloch formula. Note that since dE/dx is proportional to n_H, the flux of gamma rays from inflight annihilation is not sensitive

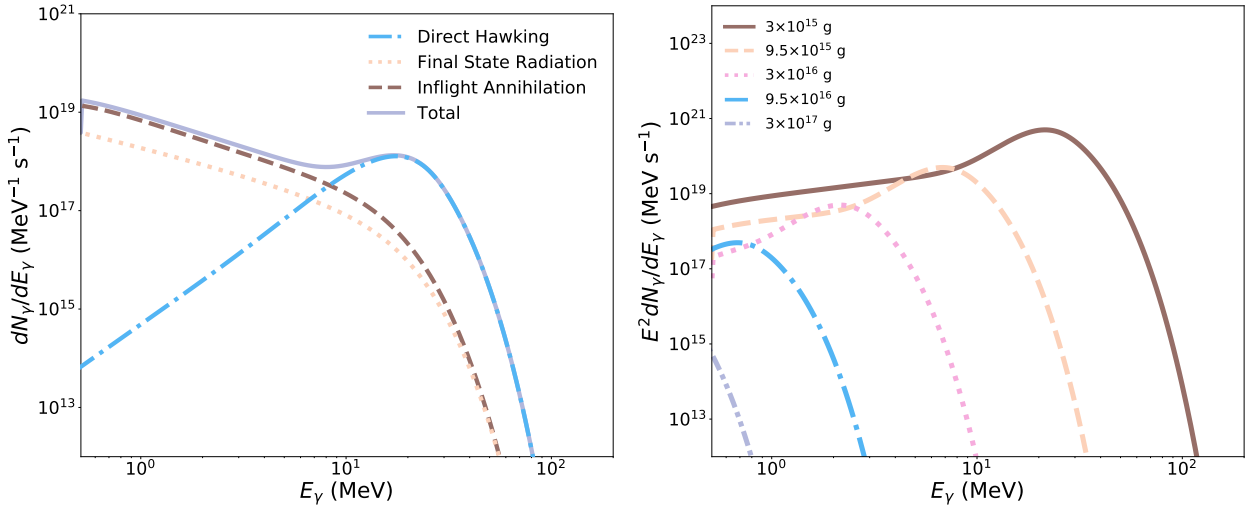

Figure 4.1: Left: The gamma-ray spectrum from a black hole with a mass of $m_{\rm BH} = 3 \times 10^{15}\,{\rm g}$, including the contributions from direct Hawking radiation, final state radiation, and the inflight annihilation of positrons. Right: The total gamma-ray spectrum from black holes for several choices of $m_{\rm BH}$.

to the density of gas.

The probability that a positron with an initial energy of E_{e^+} will survive until its energy has been reduced to E is given by

$$P_{E_{e^+} \to E} = \exp\left(- n_H \int_E^{E_{e^+}} \sigma_{\rm ann}(E') \frac{dE'}{|dE'/dx|} \right), \tag{4.3}$$

where $\sigma_{\rm ann}$ is the cross section for a positron to annihilate with an electron at rest. For positrons less energetic than a few MeV, $P_{E_{e^+} \to m_e}$ always falls in the range between 0.95 and 1.0, reflecting the fact that only a few percent of the positrons annihilate before becoming non-relativistic.

Lastly, we also include in our calculations the final state radiation from any electrons and positrons that are produced through the process of Hawking evaporation. This leads to the following contribution to the gamma-ray spectrum:

$$\frac{dN_\gamma^{\rm FSR}}{dE_\gamma} = \frac{\alpha}{2\pi} \int dE_e \frac{dN_e}{dE_e} \left(\frac{2}{E_\gamma} + \frac{E_\gamma}{E_e^2} - \frac{2}{E_e} \right) \left[\ln\left(\frac{2E_e(E_e - E_\gamma)}{m_e^2} \right) - 1 \right], \tag{4.4}$$

where dN_e/dE_e is the spectrum of electrons and positrons radiated from the black hole.

In Fig. 4.1, we show the spectrum of the gamma-ray emission from an individual black hole for several choices of $m_{\rm BH}$, and including contributions from direct Hawking radiation, final state radiation, and inflight annihilation. At the highest energies, direct Hawking radiation dominates this emission. In contrast, inflight annihilation provides the largest contribution at lower energies.

Putting these contributions together, we are now in a position to calculate the total flux of gamma-rays from a population of primordial black holes. Averaged over a solid angle, $\Delta\Omega$, this flux is given by:

$$\begin{aligned} F_\gamma(\Delta\Omega) &= \frac{dN_\gamma^{\rm tot}}{dE_\gamma}\frac{1}{4\pi}\int_{\Delta\Omega}\int_{los} n_{\rm BH}(l,\Omega)\, dl\, d\Omega, \\ &= \frac{dN_\gamma^{\rm tot}}{dE_\gamma}\frac{f_{\rm BH}}{4\pi m_{\rm BH}}\int_{\Delta\Omega}\int_{los} \rho_{\rm DM}(l,\Omega)\, dl\, d\Omega, \end{aligned} \tag{4.5}$$

where

$$\frac{dN_\gamma^{\rm tot}}{dE_\gamma} = \frac{dN_\gamma^{\rm dir}}{dE_\gamma} + \frac{dN_\gamma^{\rm IA}}{dE_\gamma} + \frac{dN_\gamma^{\rm FSR}}{dE_\gamma}, \tag{4.6}$$

$n_{\rm BH}$ is the number density of black holes, $f_{\rm BH}$ is the fraction of the dark matter that consists of black holes, and the integrals are performed over the line-of-sight and the solid angle observed. For the spatial distribution of primordial black holes in the Milky Way, we adopt a generalized Navarro-Frenk-White (NFW) halo profile [212, 213]:

$$n_{\rm BH} = \frac{n_0}{(r/R_s)^\gamma\,[1+(r/R_s)]^{3-\gamma}}, \tag{4.7}$$

where r is the distance from the Galactic Center. In our calculations, we adopt a scale radius of $R_s = 20$ kpc and have normalized n_0 such that the local density of black holes (at $r = 8.25$ kpc) is $n_{\rm BH} = 0.4\,{\rm GeV/cm}^3 \times f_{\rm BH}/m_{\rm BH}$ [233]. We take the inner slope of this profile, γ, to be a free parameter.

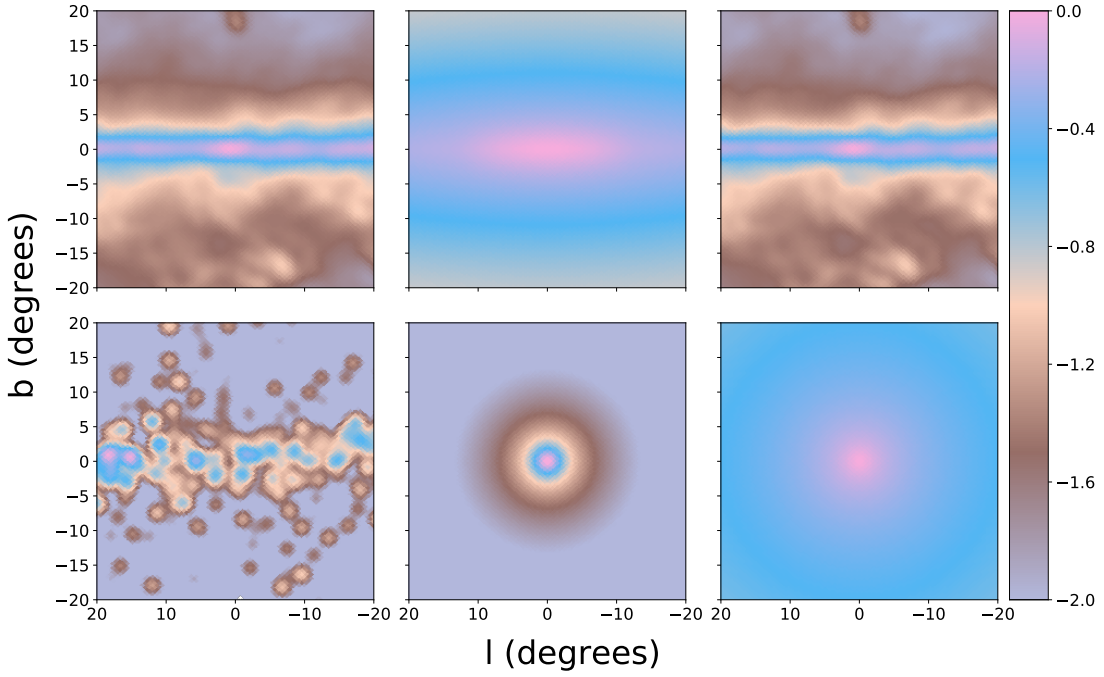

Figure 4.2: The spatial templates used in our analysis evaluated at 10 MeV after convolving with the point spread function of e-ASTROGAM. In the upper row, the templates correspond to the emission from pion production (left), inverse Compton scattering (center), and bremsstrahlung (right), as generated using the publicly available code GALPROP [264, 132]. In the lower row, the templates correspond to the gamma-ray point sources contained within the Fermi 4FGL-DR2 catalog (left), the emission associated with the Galactic Center gamma-ray excess (center), and the emission from primordial black holes (with $\gamma = 1.4$, $m_{\rm BH} = 2 \times 10^{16}\,{\rm g}$ and $f_{\rm BH} = 10^{-4}$). The scale used is logarithmic, and the brightest point in each frame is normalized to unity.

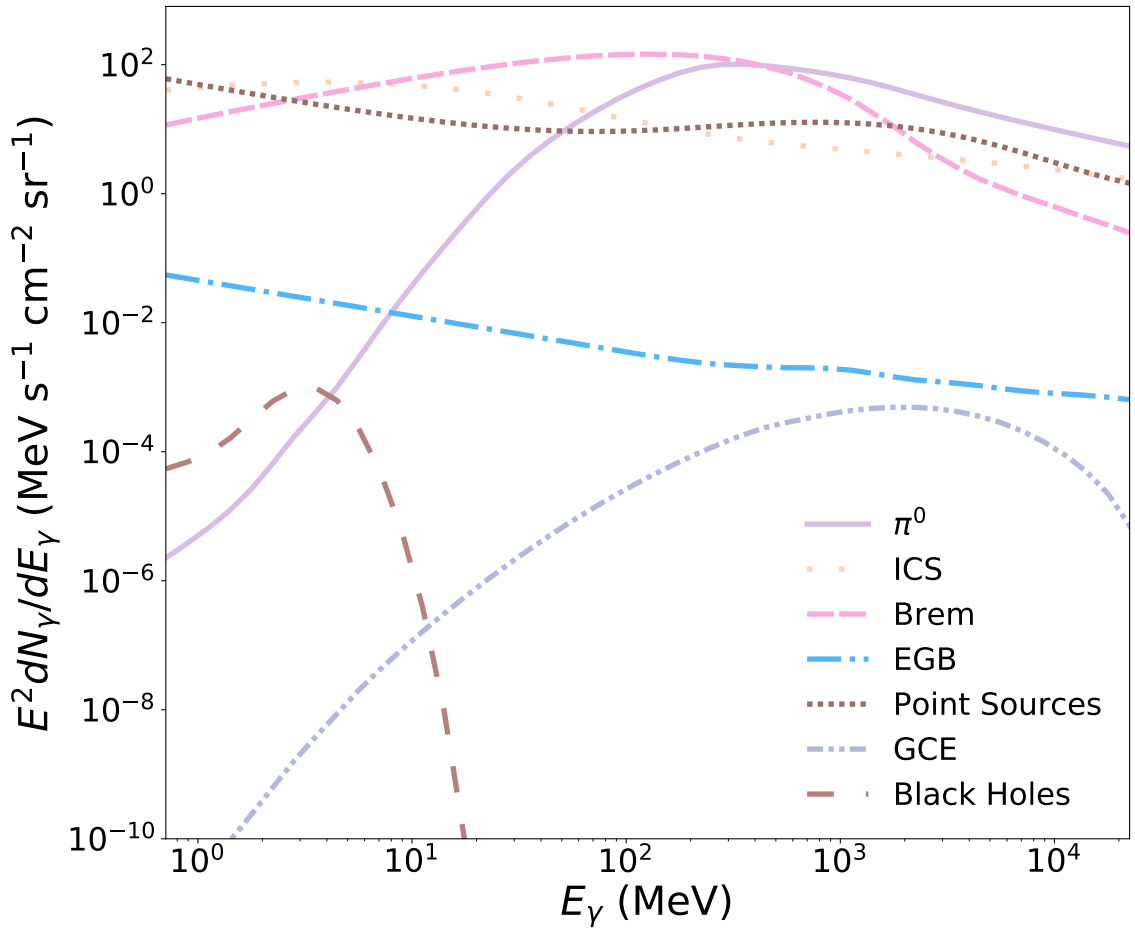

Figure 4.3: The gamma-ray spectra of the various components of our background model, and from primordial black holes (for the case of $m_{\rm BH} = 2 \times 10^{16}\,{\rm g}$, $f_{\rm BH} = 4 \times 10^{-4}$ and $\gamma = 1$). Each curve is averaged over the $40^\circ \times 40^\circ$ region-of-interest.

4.1.2 Data Simulation and Template Analysis

In order to project the sensitivity of a future MeV-scale gamma-ray telescope to the Hawking radiation from a population of primordial black holes in the Inner Galaxy, we have created a series of simulated data sets based on the proposed design of e-ASTROGAM, and analyzed this simulated data utilizing a number of spatial templates. Such template-based analyses are extremely powerful in that they allow us to simultaneously exploit both spectral and morphological distinctions between the signal being searched for and the various astrophysical backgrounds that are present.

Our analysis includes spatial templates associated with the processes of pion production,

inverse Compton scattering, and Bremsstrahlung, each of which we generated using the publicly available code GALPROP [264, 132]. In utilizing GALPROP, we have adopted the default parameters from GALPROP WebRun, which have been selected to reproduce a variety of cosmic-ray and gamma-ray data. In addition to these three templates associated with Galactic diffuse emission mechanisms, we have also included templates designed to account for known gamma-ray point sources (using the best-fit spectra and source locations, as reported in the Fermi 4FGL-DR2 catalog), and for the (isotropic) extragalactic gamma-ray background [4, 8]. For each of these two latter templates, we have extrapolated in energy from the range measured by Fermi. We have also included a template intended to account for the emission known as the Galactic Center gamma-ray excess, which we have modeled as a population of 40 GeV dark matter particles annihilating (to $b\bar{b}$) with a cross section of $\langle \sigma v \rangle = 2.2 \times 10^{-26}\,\mathrm{cm}^3/\mathrm{s}$, and that is distributed according to a halo profile with an inner slope of $\gamma = 1.2$ [150, 131, 153, 99, 9, 72, 99, 9]. In this section, we take no stance on the origin of this excess, which can be treated without loss of generality as arising from the annihilation of particle dark matter, a large population of millisecond pulsars, or from some other unknown process or mechanism [183]. The morphology of these templates, as evaluated at 10 MeV, is shown in Fig. 4.2. The scale used is logarithmic (base 10), and the brightest point in each frame is normalized to unity. For example, the brightest point in each frame is pink, while a point that is fainter by two orders of magnitude would appear purple. The gamma-ray spectrum associated with each of these templates is shown in Fig. 4.3.

In our analysis, we adopt as our region of interest a $40^\circ \times 40^\circ$ square centered on the Galactic Center. We divide this region into 0.2098 square degree HEALPix bins, corresponding to $N_{\mathrm{side}} = 128$. We also divide the spectrum into 10 energy bins per decade, from $E_\gamma = m_e$ up to 1 GeV.

To produce a simulated data set, we first convolve each of the templates by the point spread function of e-ASTROGAM, which we treat as a gaussian with a 68% containment radius as given in the upper frame of Fig. 4.4 [100]. Then, after summing the templates

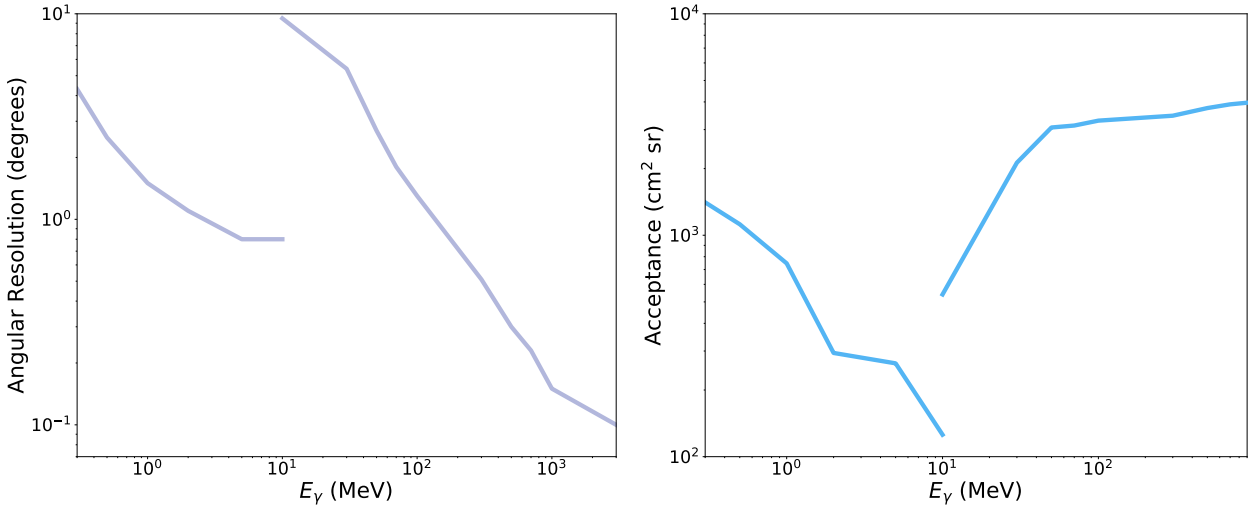

Figure 4.4: The 68% containment radius (top) and acceptance (bottom) of e-ASTROGAM as a function of gamma-ray energy [100]. At energies below (above) 10 MeV, this instrument relies primarily on Compton scattering (pair conversion).

as described above, we calculate the mean number of events in a given angular and energy bin. This is done by multiplying the flux in that bin by the acceptance of e-ASTROGAM (as given in the lower frame of Fig. 4.4), and by five years of observation time. For each bin, we then randomly draw from a Poisson distribution using the mean number of events in that bin, as described previously, to find the simulated number of events in that bin. Once we have a simulated data set for a given choice of $m_{\rm BH}$, $f_{\rm BH}$, and γ, we can calculate the likelihood for a model described by any given sum of the templates listed above.

4.1.3 Projected Constraints

To derive the projected constraints for e-ASTROGAM (or a similar instrument) on the abundance of primordial black holes, we simulate a data set assuming that no such black holes are present. Then, for each choice of $m_{\rm BH}$ and γ, we calculate the likelihood as a function of $f_{\rm BH}$, in order to place an upper limit on $f_{\rm BH}$. To identify the points in parameter space with the maximum likelihood, and to derive the appropriate confidence intervals around those points, we utilize the publicly available MINUIT algorithm [164]. Because MINUIT can occasionally identify false-minima, we use the PyMultiNest package to test the robustness

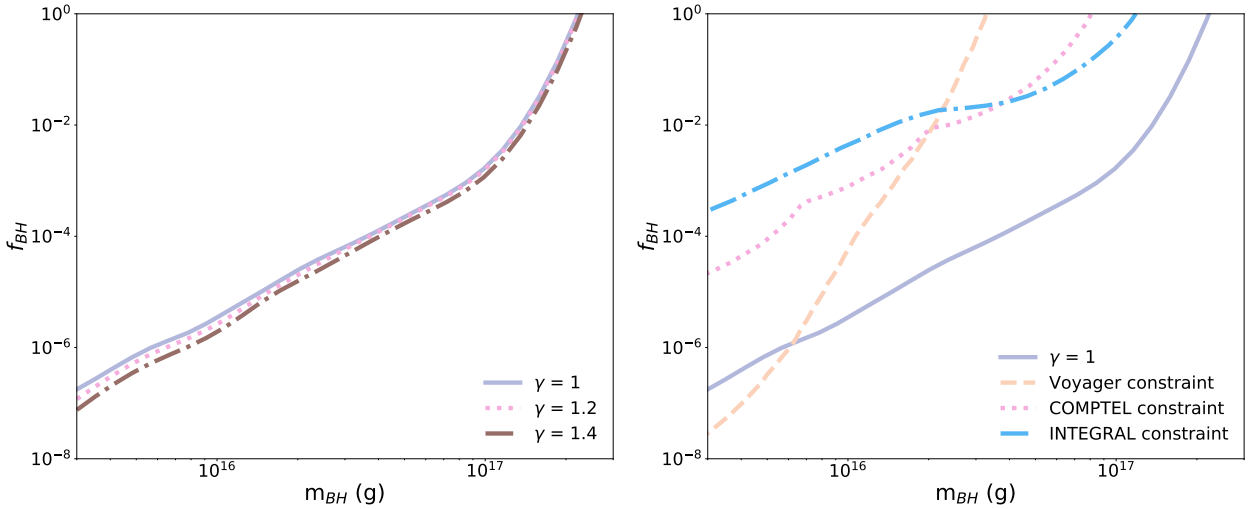

Figure 4.5: Our projected 95% confidence level upper limits on the fraction of the dark matter that could consist of primordial black holes, $f_{\rm BH}$, after 5 years of observation with e-ASTROGAM. In the left frame, we show results for black holes that are distributed according to a generalized NFW profile with $\gamma = 1.0$, 1.2, or 1.4. In the right frame, our projected constraints are compared to existing constraints derived from local measurements of the cosmic-ray electron-positron flux by the Voyager 1 satellite, and gamma-ray observations of the Inner Galaxy by COMPTEL and INTEGRAL [41, 181].

of our results by searching for global minima which may not have been encountered in our MINUIT scan [44].

In the left frame of Fig. 4.5, we show our 95% confidence-level projected upper limits on $f_{\rm BH}$ for black holes distributed according to a generalized NFW profile with $\gamma = 1.0$, 1.2, or 1.4. To reduce the impact of stochastic variations in our simulated data sets, we show as our projected constraints the average result obtained over five independent realizations. In the right frame of this figure, we compare this constraint to those previously derived from Voyager 1, as well as COMPTEL and INTEGRAL, for the specific case of $\gamma = 1$ [41, 181]. For black holes more massive than $m_{\rm BH} \sim 6 \times 10^{15}\,{\rm g}$, our projected constraints would represent the most stringent limits on the Hawking radiation from black holes.

Up to this point in our analysis, we have adopted a monochromatic distribution for the masses of the black holes. More realistically, we might expect a population of primordial black holes to contain members with a range of different masses. To this end, we repeated our

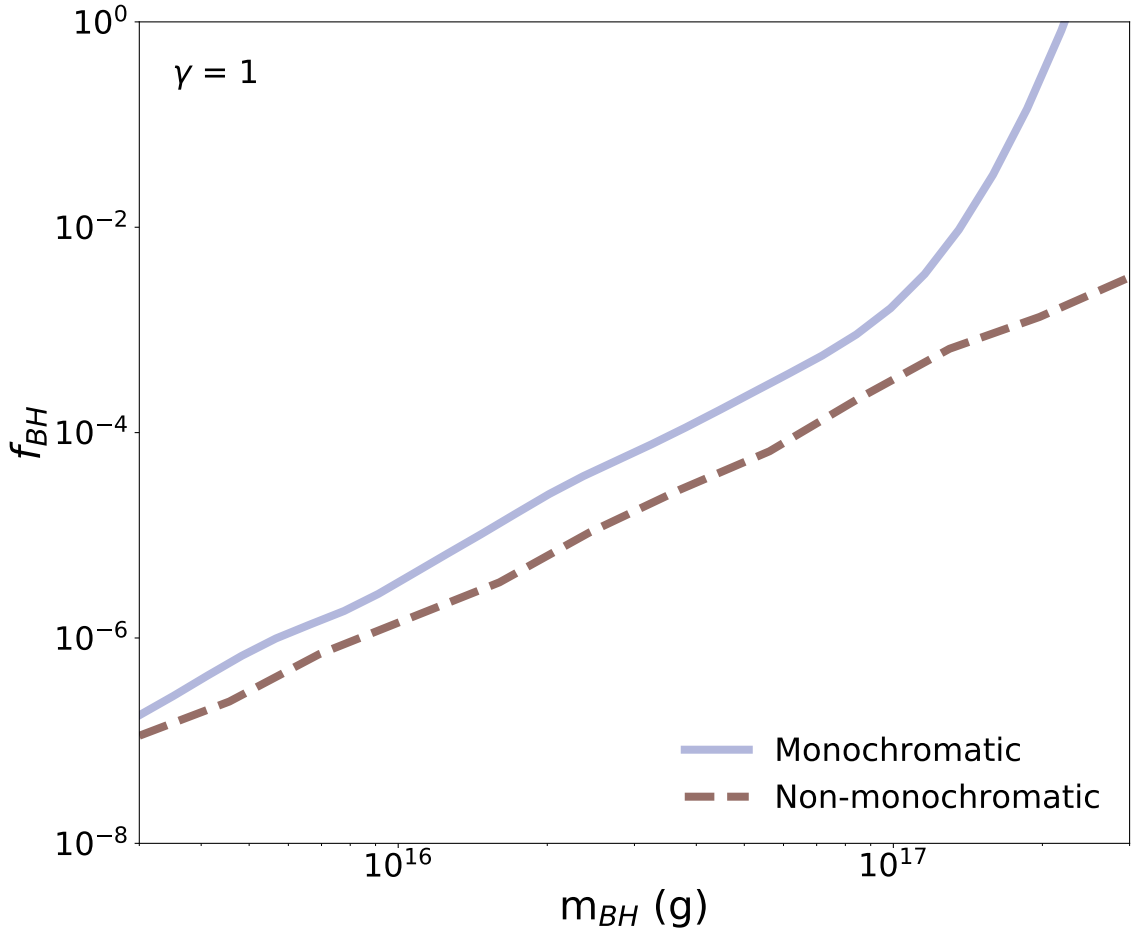

Figure 4.6: The solid curve in this figure represents the same constraint as that shown in Fig. 4.5 (for the case of $\gamma = 1$), while the dashed curve is that obtained for a population of black holes with masses that are distributed according to a log-normal distribution with a variance of $\sigma = 2$ and that is centered around $\mu = \ln(m_{\rm BH})$.

calculation considering black holes that are distributed according to a log-normal distribution with a variance of $\sigma = 2$. These results, which are shown in Fig. 4.6, are somewhat more stringent those obtained for the case of a monochromatic mass distribution.

Ideally, one would independently float the intensity and spectrum from each gamma-ray point source in a template-based analysis. Computational limitations, however, make such an approach unrealistic. For this reason, we have adopted in our calculations a single template to account for all of the known gamma-ray point sources in this region of the sky. Most of these sources are very morphologically distinct from our black hole template, making it very unlikely that this choice would significantly impact our projections. One might speculate, however, that an individual point source located near the Galactic Center could be partially degenerate with our black hole template, potentially biasing our results. To test this possibility, we have repeated our analysis including an additional template to account for the relatively bright and centrally-located point source 4FGL J1745.6-2859, which is associated with the Milky Way's supermassive black hole, Sgr A*. The constraints obtained in this way differ negligibly from those shown in Fig. 4.5, never by more than a few percent, thus indicating that the emission from individual point sources is unlikely to be confused with that from primordial black holes in our analysis.

4.1.4 Sensitivity to PBHs Capable of Generating the 511 keV Excess

Measurements of the Inner Milky Way by the INTEGRAL satellite have identified an excess of 511 keV photons, consisting of a flux of $(1.07 \pm 0.03) \times 10^{-3}$ photons cm^{-2} s^{-1} and corresponding to the injection of $\sim 2 \times 10^{43}$ positrons per second [267, 73, 268, 165, 266, 187, 230]. While various astrophysical sources of this emission have been considered, these interpretations each face considerable challenges [169, 62, 36, 134, 31, 256, 124, 231]. In light of this situation, a number of more exotic scenarios have been proposed, including those in which the 511 keV excess is produced by the annihilation, decay, or upscattering of dark matter particles, or by Q-balls, pico-charged particles, quark nuggets, or unstable MeV-scale

states produced in supernovae [38, 160, 155, 185, 154, 63, 90, 117, 226, 82, 81, 171, 113, 114, 200, 98]. It is also possible that the excess of 511 keV photons could be produced through the Hawking evaporation of a population of primordial black holes concentrated in the Inner Galaxy [121, 27, 45, 181, 197, 103]. In particular, a population of black holes with a distribution of masses that peaks around $m_{\rm BH} \sim (1-4) \times 10^{16}$ g could plausibly generate this signal if they are distributed in a very concentrated profile around the Galactic Center [181].

The observed morphology of the 511 keV excess is quite steeply concentrated around the Galactic Center [39]. As a result, if primordial black holes are to generate these excess photons, they must be distributed with a profile that is at least as centrally concentrated as $\gamma \sim 1.6$ [181, 262, 24]. This is significantly steeper than the profiles favored by numerical simulations of cold dark matter, which typically favor $\gamma \sim 1.0 - 1.4$ [130, 133, 192, 271, 272, 47, 242, 104, 105, 243, 35]. Such a scenario thus requires a greater degree of adiabatic contraction than is suggested by current simulations [128].

To project the sensitivity of e-ASTROGAM to a population of black holes that could be responsible for the observed 511 keV excess, we simulate a data set for the case of $m_{\rm BH} = 2 \times 10^{16}\,{\rm g}$, $f_{\rm BH} = 4 \times 10^{-4}$, and $\gamma = 1.6$ [181]. We then calculate the maximum value of the likelihood that is obtained as a function of these three parameters. In Fig. 4.7, we show the results of this analysis. This figure demonstrates that an instrument such as e-ASTROGAM would not only be able to detect the Hawking radiation from a black hole population responsible for the 511 keV excess, but would be able to characterize the properties of such a population with remarkable precision. While such a result could be impacted by systematic uncertainties that we have not accounted for in our analysis, we consider it clear that e-ASTROGAM would be able to quite accurately detect and measure the gamma-ray emission produced by such a population of primordial black holes.

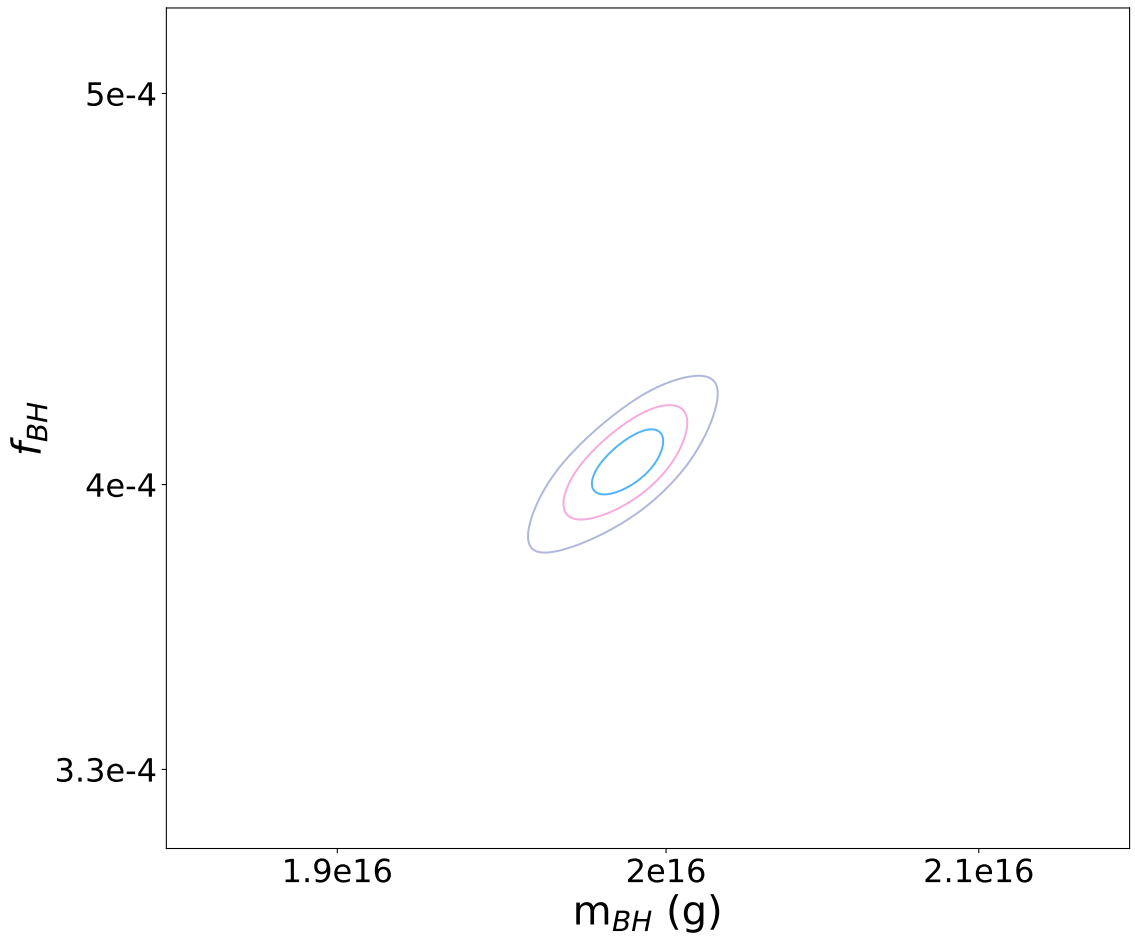

Figure 4.7: The ability of e-ASTROGAM to measure the properties of a black hole population in a scenario in which $m_{\rm BH} = 2 \times 10^{16}\,{\rm g}$, $f_{\rm BH} = 4 \times 10^{-4}$, and $\gamma = 1.6$, as motivated by the 511 keV excess observed by INTEGRAL [181]. The contours reflect the projected 1σ, 2σ, and 3σ constraints of these quantities.

4.2 The 511 keV Excess and Primordial Black Holes

The INTEGRAL satellite has detected an excess of 511 keV photons from the inner Milky Way relative to astrophysical expectations. This signal consists of a flux of $(1.07 \pm 0.03) \times 10^{-3}$ photons cm^{-2} s^{-1}, requiring the injection of $\sim 2 \times 10^{43}$ positrons per second [267, 73, 268, 165, 266, 187, 230]. A variety of potential astrophysical sources for this signal have been proposed, including type Ia supernovae, gamma-ray bursts, microquasars, low-mass X-ray binaries, and neutron star mergers [169, 62, 36, 134, 31, 256, 124]. However, given the challenges involved in explaining the observed characteristics of this signal, a number of more exotic scenarios have also been put forth [231]. In particular, the annihilations of MeV-scale dark matter particles have been considered in detail within this context, although this possibility is constrained by measurements of the damping tail of the cosmic microwave background [38, 160, 155, 185, 273, 111, 112, 237]. Explanations featuring decaying or upscattering dark matter particles also remain potentially viable [154, 63, 90, 117, 226, 82, 81]. Other exotic scenarios involving Q-balls, pico-charged particles, quark nuggets, or unstable MeV-scale states produced in supernovae have also been discussed within this context [171, 113, 114, 200, 98].

Another possibility that we will consider here is that the excess positrons could be produced through the Hawking evaporation of a population of primordial black holes concentrated in the Inner Galaxy [141, 126, 121, 27, 45, 197, 103]. As we will show, black holes with masses in the range of $m_{\rm BH} \sim (1-4) \times 10^{16}$ g could produce the required flux of positrons while remaining consistent with all existing constraints, including those from the COMPTEL, INTEGRAL, and Voyager 1 satellites [198, 87, 41, 60, 53, 97].

Here, we discuss the possibility that primordial black holes could be the source of the positrons responsible for INTEGRAL's 511 keV excess. After identifying the regions of parameter space that can accommodate this signal, we calculate the gamma-ray spectrum from these black holes (including direct Hawking radiation, photons from the inflight annihilation of positrons, and final-state radiation), and derive constraints based on data from

the gamma-ray telescopes INTEGRAL and COMPTEL. In scenarios in which black holes can produce the observed 511 keV signal, we find that the number density of black holes in the local halo is $\sim 10^{12}\,\mathrm{pc}^{-3}$, corresponding to a median instantaneous distance of ~ 10 AU to the nearest such black hole, well within the boundaries of our Solar System. Given the significant velocities of any primordial black holes in the Milky Way's halo, we should expect individual black holes to regularly pass through the inner Solar System. Even at such close distances, however, it would be very challenging to detect the Hawking radiation from an individual black hole in this mass range. On the other hand, it should be possible to definitively test this class of scenarios by characterizing the diffuse MeV-scale gamma-ray emission from the halo of the Milky Way with proposed gamma-ray telescopes such as AMEGO or e-ASTROGAM.

4.2.1 Dark Matter Distribution

Black holes radiate all particle species lighter than or comparable to their temperature, which is related to the mass of the black hole, as described in equation 2.6. For context, the Schwarzschild radius of a black hole is given by $r_s = 2m_{\mathrm{BH}}/M_{\mathrm{Pl}}^2 \simeq 1.5 \times 10^{-12}\,\mathrm{cm} \times (m_{\mathrm{BH}}/10^{16}\mathrm{g})$. This radiation causes a black hole to lose mass at a rate described in equation 2.7. Additionally, we will be again utilizing the spectrum of Hawking radiation from an individual black hole, as given in equation 4.1.

4.2.2 Parameter Space

In order to identify the parameter space in which primordial black holes could produce the observed 511 keV excess, we calculate the flux and spatial distribution of the positrons injected from these objects and compare this to the intensity and morphology of the 511 keV signal as reported in Ref. [39]. The flux of 511 keV photons from black holes near the Galactic Center observed over a region of solid angle, $\Delta\Omega$, is given by equation 4.5, where n_{BH} is the number density of black holes, L_{511} is the number of 511 keV photons produced

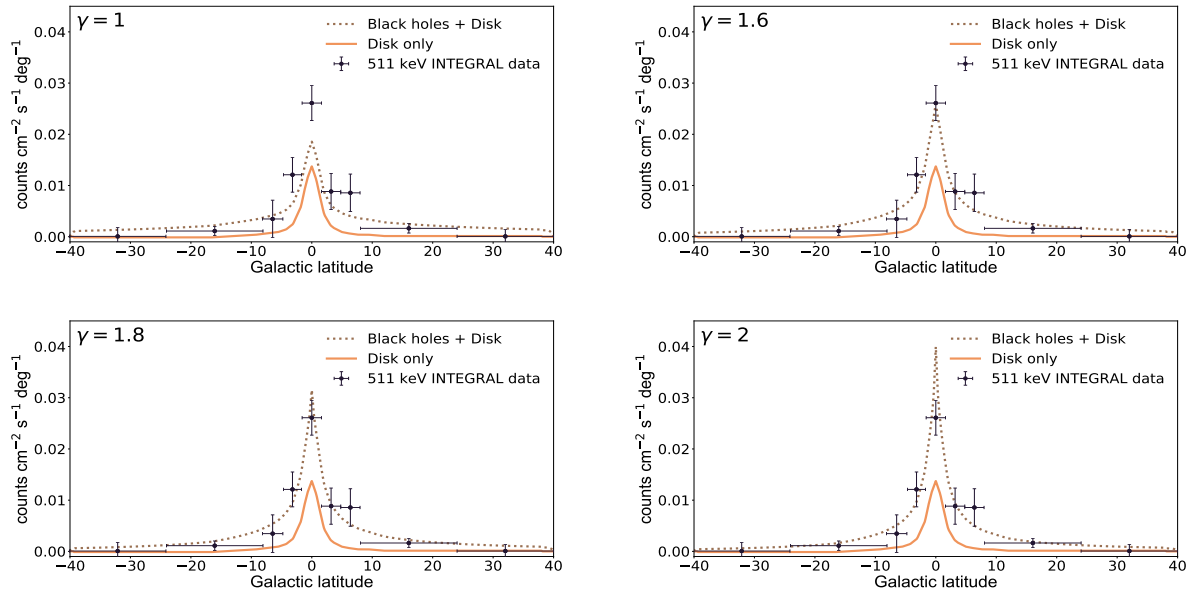

Figure 4.8: The predicted flux and angular profile of 511 keV photons, averaged over $-8^\circ < l < +8^\circ$, and compared to the measurements of the INTEGRAL satellite [39]. Results are shown for four choices of the density profile's inner slope, γ. In each frame, we have selected values of $m_{\rm BH}$ and $f_{\rm DM}$ which provide the best possible normalization to this data. The solid curves represent an estimate for the contribution from astrophysical sources in the Galactic Disk, while the dashed curves correspond to the total contribution from disk sources and primordial black holes [236].

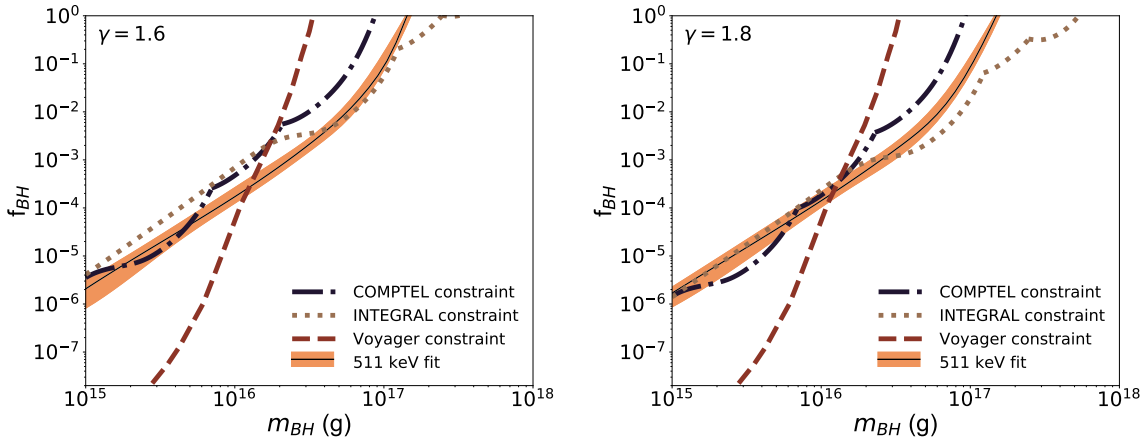

Figure 4.9: In each frame, the orange band denotes the 2σ region of parameter space in which the 511 keV excess observed by INTEGRAL could be produced through the Hawking evaporation of primordial black holes. Also shown are the constraints on this parameter space derived from the measurements of the INTEGRAL, COMPTEL, and Voyager 1 satellites. Black holes with masses of $\sim (1-4) \times 10^{16}$ g could produce the observed excess if they constitute a small fraction of the total dark matter and are distributed according to a halo profile with a very steep inner slope, $\gamma \simeq 1.6 - 1.8$.

by a given black hole per unit time, and the integrals are performed over solid angle and the line-of-sight, l. In the second line, we have written the number density of black holes in terms of the dark matter density, $n_{\rm BH} = f_{\rm BH}\,\rho_{\rm DM}/m_{\rm BH}$, where $f_{\rm BH}$ is the fraction of the total dark matter that consists of black holes. When a black hole emits a positron, it can either directly annihilate to produce two 511 keV photons, or form a positronium bound state with an electron, which results 25% of the time in two 511 keV photons, and 75% of the time in three photons, each with $E_\gamma < 511$ keV. Given that observations indicate that the positronium fraction in the interstellar medium of the Milky Way is $f = 0.967 \pm 0.022$, the number of 511 keV photons produced per positron is $2(1-f) + 2f/4 \approx 0.55$ [165].

For the dark matter distribution, we again adopt a generalized Navarro-Frenk-White (NFW) halo profile, as described in equation 4.7. We again take the inner slope of this profile, γ, to be a free parameter.

In Fig. 4.8, we have plotted the 511 keV emission predicted from primordial black holes as a function of galactic latitude (averaging over $-8^\circ < l < +8^\circ$), for four choices of the density profile's inner slope, γ. In each frame, we compare the predicted profile of this emission to the measurements by INTEGRAL [39]. In addition to the 511 keV emission resulting from positrons radiated from black holes, we have included an estimate for the contribution from astrophysical positron emission in the disk, as described in Ref. [236]. Given the uncertainties regarding the magnitude of the astrophysical contribution, we have allowed its normalization to float from its default value by up to a factor of two. From this figure, it is clear that a very steep density profile is required if primordial black holes are to produce the observed intensity of the 511 keV emission from the inner few degrees around the Galactic Center [262, 24]. Formally, our fit to this data favors $\gamma = 2.2 \pm 0.6$ (at 2σ), although a somewhat larger range could plausibly be accommodated if all of the related uncertainties were taken into account. While this range is well above that typically favored by numerical simulations of cold dark matter ($\gamma \sim 1 - 1.4$), the lower portion of the range favored by our fit could be potentially viable if adiabatic contraction is efficient

[129, 130, 133, 192, 271, 272, 246, 260, 86, 240, 47, 242, 104, 105, 243, 35, 128]. In light of this, we chose to focus on the lowest portion of the range favored by our fit, characterized by $\gamma \sim 1.6 - 1.8$.

In each frame of Fig. 4.8, we have selected values of $m_{\rm BH}$ and $f_{\rm DM}$ which provide the best possible normalization to the INTEGRAL data. The orange bands shown in Fig. 4.9 represent the range of these parameters that lead to the best-fit normalization for the 511 keV signal (for results using other values of γ, see the Supplementary Material).

In addition to electrons and positrons, black holes produce gamma rays which can be used to constrain this class of scenarios. Photons can be produced directly as the products of Hawking evaporation (see Eq. 4.1), as well as through the inflight annihilation of positrons, and as final state radiation. This inflight annihilation, final state radiation, and the contribution directly from black hole evaporation, make up our 511 keV photon emission from black holes, and takes into account electron propagation in the Milky Way. The flux of these gamma rays from a population of black holes observed over a solid angle, $\Delta\Omega$, is given by equation 4.5, where $dN_\gamma^{\rm tot}/dE_\gamma$ is the gamma-ray spectrum from an individual black hole, including the contributions from direct Hawking evaporation, inflight positron annihilation, and final state radiation. In Fig. 4.10, we plot the spectrum of the gamma-ray emission from a black hole with a mass of $m_{\rm BH} = 2 \times 10^{16}\,{\rm g}$, showing separately each of these contributions. At the highest energies, the direct Hawking radiation dominates, while inflight annihilation provides the largest contribution at lower energies.

4.2.3 Inflight Annihilation and Final State Radiation

We also want to describe the calculation of the contributions from inflight annihilation and final state radiation.

In the energy range of interest for this study, most positrons lose energy via ionization and become non-relativistic before annihilating. A small fraction of such positrons, however, will annihilate inflight prior to reaching non-relativistic velocities. Such annihilations can

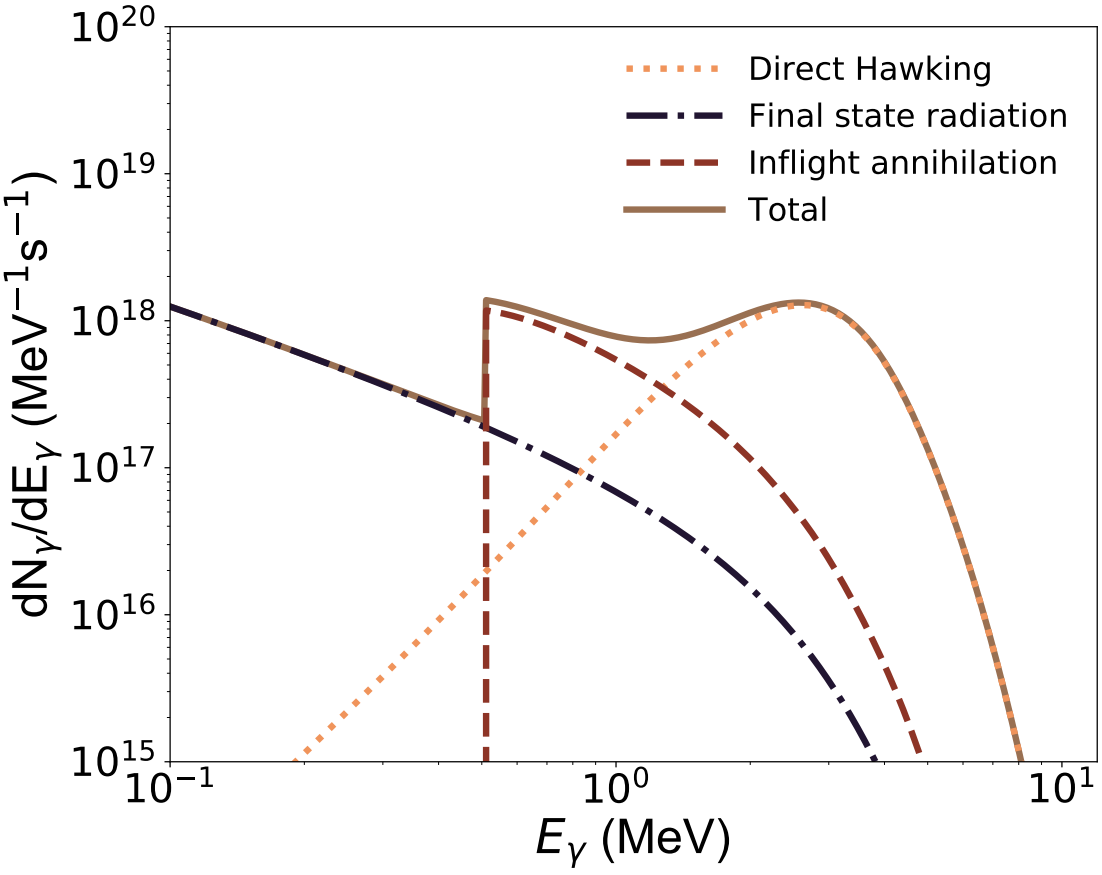

Figure 4.10: The gamma-ray emission from a black hole with a mass of $m_{\mathrm{BH}} = 2 \times 10^{16}\,\mathrm{g}$, showing separately the contributions from direct Hawking radiation, inflight positron annihilation, and final state radiation.

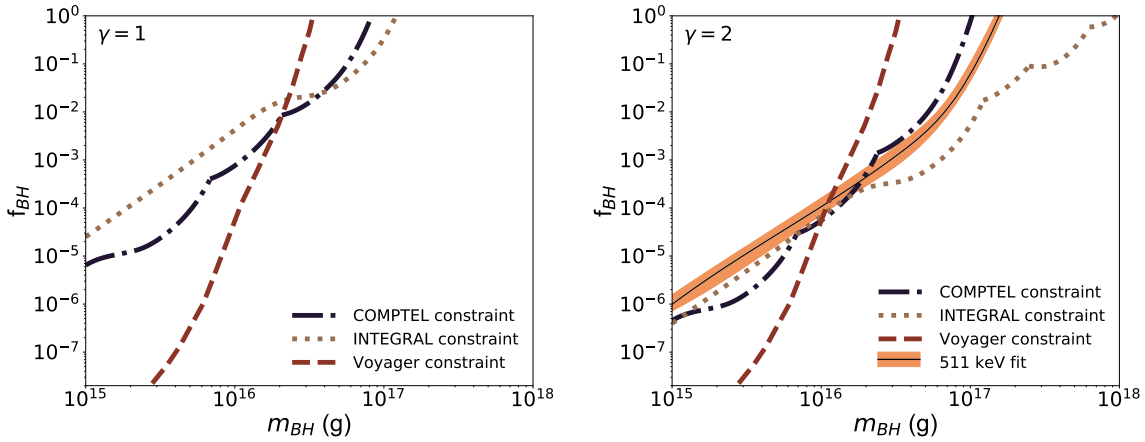

Figure 4.11: As in Fig. 2, but for black hole distributions with an inner slope of $\gamma = 1$ (left) or $\gamma = 2$ (right). In the $\gamma = 1$ case, we do not show any region for the 511 keV excess, as the angular distribution of this signal cannot be accommodated for this choice of halo profile. In the $\gamma = 2$ case, the region favored by the 511 keV excess is ruled out by a combination of the constraints from COMPTEL, INTEGRAL, and Voyager 1.

produce photons with energies greater than 511 keV, thus contributing to the continuum spectrum of diffuse gamma rays.

Following Ref. [32], the spectrum of gamma rays from the inflight annihilation of positrons is given by equation 4.2, the probability that a positron of energy E_{e^+} will survive until its energy has been reduced to E is given by equation 4.3, and the contribution to the gamma ray spectrum from final state radiation is given by equation 4.4.

4.2.4 Results For Other Values of γ

In Fig. 2, we showed the regions of black hole parameter space that can accommodate the observed characteristics of the 511 keV excess, along with the constraints from gamma-ray and cosmic-ray electron measurements, for halo profiles with an inner slope of $\gamma = 1.6$ or 1.8. In Fig. 4.11, we show the corresponding results for the cases of $\gamma = 1$ or $\gamma = 2$. In the $\gamma = 1$ frame, we do not show any region for the 511 keV excess, as the angular distribution of this signal cannot be accommodated for this choice of halo profile. In the $\gamma = 2$ case, the region favored by the 511 keV excess is ruled out by a combination of the constraints from

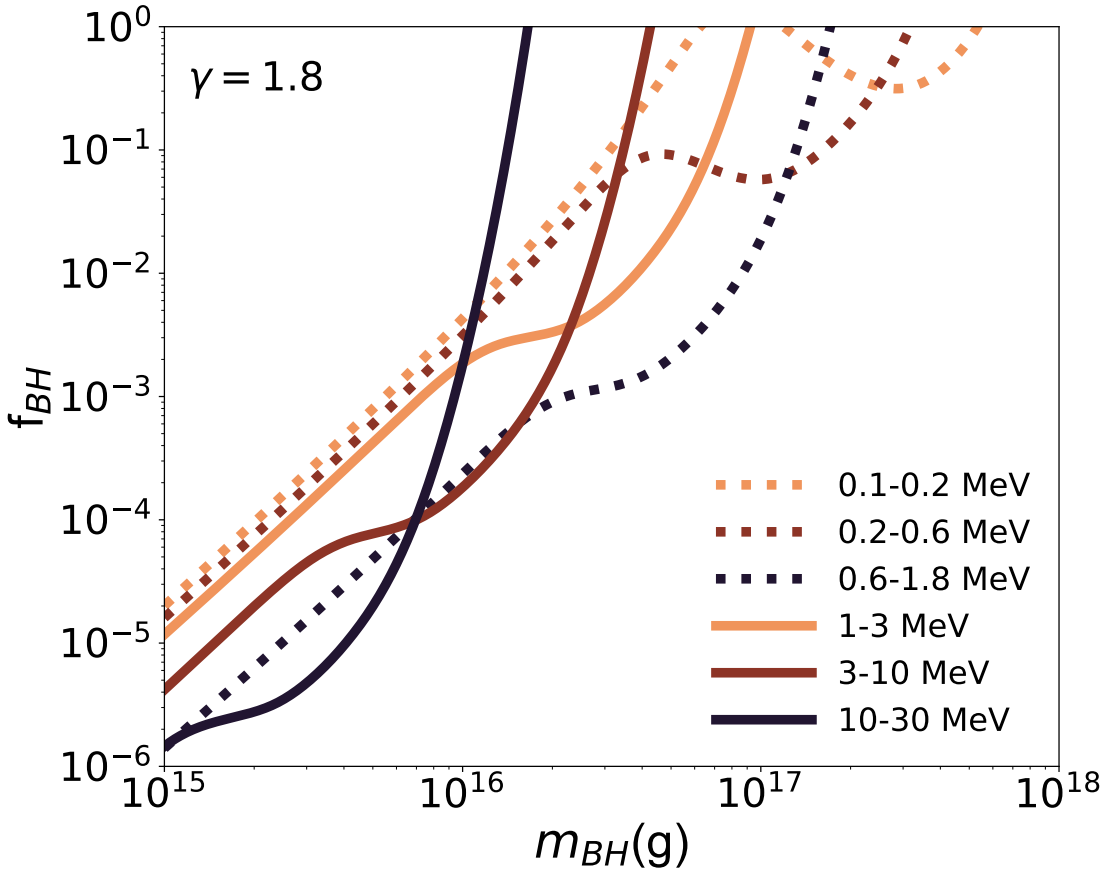

Figure 4.12: the constraints on the black hole parameter space from individual energy bins of data from the INTEGRAL (dashed) and COMPTEL (solid) satellites, for the case of $\gamma = 1.8$.

COMPTEL, INTEGRAL, and Voyager 1.

4.2.5 Bin-by-Bin Gamma-Ray Constraints

In Fig. 4.12, we show the constraints on the black hole parameter space as derived from individual energy bins of INTEGRAL and COMPTEL data, for the case of $\gamma = 1.8$. INTEGRAL provides the most stringent constraints on black holes more massive than $\sim 2 \times 10^{16}\,\mathrm{g}$, while COMPTEL (and Voyager 1) are most restrictive for smaller values of m_{BH}.

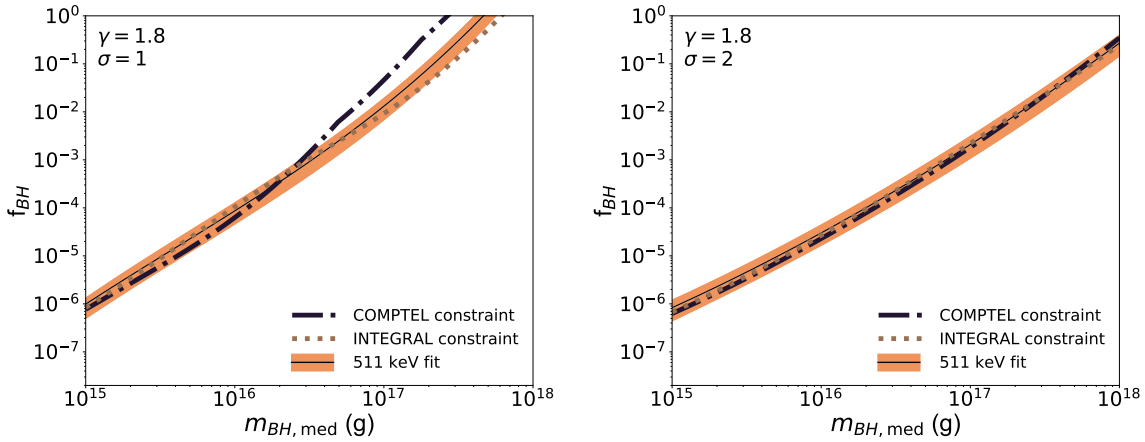

Figure 4.13: As in Fig. 2, but for black hole distributions with an inner slope of $\gamma = 1.8$, with a non-monochromatic mass distribution. We do not show the Voyager constraints, as they are specific to a monochromatic mass spectrum. The non-monochromatic mass spectrum is calculated using a log normal distribution, with the median black hole mass being plotted on the x axis, with $\sigma = 1$ in the left plot, and $\sigma = 2$ on the right.

4.2.6 Non-Monocromatic Mass Spectrum

In addition, we show the constraints in the black hole parameter space for a non-monochromatic mass spectrum in Fig. 4.13. For this mass spectrum, we follow a log-normal distribution and plot the parameter space as a function of median black hole mass, with $\sigma = 1$ (left) and $\sigma = 2$ (right). We consider a value of $\gamma = 1.8$.

4.2.7 Constraining the Abundance of PBHs

To constrain the abundance of primordial black holes in the Inner Galaxy, we make use of gamma-ray measurements from the INTEGRAL and COMPTEL satellites (for lower mass black holes, one would instead derive constraints from gamma-ray measurements at higher energies, such as those from EGRET or Fermi) [40, 253, 202, 10]. We utilize the gamma-ray fluxes as measured in the 0.1-0.2 MeV, 0.2-0.6 MeV and 0.6-1.8 MeV bands by INTEGRAL, and in the 1-3 MeV, 3-10 MeV, and 10-30 MeV bands by COMPTEL. For each INTEGRAL band, we integrate the predicted gamma-ray flux over each of the angular bins presented. We then vary $f_{\rm BH}$ until we identify the value at which the total χ^2 has increased from

its best fit at the 2σ level [198, 74]. For our comparison to the COMPTEL data, the large systematic (and highly correlated) error bars make it inappropriate to conduct a χ^2 analysis, so we simply require that our predicted flux does not exceed any of the measurements by more than 2σ [87]. We also apply constraints derived from the local electron/positron flux as measured by Voyager 1 [41].

In Fig. 4.9, we plot the INTEGRAL, COMPTEL, and Voyager 1 constraints on the value of $f_{\rm BH}$, as a function of $m_{\rm BH}$, for $\gamma = 1.6$ or 1.8. After taking these constraints into account, we conclude that $\sim (1-4) \times 10^{16}$ g black holes could produce the observed 511 keV excess if they constitute a small fraction of the total dark matter halo, $f_{\rm BH} \sim 0.0001 - 0.004$, and are distributed according to a halo profile with a very steep inner slope. For this range of parameters, there are approximately $\sim 10^{22} - 10^{23}$ black holes in the innermost kpc of the Milky Way. It is plausible that black holes in this mass range could have been formed in the very early universe. In particular, the horizon enclosed a total mass of $\sim 10^{16}$ g when the universe was at a temperature of $\sim 10^8$ GeV [142, 125, 177, 79, 170, 180, 46, 278, 279, 77, 156, 195, 194, 196, 270, 251, 146, 186]. Note that although we have adopted a monochromatic mass distribution in our calculations, a distributions of masses with a variance as large as roughly an order of magnitude could plausibly produce the observed 511 keV signal without conflicting with existing constraints. We also note that in the presence of a sizable population of primordial black holes, the remaining dark matter cannot consist of particles that are capable of producing photons or other readily detectable particles through their self-annihilations [55, 11].

4.2.8 Black Holes in Our Solar System

In the regions of parameter space in which primordial black holes could generate the observed 511 keV excess, the number density of black holes in the vicinity of the Solar System is given

by:

$$n_{\rm BH}^{\rm local} = \frac{f_{\rm BH}\rho_{\rm DM}^{\rm local}}{m_{\rm BH}} \tag{4.8}$$
$$\simeq 1.0 \times 10^{12}\,{\rm pc}^{-3} \times \left(\frac{f_{\rm BH}}{10^{-3}}\right)\left(\frac{2\times 10^{16}\,{\rm g}}{m_{\rm BH}}\right)$$
$$\simeq 1.2 \times 10^{-4}\,{\rm AU}^{-3} \times \left(\frac{f_{\rm BH}}{10^{-3}}\right)\left(\frac{2\times 10^{16}\,{\rm g}}{m_{\rm BH}}\right),$$

where we have again adopted a local dark matter density of $\rho_{\rm DM}^{\rm local} = 0.4\,{\rm GeV/cm}^3$. For this number density, we should expect the closest black hole to be located at a distance of only $d \sim (3/4\pi n_{\rm BH})^{1/3} \sim \mathcal{O}(10\,{\rm AU})$, and for the Solar System to contain several hundred black holes at any given moment. Considering the significant velocities expected of any black holes that are part of the Milky Way's dark matter halo, we conclude that black holes should regularly pass through the inner Solar System in this class of scenarios. Over a ten year window, for example, and adopting a representative velocity of 300 km/s, we predict a closest approach of a few AU or less. At such close proximity, one might think that the Hawking radiation from an individual black hole could be detectable, especially in light of proposed satellite-based gamma-ray telescopes optimized for sensitivity to MeV-scale photons, such as AMEGO and e-ASTROGAM [51, 101, 249]. Even for these future missions, however, the design sensitivity to point sources of MeV-scale photons is only $\sim 10^{-6}\,{\rm MeV\,cm^{-2}\,s^{-1}}$. In comparison, the gamma-ray flux from an individual black hole is predicted to be $\sim 10^{-10}\,{\rm MeV\,cm^{-2}\,s^{-1}} \times (10\,{\rm AU}/d)^2\,(2\times 10^{16}\,{\rm g}/m_{\rm BH})^2$, leading to a detectable signal only for a black hole closer d1AU. Even if we were to be lucky enough to have a black hole at such a close proximity, its proper motion would significantly complicate the search for its Hawking radiation.

A more promising way to test this class of scenarios is to use a telescope such as AMEGO or e-ASTROGAM to detect and characterize the diffuse gamma-ray emission generated by black holes in the Milky Way's inner halo, or as they contribute to the isotropic gamma-ray background [51, 101, 232]. Instruments such as AMEGO or e-ASTROGAM should be able to improve substantially (by approximately an order of magnitude) on the limits derived in

study using COMPTEL and INTEGRAL data, making it possible to definitively test the range of parameter space in which primordial black holes could produce the observed 511 keV signal.

CHAPTER 5

CONCLUSION

It is plausible that the early universe contained a substantial population of black holes. These black holes are called "primordial black holes" and are defined as black holes that formed shortly after the big bang. Primordial black holes could have formed via phase transitions, quantum fluctuations, or inflation, among other mechanisms. The emitted Hawking radiation, and gravitational properties of primordial black holes make them an intriguing dark matter candidate. If these black holes still exist today, they could make up some or most of the dark matter in the universe. Even primordial black holes that evaporated in the early universe are interesting and commonly studied as the effects of their evaporation could have been significant. In this thesis, we discuss primordial black holes and their observational consequences, both to examine primordial black holes in the early universe, as well as observations today that could probe Hawking evaporation from currently evaporating black holes.

In this thesis we discussed black holes that evaporated during or shortly after the BBN era, which can be constrained by measurements of the primordial light element abundances. We revisited the impact of evaporating black holes on BBN, updating the relevant measurements and expanding the discussion to include cases in which black holes can evaporate into particles beyond the Standard Model.

Recent improvements in the determination of the primordial deuterium abundance have made it possible to significantly strengthen the constraints on primordial black holes relative to those presented in previous work. Our main results are shown in Fig. 3.3, where (assuming only Standard Model particle content) we summarize our constraints on the initial abundance of primordial black holes which evaporate on a timescale of 10^{-1} to $10^{13}\,\mathrm{s}$ (corresponding to a mass range of $\sim 6\times10^{8}$ to $\sim 2\times10^{13}$ grams). For $t_{\rm evap} \lesssim 80\,\mathrm{s}$, these constraints are largely the consequence of the neutron abundance at early times, which is sensitive to the expansion rate at the time of proton-neutron freeze-out, as well as to the presence of energetic mesons which can convert protons into neutrons (and vice versa). For longer-lived black holes, the constraints are instead dominated by the hadrodissociation and photodissociation of

helium nuclei, each of which can significantly increase the observed abundance of primordial deuterium.

Whereas previous work studying the impact of primordial black holes on BBN have focused on Hawking evaporation into Standard Model particles, we have extended this discussion to include scenarios beyond the Standard Model. Given the purely gravitational nature of Hawking evaporation, black holes produce all particle species lighter than the black hole's temperature, regardless of their charges or couplings. As a consequence, the rate at which black holes evaporate and the types of particles that are produced through this process depend on the complete particle spectrum, including any and all such species that might exist beyond the confines of the Standard Model. From this perspective, it is particularly interesting to consider scenarios that feature large numbers of feebly-coupled degrees-of-freedom. In exploring such hidden sector models, we have considered constraints on light, stable products of Hawking radiation (which act as dark radiation), as well as massive stable particles (which act as dark matter). For $t_{\rm evap} \lesssim 10^2\,{\rm s}$, we have placed constraints on black holes with light hidden sectors that are comparably stringent to those derived from measurements of the CMB (longer-lived black holes are more strongly restricted by the CMB). For relatively short-lived black holes ($t_{\rm evap} \lesssim 10^3\,{\rm s}$), we have identified a wide range of scenarios in which the entirety of the dark matter abundance could be produced through Hawking evaporation, especially if $m_{\rm DM} \sim {\rm GeV} - {\rm PeV}$ (other values of $m_{\rm DM}$ are also possible, but only if $g_{\star,H}$ is very large or $t_{\rm evap} \lesssim 10^{-1}\,{\rm s}$). For longer-lived black holes, the combined constraints from the measured deuterium abundance and large scale structure (as related to the dark matter's free-streaming length) are more restrictive. We also consider evaporating black holes within the context of TeV-scale supersymmetry, finding a non-negligible impact on the resulting constraints, and identifying scenarios in which Hawking evaporation could produce an abundance of neutralinos (or other LSPs) that is in good agreement with the measured dark matter density. The epoch of BBN provides us with critical information pertaining to the energy content of the universe at early times. Measurements of the primordial element

abundances serve as a window into this period, enabling us to test and constrain a wide range of possible new phenomena, including that of primordial black holes.

Additionally, we have evaluated the ability of future MeV-scale gamma-ray telescopes such as e-ASTROGAM or AMEGO to detect and characterize the Hawking radiation from a population of primordial black holes located in the inner volume of the Milky Way. These black holes are much more massive and longer lived than the black holes that may have affected BBN. We have calculated the gamma-ray emission from black holes, including contributions from direct Hawking radiation, inflight positron annihilation, and final state radiation. We then performed an analysis utilizing a series of spatial templates, allowing us to fully exploit the morphological and spectral information provided by such an instrument. We have included in our analysis templates associated with pion production, inverse Compton scattering, bremsstrahlung, known point sources, the Galactic Center gamma-ray excess, and the extragalactic gamma-ray background, as well as that associated with the Hawking radiation from a population of primordial black holes.

At the present time, the strongest constraints on Hawking radiation come from the Voyager 1, COMPTEL, and INTEGRAL satellites [181, 87, 198, 41, 97]. More specifically, local measurements of the cosmic-ray electron-positron flux by Voyager 1 provide the strongest constraint on black holes lighter than $m_{\rm BH} \sim (1-2) \times 10^{16}\,{\rm g}$ [41], while MeV-scale gamma-ray observations of the Inner Galaxy by COMPTEL and INTEGRAL provide the leading constraints in the mass range of $m_{\rm BH} \sim 10^{16} - 10^{17}\,{\rm g}$ [181, 87, 198, 87]. In the absence of a black hole population, we project that e-ASTROGAM will be able to provide the strongest constraints on black holes in the mass range of $m_{\rm BH} \sim (0.6-20) \times 10^{16}\,{\rm g}$. Over much of this mass range, the sensitivity of e-ASTROGAM will exceed that of existing or past experiments by roughly two orders of magnitude.

It has been previously pointed out that primordial black holes could be responsible for the excess of 511 keV photons observed from the Inner Galaxy by the INTEGRAL satellite. This requires the mass distribution of the black hole population to peak at around $m_{\rm BH} \sim$

$(1-4)\times10^{16}\,\mathrm{g}$, and for these objects to be distributed in a very concentrated profile around the Galactic Center [181]. In such a scenario, we find that an instrument such as AMEGO or e-ASTROGAM would not only clearly detect the Hawking radiation from such a population, but would be able to quite precisely measure the abundance and mass distribution of the responsible black holes.

Finally, this thesis discussed primordial black holes in their capacity to produce the excess of 511 keV photons observed from the Inner Galaxy by the INTEGRAL satellite. To reproduce the angular distribution of this signal, the black holes must be distributed with a very cuspy halo profile, featuring an inner slope of $\gamma \sim 1.6$ or higher. Furthermore, to be consistent with gamma-ray constraints from COMPTEL and INTEGRAL, and cosmic-ray electron constraints from Voyager 1, the bulk of these black holes must have masses in the range of $m_{\rm BH} \sim (1-4)\times10^{16}\,\mathrm{g}$. To provide the observed normalization of this signal, these black holes must constitute a relatively small fraction of the total dark matter abundance, $f_{\rm DM} \sim 0.0001 - 0.004$.

In our calculations, we have included the photons, electrons and positrons that are directly produced through Hawking radiation, as well as the gamma-rays that are generated through the inflight annihilation of positrons, and as final state radiation. For the range of $m_{\rm BH}$ and $f_{\rm DM}$ required in this scenario, we predict that the local halo of the Milky Way should contain a considerable number density of black holes, $n_{\rm BH}^{\rm local} \sim 10^{12}\,\mathrm{pc}^{-3}$. Although such black holes would be very challenging to detect individually, future satellite-based gamma-ray telescopes such as AMEGO or e-ASTROGAM will be able to definitively test this class of scenarios by measuring the spectrum and morphology of the MeV-scale emission from the Inner Galaxy.

Black holes are one of the most mysterious and thought provoking objects in the universe. They have captured the imagination of both laypeople and astrophysicists for decades. These mysterious objects are so gravitationally strong that nothing, not even light, can escape from beyond their event horizon. Black holes can be hugely massive monsters lying in wait at

the center of galaxies, including our own, produced in the explosion at the end of a colossal star's life, or in the first moments of the universe. Their effects on the universe have been a source of massive research efforts, motivated by their potential as a dark matter candidate and their ability to radiate away particles via Hawking evaporation. In this thesis, we have explored the current understanding primordial black holes as dark matter. We applied that knowledge to present novel work on the impact of PBHs on Big Bang nucleosynthesis, as well as the potential observational consequences of primordial black holes in the center of the Milky Way galaxy. While much remains to be discovered, this research represents an advance in our understanding of primordial black holes and provides a strong foundation for future work in this exciting field.

"*And it's fine to fake it 'til you make it*

'Til you do, 'til it's true."

— Taylor Swift

REFERENCES

[1] Aaboud, M., et al. 2018, Phys. Rev. D, 97, 112001

[2] Abbott, R., Abbott, T. D., Abraham, S., et al. 2021, The Astrophysical Journal Letters, 915, L5

[3] —. 2021, The Astrophysical Journal Letters, 915, L5

[4] Abdollahi, S., et al. 2020, Astrophys. J. Suppl., 247, 33

[5] Accetta, F. S., & Trester, J. J. 1989, Phys. Rev. D, 39, 2854

[6] Acharya, S. K., & Khatri, R. 2020, JCAP, 06, 018

[7] —. 2020, JCAP, 02, 010

[8] Ackermann, M., et al. 2015, Astrophys. J., 799, 86

[9] —. 2017, Astrophys. J., 840, 43

[10] —. 2018, Astrophys. J., 857, 49

[11] Adamek, J., Byrnes, C. T., Gosenca, M., & Hotchkiss, S. 2019, Phys. Rev. D, 100, 023506

[12] Afshordi, N., McDonald, P., & Spergel, D. N. 2003, The Astrophysical Journal, 594, L71

[13] Aghanim, N., et al. 2020, Astron. Astrophys., 641, A6, [Erratum: Astron.Astrophys. 652, C4 (2021)]

[14] Akiyama, K., et al. 2019, Astrophys. J. Lett., 875, L1

[15] Alcock, C., Allsman, R. A., Alves, D., et al. 1998, The Astrophysical Journal, 499, L9

[16] Ali-Haïmoud, Y., Kovetz, E. D., & Kamionkowski, M. 2017, Phys. Rev. D, 96, 123523

[17] Allahverdi, R., Dent, J., & Osinski, J. 2018, Phys. Rev. D, 97, 055013

[18] Anastasopoulos, P., Bianchi, M., Dudas, E., & Kiritsis, E. 2006, JHEP, 11, 057

[19] Ando, S., Cyburt, R. H., Hong, S. W., & Hyun, C. H. 2006, Phys. Rev. C, 74, 025809

[20] Arbey, A. 2012, Comput. Phys. Commun., 183, 1822

[21] Arbey, A., Auffinger, J., Hickerson, K. P., & Jenssen, E. S. 2020, Comput. Phys. Commun., 248, 106982

[22] Arkani-Hamed, N., Cohen, T., D'Agnolo, R. T., et al. 2016, Phys. Rev. Lett., 117, 251801

[23] Arvanitaki, A., Dimopoulos, S., Dubovsky, S., Kaloper, N., & March-Russell, J. 2010, Phys. Rev. D, 81, 123530

[24] Ascasibar, Y., Jean, P., Boehm, C., & Knoedlseder, J. 2006, Mon. Not. Roy. Astron. Soc., 368, 1695

[25] Aver, E., Olive, K. A., & Skillman, E. D. 2015, JCAP, 07, 011

[26] Baldes, I., Decant, Q., Hooper, D. C., & Lopez-Honorez, L. 2020, JCAP, 08, 045

[27] Bambi, C., Dolgov, A. D., & Petrov, A. A. 2008, Phys. Lett. B, 670, 174, [Erratum: Phys.Lett.B 681, 504–504 (2009)]

[28] Barabash, A. S. 2009, Foundations of Physics, 40, 703

[29] Bardeen, J. M., Carter, B., & Hawking, S. W. 1973, Commun. Math. Phys., 31, 161

[30] Barnacka, A., Glicenstein, J.-F., & Moderski, R. 2012, Physical Review D, 86, doi:10.1103/physrevd.86.043001

[31] Bartels, R., Calore, F., Storm, E., & Weniger, C. 2018, Mon. Not. Roy. Astron. Soc., 480, 3826

[32] Beacom, J. F., Bell, N. F., & Bertone, G. 2005, Phys. Rev. Lett., 94, 171301

[33] Beacom, J. F., & Yüksel, H. 2006, Phys. Rev. Lett., 97, 071102

[34] Berlin, A., Blinov, N., & Li, S. W. 2019, Phys. Rev. D, 100, 015038

[35] Bernal, N., Necib, L., & Slatyer, T. R. 2016, JCAP, 12, 030

[36] Bertone, G., Kusenko, A., Palomares-Ruiz, S., Pascoli, S., & Semikoz, D. 2006, Phys. Lett. B, 636, 20

[37] Bird, S., Cholis, I., Muñoz, J. B., et al. 2016, Phys. Rev. Lett., 116, 201301

[38] Boehm, C., Hooper, D., Silk, J., Casse, M., & Paul, J. 2004, Phys. Rev. Lett., 92, 101301

[39] Bouchet, L., Roques, J.-P., & Jourdain, E. 2010, Astrophys. J., 720, 1772

[40] Bouchet, L., Strong, A. W., Porter, T. A., et al. 2011, Astrophys. J., 739, 29

[41] Boudaud, M., & Cirelli, M. 2019, Phys. Rev. Lett., 122, 041104

[42] Braun, V., He, Y.-H., Ovrut, B. A., & Pantev, T. 2005, JHEP, 06, 039

[43] Bringmann, T., Kahlhoefer, F., Schmidt-Hoberg, K., & Walia, P. 2018, Phys. Rev. D, 98, 023543

[44] Buchner, J., Georgakakis, A., Nandra, K., et al. 2014, Astron. Astrophys., 564, A125

[45] Cai, R.-G., Ding, Y.-C., Yang, X.-Y., & Zhou, Y.-F. 2020, arXiv:2007.11804

[46] Cai, R.-G., Liu, T.-B., & Wang, S.-J. 2018, Phys. Rev. D, 98, 043538

[47] Calore, F., Bozorgnia, N., Lovell, M., et al. 2015, JCAP, 12, 053

[48] Cang, J., Gao, Y., & Ma, Y.-Z. 2021, , 2021, 051

[49] —. 2022, , 2022, 012

[50] Capela, F., Pshirkov, M., & Tinyakov, P. 2013, Physical Review D, 87, doi:10.1103/physrevd.87.023507

[51] Caputo, R., et al. 2019, arXiv:1907.07558

[52] Carr, B., Kohri, K., Sendouda, Y., & Yokoyama, J. 2021, Reports on Progress in Physics, 84, 116902

[53] —. 2021, Rept. Prog. Phys., 84, 116902

[54] Carr, B., Kuhnel, F., & Sandstad, M. 2016, Phys. Rev. D, 94, 083504

[55] Carr, B., Kuhnel, F., & Visinelli, L. 2020, arXiv:2011.01930

[56] Carr, B., & Kühnel, F. 2020, Annual Review of Nuclear and Particle Science, 70, 355

[57] Carr, B. J. 1975, Astrophys. J., 201, 1

[58] Carr, B. J. 1976, ApJ, 206, 8

[59] Carr, B. J., Kohri, K., Sendouda, Y., & Yokoyama, J. 2010, Physical Review D, 81, doi:10.1103/physrevd.81.104019

[60] —. 2010, Phys. Rev. D, 81, 104019

[61] Carroll, S. M. 1997, Lecture Notes on General Relativity, doi:10.48550/ARXIV.GR-QC/9712019

[62] Casse, M., Cordier, B., Paul, J., & Schanne, S. 2004, Astrophys. J. Lett., 602, L17

[63] Cembranos, J. A. R., & Strigari, L. E. 2008, Phys. Rev. D, 77, 123519

[64] Chacko, Z., Craig, N., Fox, P. J., & Harnik, R. 2017, JHEP, 07, 023

[65] Chacko, Z., Curtin, D., Geller, M., & Tsai, Y. 2018, JHEP, 09, 163

[66] Chacko, Z., Goh, H.-S., & Harnik, R. 2006, Phys. Rev. Lett., 96, 231802

[67] Chandrasekhar, S. 1994, Journal of Astrophysics and Astronomy, 15, 105

[68] Chluba, J. 2013, Mon. Not. Roy. Astron. Soc., 436, 2232

[69] Chluba, J., & Jeong, D. 2014, Mon. Not. Roy. Astron. Soc., 438, 2065

[70] Chluba, J., Ravenni, A., & Acharya, S. K. 2020, Mon. Not. Roy. Astron. Soc., 498, 959

[71] Chluba, J., & Sunyaev, R. A. 2012, Mon. Not. Roy. Astron. Soc., 419, 1294

[72] Cholis, I., Zhong, Y.-M., McDermott, S. D., & Surdutovich, J. P. 2021, arXiv:2112.09706

[73] Churazov, E., Sunyaev, R., Sazonov, S., Revnivtsev, M., & Varshalovich, D. 2005, Mon. Not. Roy. Astron. Soc., 357, 1377

[74] Cirelli, M., Fornengo, N., Kavanagh, B. J., & Pinetti, E. 2020, arXiv:2007.11493

[75] Clark, S., Dutta, B., Gao, Y., Strigari, L. E., & Watson, S. 2017, Phys. Rev. D, 95, 083006

[76] Cleaver, G., Cvetic, M., Espinosa, J. R., et al. 1999, Phys. Rev. D, 59, 055005

[77] Clesse, S., & García-Bellido, J. 2015, Phys. Rev. D, 92, 023524

[78] Clesse, S., & García-Bellido, J. 2017, Physics of the Dark Universe, 15, 142

[79] Clesse, S., & García-Bellido, J. 2017, Phys. Dark Univ., 15, 142

[80] Clesse, S., & García-Bellido, J. 2016, Detecting the gravitational wave background from primordial black hole dark matter, doi:10.48550/ARXIV.1610.08479

[81] Cline, J. M., & Frey, A. R. 2012, Annalen Phys., 524, 579

[82] Cline, J. M., Frey, A. R., & Chen, F. 2011, Phys. Rev. D, 83, 083511

[83] Coc, A., Goriely, S., Xu, Y., Saimpert, M., & Vangioni, E. 2012, Astrophys. J., 744, 158

[84] Coc, A., Petitjean, P., Uzan, J.-P., et al. 2015, Phys. Rev. D, 92, 123526

[85] Coc, A., & Vangioni, E. 2017, Int. J. Mod. Phys. E, 26, 1741002

[86] Colin, P., Valenzuela, O., & Klypin, A. 2006, Astrophys. J., 644, 687

[87] Coogan, A., Morrison, L., & Profumo, S. 2020, arXiv:2010.04797

[88] Cooke, R., Pettini, M., Jorgenson, R. A., Murphy, M. T., & Steidel, C. C. 2014, Astrophys. J., 781, 31

[89] Coriano, C., Faraggi, A. E., & Guzzi, M. 2008, Eur. Phys. J. C, 53, 421

[90] Craig, N. J., & Raby, S. 2009, arXiv:0908.1842

[91] Cvetic, M., Halverson, J., & Langacker, P. 2011, JHEP, 11, 058

[92] Cvetic, M., Shiu, G., & Uranga, A. M. 2001, Nucl. Phys. B, 615, 3

[93] Cyburt, R. H. 2004, Phys. Rev. D, 70, 023505

[94] Cyburt, R. H., Ellis, J., Fields, B. D., et al. 2009, JCAP, 10, 021

[95] Cyburt, R. H., Ellis, J. R., Fields, B. D., & Olive, K. A. 2003, Phys. Rev. D, 67, 103521

[96] Cyburt, R. H., Fields, B. D., Olive, K. A., & Yeh, T.-H. 2016, Rev. Mod. Phys., 88, 015004

[97] Dasgupta, B., Laha, R., & Ray, A. 2020, Phys. Rev. Lett., 125, 101101

[98] Davoudiasl, H., & Perez, G. 2010, JHEP, 04, 058

[99] Daylan, T., Finkbeiner, D. P., Hooper, D., et al. 2016, Phys. Dark Univ., 12, 1

[100] De Angelis, A., et al. 2017, Exper. Astron., 44, 25

[101] —. 2017, Exper. Astron., 44, 25

[102] Depta, P. F., Hufnagel, M., Schmidt-Hoberg, K., & Wild, S. 2019, JCAP, 04, 029

[103] DeRocco, W., & Graham, P. W. 2019, Phys. Rev. Lett., 123, 251102

[104] Di Cintio, A., Brook, C. B., Dutton, A. A., et al. 2014, Mon. Not. Roy. Astron. Soc., 441, 2986

[105] Di Cintio, A., Brook, C. B., Macciò, A. V., et al. 2014, Mon. Not. Roy. Astron. Soc., 437, 415

[106] Douchin, F., & Haensel, P. 2001, Astronomy &amp Astrophysics, 380, 151

[107] Dvali, G. 2010, Fortsch. Phys., 58, 528

[108] Dvali, G., & Redi, M. 2009, Phys. Rev. D, 80, 055001

[109] Eddington, A. S. 1920, Nature, 106, 14

[110] Einstein, A. 1916, Annalen der Physik, 354, 769

[111] Ema, Y., Sala, F., & Sato, R. 2021, Eur. Phys. J. C, 81, 129

[112] Escudero, M. 2019, JCAP, 02, 007

[113] Farzan, Y., & Rajaee, M. 2017, JHEP, 12, 083

[114] —. 2020, Phys. Rev. D, 102, 103532

[115] Fields, B. D. 2011, Ann. Rev. Nucl. Part. Sci., 61, 47

[116] Fields, B. D., Olive, K. A., Yeh, T.-H., & Young, C. 2020, JCAP, 03, 010, [Erratum: JCAP 11, E02 (2020)]

[117] Finkbeiner, D. P., & Weiner, N. 2007, Phys. Rev. D, 76, 083519

[118] Finkelstein, D. 1958, Phys. Rev., 110, 965

[119] Forestell, L., Morrissey, D. E., & White, G. 2019, JHEP, 01, 074

[120] Fox, P., Pierce, A., & Thomas, S. D. 2004, arXiv:hep-th/0409059

[121] Frampton, P. H., & Kephart, T. W. 2005, Mod. Phys. Lett. A, 20, 1573

[122] Fromholz, P., Poisson, E., & Will, C. M. 2014, American Journal of Physics, 82, 295

[123] Fujita, T., Kawasaki, M., Harigaya, K., & Matsuda, R. 2014, Phys. Rev. D, 89, 103501

[124] Fuller, G. M., Kusenko, A., Radice, D., & Takhistov, V. 2019, Phys. Rev. Lett., 122, 121101

[125] Garcia-Bellido, J., Linde, A. D., & Wands, D. 1996, Phys. Rev. D, 54, 6040

[126] Gibbons, G. W., & Hawking, S. W. 1977, Phys. Rev. D, 15, 2738

[127] Giedt, J. 2001, Annals Phys., 289, 251

[128] Gnedin, O. Y., Ceverino, D., Gnedin, N. Y., et al. 2011, arXiv:1108.5736

[129] —. 2011, Halo Contraction Effect in Hydrodynamic Simulations of Galaxy Formation, arXiv:1108.5736

[130] Gnedin, O. Y., Kravtsov, A. V., Klypin, A. A., & Nagai, D. 2004, Astrophys. J., 616, 16

[131] Goodenough, L., & Hooper, D. 2009, arXiv:0910.2998

[132] Górski, K. M., Hivon, E., Banday, A. J., et al. 2005, ApJ, 622, 759

[133] Governato, F., Zolotov, A., Pontzen, A., et al. 2012, Monthly Notices of the Royal Astronomical Society, 422, 1231?1240

[134] Guessoum, N., Jean, P., & Prantzos, N. 2006, Astron. Astrophys., 457, 753

[135] Halverson, J., & Langacker, P. 2018, PoS, TASI2017, 019

[136] Halverson, J., Nelson, B. D., & Ruehle, F. 2017, Phys. Rev. D, 95, 043527

[137] Hamada, Y., & Iso, S. 2017, PTEP, 2017, 033B02

[138] Hawking, S. 1971, MNRAS, 152, 75

[139] Hawking, S. W. 1971, Phys. Rev. Lett., 26, 1344

[140] —. 1974, Nature, 248, 30

[141] —. 1975, Commun. Math. Phys., 43, 199, [Erratum: Commun.Math.Phys. 46, 206 (1976)]

[142] Hawking, S. W., Moss, I. G., & Stewart, J. M. 1982, Phys. Rev. D, 26, 2681

[143] Hawking, S. W., Perry, M. J., & Strominger, A. 2016, Physical Review Letters, 116, doi:physrevlett.116.231301

[144] Hewish, A. 1970, Annual Review of Astronomy and Astrophysics, 8, 265

[145] Hindmarsh, M., Lüben, M., Lumma, J., & Pauly, M. 2021, SciPost Physics Lecture Notes, doi:10.21468/scipostphyslectnotes.24

[146] Holman, R., Kolb, E. W., & Wang, Y. 1990, Phys. Rev. Lett., 65, 17

[147] Holtmann, E., Kawasaki, M., Kohri, K., & Moroi, T. 1999, Phys. Rev. D, 60, 023506

[148] Hook, A. 2014, Phys. Rev. D, 90, 083535

[149] Hooper, D. 2024, Particle Cosmology and Astrophysics (Princeton University Press)

[150] Hooper, D., & Goodenough, L. 2011, Phys. Lett. B, 697, 412

[151] Hooper, D., Krnjaic, G., March-Russell, J., McDermott, S. D., & Petrossian-Byrne, R. 2020, arXiv:2004.00618

[152] Hooper, D., Krnjaic, G., & McDermott, S. D. 2019, JHEP, 08, 001

[153] Hooper, D., & Linden, T. 2011, Phys. Rev. D, 84, 123005

[154] Hooper, D., & Wang, L.-T. 2004, Phys. Rev. D, 70, 063506

[155] Hooper, D., & Zurek, K. M. 2008, Phys. Rev. D, 77, 087302

[156] Hsu, S. D. H. 1990, Phys. Lett. B, 251, 343

[157] Huang, G.-y., Ohlsson, T., & Zhou, S. 2018, Phys. Rev. D, 97, 075009

[158] Hufnagel, M., Schmidt-Hoberg, K., & Wild, S. 2018, JCAP, 02, 044

[159] —. 2018, JCAP, 11, 032

[160] Huh, J.-H., Kim, J. E., Park, J.-C., & Park, S. C. 2008, Phys. Rev. D, 77, 123503

[161] Iocco, F., Mangano, G., Miele, G., Pisanti, O., & Serpico, P. D. 2009, Phys. Rept., 472, 1

[162] Isi, M., Farr, W. M., Giesler, M., Scheel, M. A., & Teukolsky, S. A. 2021, Phys. Rev. Lett., 127, 011103

[163] Izotov, Y. I., Thuan, T. X., & Guseva, N. G. 2014, Mon. Not. Roy. Astron. Soc., 445, 778

[164] James, F., & Roos, M. 1975, Comput. Phys. Commun., 10, 343

[165] Jean, P., Knodlseder, J., Gillard, W., et al. 2006, Astron. Astrophys., 445, 579

[166] Jedamzik, K. 2004, Phys. Rev. D, 70, 063524

[167] —. 2006, Phys. Rev. D, 74, 103509

[168] Jedamzik, K., & Pospelov, M. 2009, New J. Phys., 11, 105028

[169] Kalemci, E., Boggs, S. E., Milne, P. A., & Reynolds, S. P. 2006, Astrophys. J. Lett., 640, L55

[170] Kannike, K., Marzola, L., Raidal, M., & Veermäe, H. 2017, JCAP, 09, 020

[171] Kasuya, S., & Takahashi, F. 2005, Phys. Rev. D, 72, 085015

[172] Kavanagh, B. J., Gaggero, D., & Bertone, G. 2018, Phys. Rev. D, 98, 023536

[173] Kawasaki, M., Kohri, K., & Moroi, T. 2001, Phys. Rev. D, 63, 103502

[174] —. 2005, Phys. Rev. D, 71, 083502

[175] —. 2005, Phys. Lett. B, 625, 7

[176] Kawasaki, M., Kohri, K., Moroi, T., & Takaesu, Y. 2018, Phys. Rev. D, 97, 023502

[177] Kawasaki, M., Kusenko, A., Tada, Y., & Yanagida, T. T. 2016, Phys. Rev. D, 94, 083523

[178] Kawasaki, M., & Moroi, T. 1995, Astrophys. J., 452, 506

[179] —. 1995, Prog. Theor. Phys., 93, 879

[180] Kawasaki, M., Sugiyama, N., & Yanagida, T. 1998, Phys. Rev. D, 57, 6050

[181] Keith, C., & Hooper, D. 2021, Phys. Rev. D, 104, 063033

[182] Keith, C., Hooper, D., Blinov, N., & McDermott, S. D. 2020, Phys. Rev. D, 102, 103512

[183] Keith, C., Hooper, D., & Linden, T. 2022, arXiv:2212.08080

[184] Kerr, R. P. 1963, Phys. Rev. Lett., 11, 237

[185] Khalil, S., & Seto, O. 2008, JCAP, 10, 024

[186] Khlopov, M. Y., & Polnarev, A. G. 1980, Phys. Lett. B, 97, 383

[187] Kierans, C. A., et al. 2020, Astrophys. J., 895, 44

[188] Kohri, K. 2001, Phys. Rev. D, 64, 043515

[189] Kohri, K., Moroi, T., & Yotsuyanagi, A. 2006, Phys. Rev. D, 73, 123511

[190] Kohri, K., & Yokoyama, J. 2000, Phys. Rev. D, 61, 023501

[191] Kolb, E. W., & Turner, M. S. 1990, The Early Universe, Vol. 69, doi:10.1201/9780429492860

[192] Kuhlen, M., Guedes, J., Pillepich, A., Madau, P., & Mayer, L. 2013, Astrophys. J., 765, 10

[193] Kusakabe, M., Kajino, T., Yoshida, T., et al. 2009, Phys. Rev. D, 79, 123513

[194] La, D., & Steinhardt, P. J. 1989, Phys. Lett. B, 220, 375

[195] —. 1989, Phys. Rev. Lett., 62, 376, [Erratum: Phys.Rev.Lett. 62, 1066 (1989)]

[196] La, D., Steinhardt, P. J., & Bertschinger, E. W. 1989, Phys. Lett. B, 231, 231

[197] Laha, R. 2019, Phys. Rev. Lett., 123, 251101

[198] Laha, R., Muñoz, J. B., & Slatyer, T. R. 2020, Phys. Rev. D, 101, 123514

[199] LAT Collaboration. 2018, Search for Gamma-Ray Emission from Local Primordial Black Holes with the Fermi Large Area Telescope, doi:10.48550/ARXIV.1802.00100

[200] Lawson, K., & Zhitnitsky, A. 2017, JCAP, 02, 049

[201] Lebedev, O., Nilles, H. P., Raby, S., et al. 2008, Phys. Rev. D, 77, 046013

[202] Lehoucq, R., Casse, M., Casandjian, J. M., & Grenier, I. 2009, Astron. Astrophys., 502, 37

[203] Lennon, O., March-Russell, J., Petrossian-Byrne, R., & Tillim, H. 2018, JCAP, 04, 009

[204] Lunardini, C., & Perez-Gonzalez, Y. F. 2020, JCAP, 08, 014

[205] MacGibbon, J. H. 1991, Phys. Rev. D, 44, 376

[206] MacGibbon, J. H., & Webber, B. R. 1990, Phys. Rev. D, 41, 3052

[207] Masina, I. 2020, Eur. Phys. J. Plus, 135, 552

[208] McMaken, T. 2022, Monthly Notices of the Royal Astronomical Society, 511, 1218

[209] Mirabel, F. 2017, New Astronomy Reviews, 78, 1

[210] Montgomery, C., Orchiston, W., & Whittingham, I. 2009, Journal of Astronomical History and Heritage, 12, 90

[211] Morrison, L., Profumo, S., & Yu, Y. 2019, JCAP, 05, 005

[212] Navarro, J. F., Frenk, C. S., & White, S. D. M. 1996, Astrophys. J., 462, 563

[213] —. 1997, Astrophys. J., 490, 493

[214] Newman, E. T., Couch, E., Chinnapared, K., et al. 1965, Journal of Mathematical Physics, 6, 918

[215] Niikura, H., et al. 2019, Nature Astron., 3, 524

[216] Olive, K. A., Schramm, D. N., Scully, S. T., & Truran, J. W. 1997, Astrophys. J., 479, 752

[217] Oppenheimer, J. R., & Volkoff, G. M. 1939, Phys. Rev., 55, 374

[218] Page, D. N. 1976, Phys. Rev. D, 14, 3260

[219] —. 1976, Phys. Rev. D, 13, 198

[220] Peimbert, M., Luridiana, V., & Peimbert, A. 2007, Astrophys. J., 666, 636

[221] Penrose, R. 1965, Phys. Rev. Lett., 14, 57

[222] Pisanti, O., Cirillo, A., Esposito, S., et al. 2008, Comput. Phys. Commun., 178, 956

[223] Pitrou, C., Coc, A., Uzan, J.-P., & Vangioni, E. 2018, Phys. Rept., 754, 1

[224] —. 2020, JPS Conf. Proc., 31, 011034

[225] Pospelov, M., & Pradler, J. 2010, Ann. Rev. Nucl. Part. Sci., 60, 539

[226] Pospelov, M., & Ritz, A. 2007, Phys. Lett. B, 651, 208

[227] Poulin, V., Lesgourgues, J., & Serpico, P. D. 2017, JCAP, 03, 043

[228] Poulin, V., & Serpico, P. D. 2015, Phys. Rev. D, 91, 103007

[229] Poulter, H., Ali-Haïmoud, Y., Hamann, J., White, M., & Williams, A. G. 2019, arXiv:1907.06485

[230] Prantzos, N. 2006, Astron. Astrophys., 449, 869

[231] Prantzos, N., et al. 2011, Rev. Mod. Phys., 83, 1001

[232] Ray, A., Laha, R., Muñoz, J. B., & Caputo, R. 2021, arXiv:2102.06714

[233] Read, J. I. 2014, J. Phys. G, 41, 063101

[234] Rees, M. J., & Volonteri, M. 2006, Proceedings of the International Astronomical Union, 2, 51

[235] Riemer-Sørensen, S., & Jenssen, E. S. 2017, Universe, 3, 44

[236] Robin, A. C., Reyle, C., Derriere, S., & Picaud, S. 2003, Astron. Astrophys., 409, 523

[237] Sabti, N., Alvey, J., Escudero, M., Fairbairn, M., & Blas, D. 2020, JCAP, 01, 004

[238] Sarkar, S. 1996, Rept. Prog. Phys., 59, 1493

[239] Sasaki, M., Suyama, T., Tanaka, T., & Yokoyama, S. 2018, Class. Quant. Grav., 35, 063001

[240] Scannapieco, C., Wadepuhl, M., Parry, O. H., et al. 2012, Monthly Notices of the Royal Astronomical Society, 423, 1726?1749

[241] Schaffer, S. 1979, Journal for the History of Astronomy, 10, 42

[242] Schaller, M., Frenk, C. S., Bower, R. G., et al. 2015, Mon. Not. Roy. Astron. Soc., 451, 1247

[243] Schaller, M., et al. 2016, Mon. Not. Roy. Astron. Soc., 455, 4442

[244] Schramm, D. N., & Turner, M. S. 1998, Rev. Mod. Phys., 70, 303

[245] Schwarzschild, K. 1916, doi:10.48550/ARXIV.PHYSICS/9905030

[246] Sellwood, J. A. 2003, Astrophys. J., 587, 638

[247] Semikoz, D. V. 1994, ApJ, 436, 254

[248] Sirunyan, A. M., et al. 2017, Phys. Rev. D, 96, 032003

[249] Sobrinho, J. L. G., & Augusto, P. 2014, Mon. Not. Roy. Astron. Soc., 441, 2878

[250] Steigman, G. 2007, Ann. Rev. Nucl. Part. Sci., 57, 463

[251] Steinhardt, P. J., & Accetta, F. S. 1990, Phys. Rev. Lett., 64, 2740

[252] Stöcker, P., Krämer, M., Lesgourgues, J., & Poulin, V. 2018, JCAP, 03, 018

[253] Strong, A. W., Bloemen, H., Diehl, R., Hermsen, W., & Schoenfelder, V. 1999, Astrophys. Lett. Commun., 39, 209

[254] Svrcek, P. 2006, arXiv:hep-th/0607086

[255] Svrcek, P., & Witten, E. 2006, JHEP, 06, 051

[256] Takhistov, V. 2020, PoS, ICRC2019, 803

[257] Tanabashi, M., et al. 2018, Phys. Rev. D, 98, 030001

[258] Taylor, B. E., Chambers, C. M., & Hiscock, W. A. 1998, Phys. Rev. D, 58, 044012

[259] Tisserand, P., Guillou, L. L., Afonso, C., et al. 2007, Astronomy &amp Astrophysics, 469, 387

[260] Valenzuela, O., & Klypin, A. 2003, Mon. Not. Roy. Astron. Soc., 345, 406

[261] Villanueva-Domingo, P., Mena, O., & Palomares-Ruiz, S. 2021, Frontiers in Astronomy and Space Sciences, 8, doi:10.3389/fspas.2021.681084

[262] Vincent, A. C., Martin, P., & Cline, J. M. 2012, JCAP, 04, 022

[263] Visser, M. 2007, The Kerr spacetime: A brief introduction, doi:10.48550/ARXIV.0706.0622

[264] Vladimirov, A. E., Digel, S. W., Jóhannesson, G., et al. 2011, Computer Physics Communications, 182, 1156

[265] Volonteri, M. 2010, The Astronomy and Astrophysics Review, 18, 279

[266] Weidenspointner, G. 2008, Nature, 451, 159

[267] Weidenspointner, G., et al. 2004, in 5th INTEGRAL Workshop: The INTEGRAL Universe

[268] Weidenspointner, G., et al. 2007, ESA Spec. Publ., 622, 25

[269] Weinberg, E. J. 1989, Phys. Rev. D, 40, 3950

[270] —. 1989, Phys. Rev. D, 40, 3950

[271] Weinberg, M. D., & Katz, N. 2002, Astrophys. J., 580, 627

[272] —. 2007, Mon. Not. Roy. Astron. Soc., 375, 460

[273] Wilkinson, R. J., Vincent, A. C., Bœhm, C., & McCabe, C. 2016, Phys. Rev. D, 94, 103525

[274] Woosley, S., & Heger, A. 2007, Physics Reports, 442, 269

[275] Woosley, S. E., & Heger, A. 2015, The Astrophysical Journal, 810, 34

[276] Xu, Y., Takahashi, K., Goriely, S., et al. 2013, Nucl. Phys. A, 918, 61

[277] Yoo, C.-M., Harada, T., Garriga, J., & Kohri, K. 2018, PTEP, 2018, 123E01

[278] —. 2018, PTEP, 2018, 123E01

[279] Young, S., & Byrnes, C. T. 2015, JCAP, 04, 034

[280] Zel'dovich, Y. B., & Novikov, I. D. 1967, Soviet Ast., 10, 602

REFERENCES

[1] Aaboud, M., et al. 2018, Phys. Rev. D, 97, 112001

[2] Abbott, R., Abbott, T. D., Abraham, S., et al. 2021, The Astrophysical Journal Letters, 915, L5

[3] —. 2021, The Astrophysical Journal Letters, 915, L5

[4] Abdollahi, S., et al. 2020, Astrophys. J. Suppl., 247, 33

[5] Accetta, F. S., & Trester, J. J. 1989, Phys. Rev. D, 39, 2854

[6] Acharya, S. K., & Khatri, R. 2020, JCAP, 06, 018

[7] —. 2020, JCAP, 02, 010

[8] Ackermann, M., et al. 2015, Astrophys. J., 799, 86

[9] —. 2017, Astrophys. J., 840, 43

[10] —. 2018, Astrophys. J., 857, 49

[11] Adamek, J., Byrnes, C. T., Gosenca, M., & Hotchkiss, S. 2019, Phys. Rev. D, 100, 023506

[12] Afshordi, N., McDonald, P., & Spergel, D. N. 2003, The Astrophysical Journal, 594, L71

[13] Aghanim, N., et al. 2020, Astron. Astrophys., 641, A6, [Erratum: Astron.Astrophys. 652, C4 (2021)]

[14] Akiyama, K., et al. 2019, Astrophys. J. Lett., 875, L1

[15] Alcock, C., Allsman, R. A., Alves, D., et al. 1998, The Astrophysical Journal, 499, L9

[16] Ali-Haïmoud, Y., Kovetz, E. D., & Kamionkowski, M. 2017, Phys. Rev. D, 96, 123523

[17] Allahverdi, R., Dent, J., & Osinski, J. 2018, Phys. Rev. D, 97, 055013

[18] Anastasopoulos, P., Bianchi, M., Dudas, E., & Kiritsis, E. 2006, JHEP, 11, 057

[19] Ando, S., Cyburt, R. H., Hong, S. W., & Hyun, C. H. 2006, Phys. Rev. C, 74, 025809

[20] Arbey, A. 2012, Comput. Phys. Commun., 183, 1822

[21] Arbey, A., Auffinger, J., Hickerson, K. P., & Jenssen, E. S. 2020, Comput. Phys. Commun., 248, 106982

[22] Arkani-Hamed, N., Cohen, T., D'Agnolo, R. T., et al. 2016, Phys. Rev. Lett., 117, 251801

[23] Arvanitaki, A., Dimopoulos, S., Dubovsky, S., Kaloper, N., & March-Russell, J. 2010, Phys. Rev. D, 81, 123530

[24] Ascasibar, Y., Jean, P., Boehm, C., & Knoedlseder, J. 2006, Mon. Not. Roy. Astron. Soc., 368, 1695

[25] Aver, E., Olive, K. A., & Skillman, E. D. 2015, JCAP, 07, 011

[26] Baldes, I., Decant, Q., Hooper, D. C., & Lopez-Honorez, L. 2020, JCAP, 08, 045

[27] Bambi, C., Dolgov, A. D., & Petrov, A. A. 2008, Phys. Lett. B, 670, 174, [Erratum: Phys.Lett.B 681, 504–504 (2009)]

[28] Barabash, A. S. 2009, Foundations of Physics, 40, 703

[29] Bardeen, J. M., Carter, B., & Hawking, S. W. 1973, Commun. Math. Phys., 31, 161

[30] Barnacka, A., Glicenstein, J.-F., & Moderski, R. 2012, Physical Review D, 86, doi:10.1103/physrevd.86.043001

[31] Bartels, R., Calore, F., Storm, E., & Weniger, C. 2018, Mon. Not. Roy. Astron. Soc., 480, 3826

[32] Beacom, J. F., Bell, N. F., & Bertone, G. 2005, Phys. Rev. Lett., 94, 171301

[33] Beacom, J. F., & Yüksel, H. 2006, Phys. Rev. Lett., 97, 071102

[34] Berlin, A., Blinov, N., & Li, S. W. 2019, Phys. Rev. D, 100, 015038

[35] Bernal, N., Necib, L., & Slatyer, T. R. 2016, JCAP, 12, 030

[36] Bertone, G., Kusenko, A., Palomares-Ruiz, S., Pascoli, S., & Semikoz, D. 2006, Phys. Lett. B, 636, 20

[37] Bird, S., Cholis, I., Muñoz, J. B., et al. 2016, Phys. Rev. Lett., 116, 201301

[38] Boehm, C., Hooper, D., Silk, J., Casse, M., & Paul, J. 2004, Phys. Rev. Lett., 92, 101301

[39] Bouchet, L., Roques, J.-P., & Jourdain, E. 2010, Astrophys. J., 720, 1772

[40] Bouchet, L., Strong, A. W., Porter, T. A., et al. 2011, Astrophys. J., 739, 29

[41] Boudaud, M., & Cirelli, M. 2019, Phys. Rev. Lett., 122, 041104

[42] Braun, V., He, Y.-H., Ovrut, B. A., & Pantev, T. 2005, JHEP, 06, 039

[43] Bringmann, T., Kahlhoefer, F., Schmidt-Hoberg, K., & Walia, P. 2018, Phys. Rev. D, 98, 023543

[44] Buchner, J., Georgakakis, A., Nandra, K., et al. 2014, Astron. Astrophys., 564, A125

[45] Cai, R.-G., Ding, Y.-C., Yang, X.-Y., & Zhou, Y.-F. 2020, arXiv:2007.11804

[46] Cai, R.-G., Liu, T.-B., & Wang, S.-J. 2018, Phys. Rev. D, 98, 043538

[47] Calore, F., Bozorgnia, N., Lovell, M., et al. 2015, JCAP, 12, 053

[48] Cang, J., Gao, Y., & Ma, Y.-Z. 2021, , 2021, 051

[49] —. 2022, , 2022, 012

[50] Capela, F., Pshirkov, M., & Tinyakov, P. 2013, Physical Review D, 87, doi:10.1103/physrevd.87.023507

[51] Caputo, R., et al. 2019, arXiv:1907.07558

[52] Carr, B., Kohri, K., Sendouda, Y., & Yokoyama, J. 2021, Reports on Progress in Physics, 84, 116902

[53] —. 2021, Rept. Prog. Phys., 84, 116902

[54] Carr, B., Kuhnel, F., & Sandstad, M. 2016, Phys. Rev. D, 94, 083504

[55] Carr, B., Kuhnel, F., & Visinelli, L. 2020, arXiv:2011.01930

[56] Carr, B., & Kühnel, F. 2020, Annual Review of Nuclear and Particle Science, 70, 355

[57] Carr, B. J. 1975, Astrophys. J., 201, 1

[58] Carr, B. J. 1976, ApJ, 206, 8

[59] Carr, B. J., Kohri, K., Sendouda, Y., & Yokoyama, J. 2010, Physical Review D, 81, doi:10.1103/physrevd.81.104019

[60] —. 2010, Phys. Rev. D, 81, 104019

[61] Carroll, S. M. 1997, Lecture Notes on General Relativity, doi:10.48550/ARXIV.GR-QC/9712019

[62] Casse, M., Cordier, B., Paul, J., & Schanne, S. 2004, Astrophys. J. Lett., 602, L17

[63] Cembranos, J. A. R., & Strigari, L. E. 2008, Phys. Rev. D, 77, 123519

[64] Chacko, Z., Craig, N., Fox, P. J., & Harnik, R. 2017, JHEP, 07, 023

[65] Chacko, Z., Curtin, D., Geller, M., & Tsai, Y. 2018, JHEP, 09, 163

[66] Chacko, Z., Goh, H.-S., & Harnik, R. 2006, Phys. Rev. Lett., 96, 231802

[67] Chandrasekhar, S. 1994, Journal of Astrophysics and Astronomy, 15, 105

[68] Chluba, J. 2013, Mon. Not. Roy. Astron. Soc., 436, 2232

[69] Chluba, J., & Jeong, D. 2014, Mon. Not. Roy. Astron. Soc., 438, 2065

[70] Chluba, J., Ravenni, A., & Acharya, S. K. 2020, Mon. Not. Roy. Astron. Soc., 498, 959

[71] Chluba, J., & Sunyaev, R. A. 2012, Mon. Not. Roy. Astron. Soc., 419, 1294

[72] Cholis, I., Zhong, Y.-M., McDermott, S. D., & Surdutovich, J. P. 2021, arXiv:2112.09706

[73] Churazov, E., Sunyaev, R., Sazonov, S., Revnivtsev, M., & Varshalovich, D. 2005, Mon. Not. Roy. Astron. Soc., 357, 1377

[74] Cirelli, M., Fornengo, N., Kavanagh, B. J., & Pinetti, E. 2020, arXiv:2007.11493

[75] Clark, S., Dutta, B., Gao, Y., Strigari, L. E., & Watson, S. 2017, Phys. Rev. D, 95, 083006

[76] Cleaver, G., Cvetic, M., Espinosa, J. R., et al. 1999, Phys. Rev. D, 59, 055005

[77] Clesse, S., & García-Bellido, J. 2015, Phys. Rev. D, 92, 023524

[78] Clesse, S., & García-Bellido, J. 2017, Physics of the Dark Universe, 15, 142

[79] Clesse, S., & García-Bellido, J. 2017, Phys. Dark Univ., 15, 142

[80] Clesse, S., & García-Bellido, J. 2016, Detecting the gravitational wave background from primordial black hole dark matter, doi:10.48550/ARXIV.1610.08479

[81] Cline, J. M., & Frey, A. R. 2012, Annalen Phys., 524, 579

[82] Cline, J. M., Frey, A. R., & Chen, F. 2011, Phys. Rev. D, 83, 083511

[83] Coc, A., Goriely, S., Xu, Y., Saimpert, M., & Vangioni, E. 2012, Astrophys. J., 744, 158

[84] Coc, A., Petitjean, P., Uzan, J.-P., et al. 2015, Phys. Rev. D, 92, 123526

[85] Coc, A., & Vangioni, E. 2017, Int. J. Mod. Phys. E, 26, 1741002

[86] Colin, P., Valenzuela, O., & Klypin, A. 2006, Astrophys. J., 644, 687

[87] Coogan, A., Morrison, L., & Profumo, S. 2020, arXiv:2010.04797

[88] Cooke, R., Pettini, M., Jorgenson, R. A., Murphy, M. T., & Steidel, C. C. 2014, Astrophys. J., 781, 31

[89] Coriano, C., Faraggi, A. E., & Guzzi, M. 2008, Eur. Phys. J. C, 53, 421

[90] Craig, N. J., & Raby, S. 2009, arXiv:0908.1842

[91] Cvetic, M., Halverson, J., & Langacker, P. 2011, JHEP, 11, 058

[92] Cvetic, M., Shiu, G., & Uranga, A. M. 2001, Nucl. Phys. B, 615, 3

[93] Cyburt, R. H. 2004, Phys. Rev. D, 70, 023505

[94] Cyburt, R. H., Ellis, J., Fields, B. D., et al. 2009, JCAP, 10, 021

[95] Cyburt, R. H., Ellis, J. R., Fields, B. D., & Olive, K. A. 2003, Phys. Rev. D, 67, 103521

[96] Cyburt, R. H., Fields, B. D., Olive, K. A., & Yeh, T.-H. 2016, Rev. Mod. Phys., 88, 015004

[97] Dasgupta, B., Laha, R., & Ray, A. 2020, Phys. Rev. Lett., 125, 101101

[98] Davoudiasl, H., & Perez, G. 2010, JHEP, 04, 058

[99] Daylan, T., Finkbeiner, D. P., Hooper, D., et al. 2016, Phys. Dark Univ., 12, 1

[100] De Angelis, A., et al. 2017, Exper. Astron., 44, 25

[101] —. 2017, Exper. Astron., 44, 25

[102] Depta, P. F., Hufnagel, M., Schmidt-Hoberg, K., & Wild, S. 2019, JCAP, 04, 029

[103] DeRocco, W., & Graham, P. W. 2019, Phys. Rev. Lett., 123, 251102

[104] Di Cintio, A., Brook, C. B., Dutton, A. A., et al. 2014, Mon. Not. Roy. Astron. Soc., 441, 2986

[105] Di Cintio, A., Brook, C. B., Macciò, A. V., et al. 2014, Mon. Not. Roy. Astron. Soc., 437, 415

[106] Douchin, F., & Haensel, P. 2001, Astronomy &amp Astrophysics, 380, 151

[107] Dvali, G. 2010, Fortsch. Phys., 58, 528

[108] Dvali, G., & Redi, M. 2009, Phys. Rev. D, 80, 055001

[109] Eddington, A. S. 1920, Nature, 106, 14

[110] Einstein, A. 1916, Annalen der Physik, 354, 769

[111] Ema, Y., Sala, F., & Sato, R. 2021, Eur. Phys. J. C, 81, 129

[112] Escudero, M. 2019, JCAP, 02, 007

[113] Farzan, Y., & Rajaee, M. 2017, JHEP, 12, 083

[114] —. 2020, Phys. Rev. D, 102, 103532

[115] Fields, B. D. 2011, Ann. Rev. Nucl. Part. Sci., 61, 47

[116] Fields, B. D., Olive, K. A., Yeh, T.-H., & Young, C. 2020, JCAP, 03, 010, [Erratum: JCAP 11, E02 (2020)]

[117] Finkbeiner, D. P., & Weiner, N. 2007, Phys. Rev. D, 76, 083519

[118] Finkelstein, D. 1958, Phys. Rev., 110, 965

[119] Forestell, L., Morrissey, D. E., & White, G. 2019, JHEP, 01, 074

[120] Fox, P., Pierce, A., & Thomas, S. D. 2004, arXiv:hep-th/0409059

[121] Frampton, P. H., & Kephart, T. W. 2005, Mod. Phys. Lett. A, 20, 1573

[122] Fromholz, P., Poisson, E., & Will, C. M. 2014, American Journal of Physics, 82, 295

[123] Fujita, T., Kawasaki, M., Harigaya, K., & Matsuda, R. 2014, Phys. Rev. D, 89, 103501

[124] Fuller, G. M., Kusenko, A., Radice, D., & Takhistov, V. 2019, Phys. Rev. Lett., 122, 121101

[125] Garcia-Bellido, J., Linde, A. D., & Wands, D. 1996, Phys. Rev. D, 54, 6040

[126] Gibbons, G. W., & Hawking, S. W. 1977, Phys. Rev. D, 15, 2738

[127] Giedt, J. 2001, Annals Phys., 289, 251

[128] Gnedin, O. Y., Ceverino, D., Gnedin, N. Y., et al. 2011, arXiv:1108.5736

[129] —. 2011, Halo Contraction Effect in Hydrodynamic Simulations of Galaxy Formation, arXiv:1108.5736

[130] Gnedin, O. Y., Kravtsov, A. V., Klypin, A. A., & Nagai, D. 2004, Astrophys. J., 616, 16

[131] Goodenough, L., & Hooper, D. 2009, arXiv:0910.2998

[132] Górski, K. M., Hivon, E., Banday, A. J., et al. 2005, ApJ, 622, 759

[133] Governato, F., Zolotov, A., Pontzen, A., et al. 2012, Monthly Notices of the Royal Astronomical Society, 422, 1231?1240

[134] Guessoum, N., Jean, P., & Prantzos, N. 2006, Astron. Astrophys., 457, 753

[135] Halverson, J., & Langacker, P. 2018, PoS, TASI2017, 019

[136] Halverson, J., Nelson, B. D., & Ruehle, F. 2017, Phys. Rev. D, 95, 043527

[137] Hamada, Y., & Iso, S. 2017, PTEP, 2017, 033B02

[138] Hawking, S. 1971, MNRAS, 152, 75

[139] Hawking, S. W. 1971, Phys. Rev. Lett., 26, 1344

[140] —. 1974, Nature, 248, 30

[141] —. 1975, Commun. Math. Phys., 43, 199, [Erratum: Commun.Math.Phys. 46, 206 (1976)]

[142] Hawking, S. W., Moss, I. G., & Stewart, J. M. 1982, Phys. Rev. D, 26, 2681

[143] Hawking, S. W., Perry, M. J., & Strominger, A. 2016, Physical Review Letters, 116, doi:physrevlett.116.231301

[144] Hewish, A. 1970, Annual Review of Astronomy and Astrophysics, 8, 265

[145] Hindmarsh, M., Lüben, M., Lumma, J., & Pauly, M. 2021, SciPost Physics Lecture Notes, doi:10.21468/scipostphyslectnotes.24

[146] Holman, R., Kolb, E. W., & Wang, Y. 1990, Phys. Rev. Lett., 65, 17

[147] Holtmann, E., Kawasaki, M., Kohri, K., & Moroi, T. 1999, Phys. Rev. D, 60, 023506

[148] Hook, A. 2014, Phys. Rev. D, 90, 083535

[149] Hooper, D. 2024, Particle Cosmology and Astrophysics (Princeton University Press)

[150] Hooper, D., & Goodenough, L. 2011, Phys. Lett. B, 697, 412

[151] Hooper, D., Krnjaic, G., March-Russell, J., McDermott, S. D., & Petrossian-Byrne, R. 2020, arXiv:2004.00618

[152] Hooper, D., Krnjaic, G., & McDermott, S. D. 2019, JHEP, 08, 001

[153] Hooper, D., & Linden, T. 2011, Phys. Rev. D, 84, 123005

[154] Hooper, D., & Wang, L.-T. 2004, Phys. Rev. D, 70, 063506

[155] Hooper, D., & Zurek, K. M. 2008, Phys. Rev. D, 77, 087302

[156] Hsu, S. D. H. 1990, Phys. Lett. B, 251, 343

[157] Huang, G.-y., Ohlsson, T., & Zhou, S. 2018, Phys. Rev. D, 97, 075009

[158] Hufnagel, M., Schmidt-Hoberg, K., & Wild, S. 2018, JCAP, 02, 044

[159] —. 2018, JCAP, 11, 032

[160] Huh, J.-H., Kim, J. E., Park, J.-C., & Park, S. C. 2008, Phys. Rev. D, 77, 123503

[161] Iocco, F., Mangano, G., Miele, G., Pisanti, O., & Serpico, P. D. 2009, Phys. Rept., 472, 1

[162] Isi, M., Farr, W. M., Giesler, M., Scheel, M. A., & Teukolsky, S. A. 2021, Phys. Rev. Lett., 127, 011103

[163] Izotov, Y. I., Thuan, T. X., & Guseva, N. G. 2014, Mon. Not. Roy. Astron. Soc., 445, 778

[164] James, F., & Roos, M. 1975, Comput. Phys. Commun., 10, 343

[165] Jean, P., Knodlseder, J., Gillard, W., et al. 2006, Astron. Astrophys., 445, 579

[166] Jedamzik, K. 2004, Phys. Rev. D, 70, 063524

[167] —. 2006, Phys. Rev. D, 74, 103509

[168] Jedamzik, K., & Pospelov, M. 2009, New J. Phys., 11, 105028

[169] Kalemci, E., Boggs, S. E., Milne, P. A., & Reynolds, S. P. 2006, Astrophys. J. Lett., 640, L55

[170] Kannike, K., Marzola, L., Raidal, M., & Veermäe, H. 2017, JCAP, 09, 020

[171] Kasuya, S., & Takahashi, F. 2005, Phys. Rev. D, 72, 085015

[172] Kavanagh, B. J., Gaggero, D., & Bertone, G. 2018, Phys. Rev. D, 98, 023536

[173] Kawasaki, M., Kohri, K., & Moroi, T. 2001, Phys. Rev. D, 63, 103502

[174] —. 2005, Phys. Rev. D, 71, 083502

[175] —. 2005, Phys. Lett. B, 625, 7

[176] Kawasaki, M., Kohri, K., Moroi, T., & Takaesu, Y. 2018, Phys. Rev. D, 97, 023502

[177] Kawasaki, M., Kusenko, A., Tada, Y., & Yanagida, T. T. 2016, Phys. Rev. D, 94, 083523

[178] Kawasaki, M., & Moroi, T. 1995, Astrophys. J., 452, 506

[179] —. 1995, Prog. Theor. Phys., 93, 879

[180] Kawasaki, M., Sugiyama, N., & Yanagida, T. 1998, Phys. Rev. D, 57, 6050

[181] Keith, C., & Hooper, D. 2021, Phys. Rev. D, 104, 063033

[182] Keith, C., Hooper, D., Blinov, N., & McDermott, S. D. 2020, Phys. Rev. D, 102, 103512

[183] Keith, C., Hooper, D., & Linden, T. 2022, arXiv:2212.08080

[184] Kerr, R. P. 1963, Phys. Rev. Lett., 11, 237

[185] Khalil, S., & Seto, O. 2008, JCAP, 10, 024

[186] Khlopov, M. Y., & Polnarev, A. G. 1980, Phys. Lett. B, 97, 383

[187] Kierans, C. A., et al. 2020, Astrophys. J., 895, 44

[188] Kohri, K. 2001, Phys. Rev. D, 64, 043515

[189] Kohri, K., Moroi, T., & Yotsuyanagi, A. 2006, Phys. Rev. D, 73, 123511

[190] Kohri, K., & Yokoyama, J. 2000, Phys. Rev. D, 61, 023501

[191] Kolb, E. W., & Turner, M. S. 1990, The Early Universe, Vol. 69, doi:10.1201/9780429492860

[192] Kuhlen, M., Guedes, J., Pillepich, A., Madau, P., & Mayer, L. 2013, Astrophys. J., 765, 10

[193] Kusakabe, M., Kajino, T., Yoshida, T., et al. 2009, Phys. Rev. D, 79, 123513

[194] La, D., & Steinhardt, P. J. 1989, Phys. Lett. B, 220, 375

[195] —. 1989, Phys. Rev. Lett., 62, 376, [Erratum: Phys.Rev.Lett. 62, 1066 (1989)]

[196] La, D., Steinhardt, P. J., & Bertschinger, E. W. 1989, Phys. Lett. B, 231, 231

[197] Laha, R. 2019, Phys. Rev. Lett., 123, 251101

[198] Laha, R., Muñoz, J. B., & Slatyer, T. R. 2020, Phys. Rev. D, 101, 123514

[199] LAT Collaboration. 2018, Search for Gamma-Ray Emission from Local Primordial Black Holes with the Fermi Large Area Telescope, doi:10.48550/ARXIV.1802.00100

[200] Lawson, K., & Zhitnitsky, A. 2017, JCAP, 02, 049

[201] Lebedev, O., Nilles, H. P., Raby, S., et al. 2008, Phys. Rev. D, 77, 046013

[202] Lehoucq, R., Casse, M., Casandjian, J. M., & Grenier, I. 2009, Astron. Astrophys., 502, 37

[203] Lennon, O., March-Russell, J., Petrossian-Byrne, R., & Tillim, H. 2018, JCAP, 04, 009

[204] Lunardini, C., & Perez-Gonzalez, Y. F. 2020, JCAP, 08, 014

[205] MacGibbon, J. H. 1991, Phys. Rev. D, 44, 376

[206] MacGibbon, J. H., & Webber, B. R. 1990, Phys. Rev. D, 41, 3052

[207] Masina, I. 2020, Eur. Phys. J. Plus, 135, 552

[208] McMaken, T. 2022, Monthly Notices of the Royal Astronomical Society, 511, 1218

[209] Mirabel, F. 2017, New Astronomy Reviews, 78, 1

[210] Montgomery, C., Orchiston, W., & Whittingham, I. 2009, Journal of Astronomical History and Heritage, 12, 90

[211] Morrison, L., Profumo, S., & Yu, Y. 2019, JCAP, 05, 005

[212] Navarro, J. F., Frenk, C. S., & White, S. D. M. 1996, Astrophys. J., 462, 563

[213] —. 1997, Astrophys. J., 490, 493

[214] Newman, E. T., Couch, E., Chinnapared, K., et al. 1965, Journal of Mathematical Physics, 6, 918

[215] Niikura, H., et al. 2019, Nature Astron., 3, 524

[216] Olive, K. A., Schramm, D. N., Scully, S. T., & Truran, J. W. 1997, Astrophys. J., 479, 752

[217] Oppenheimer, J. R., & Volkoff, G. M. 1939, Phys. Rev., 55, 374

[218] Page, D. N. 1976, Phys. Rev. D, 14, 3260

[219] —. 1976, Phys. Rev. D, 13, 198

[220] Peimbert, M., Luridiana, V., & Peimbert, A. 2007, Astrophys. J., 666, 636

[221] Penrose, R. 1965, Phys. Rev. Lett., 14, 57

[222] Pisanti, O., Cirillo, A., Esposito, S., et al. 2008, Comput. Phys. Commun., 178, 956

[223] Pitrou, C., Coc, A., Uzan, J.-P., & Vangioni, E. 2018, Phys. Rept., 754, 1

[224] —. 2020, JPS Conf. Proc., 31, 011034

[225] Pospelov, M., & Pradler, J. 2010, Ann. Rev. Nucl. Part. Sci., 60, 539

[226] Pospelov, M., & Ritz, A. 2007, Phys. Lett. B, 651, 208

[227] Poulin, V., Lesgourgues, J., & Serpico, P. D. 2017, JCAP, 03, 043

[228] Poulin, V., & Serpico, P. D. 2015, Phys. Rev. D, 91, 103007

[229] Poulter, H., Ali-Haïmoud, Y., Hamann, J., White, M., & Williams, A. G. 2019, arXiv:1907.06485

[230] Prantzos, N. 2006, Astron. Astrophys., 449, 869

[231] Prantzos, N., et al. 2011, Rev. Mod. Phys., 83, 1001

[232] Ray, A., Laha, R., Muñoz, J. B., & Caputo, R. 2021, arXiv:2102.06714

[233] Read, J. I. 2014, J. Phys. G, 41, 063101

[234] Rees, M. J., & Volonteri, M. 2006, Proceedings of the International Astronomical Union, 2, 51

[235] Riemer-Sørensen, S., & Jenssen, E. S. 2017, Universe, 3, 44

[236] Robin, A. C., Reyle, C., Derriere, S., & Picaud, S. 2003, Astron. Astrophys., 409, 523

[237] Sabti, N., Alvey, J., Escudero, M., Fairbairn, M., & Blas, D. 2020, JCAP, 01, 004

[238] Sarkar, S. 1996, Rept. Prog. Phys., 59, 1493

[239] Sasaki, M., Suyama, T., Tanaka, T., & Yokoyama, S. 2018, Class. Quant. Grav., 35, 063001

[240] Scannapieco, C., Wadepuhl, M., Parry, O. H., et al. 2012, Monthly Notices of the Royal Astronomical Society, 423, 1726?1749

[241] Schaffer, S. 1979, Journal for the History of Astronomy, 10, 42

[242] Schaller, M., Frenk, C. S., Bower, R. G., et al. 2015, Mon. Not. Roy. Astron. Soc., 451, 1247

[243] Schaller, M., et al. 2016, Mon. Not. Roy. Astron. Soc., 455, 4442

[244] Schramm, D. N., & Turner, M. S. 1998, Rev. Mod. Phys., 70, 303

[245] Schwarzschild, K. 1916, doi:10.48550/ARXIV.PHYSICS/9905030

[246] Sellwood, J. A. 2003, Astrophys. J., 587, 638

[247] Semikoz, D. V. 1994, ApJ, 436, 254

[248] Sirunyan, A. M., et al. 2017, Phys. Rev. D, 96, 032003

[249] Sobrinho, J. L. G., & Augusto, P. 2014, Mon. Not. Roy. Astron. Soc., 441, 2878

[250] Steigman, G. 2007, Ann. Rev. Nucl. Part. Sci., 57, 463

[251] Steinhardt, P. J., & Accetta, F. S. 1990, Phys. Rev. Lett., 64, 2740

[252] Stöcker, P., Krämer, M., Lesgourgues, J., & Poulin, V. 2018, JCAP, 03, 018

[253] Strong, A. W., Bloemen, H., Diehl, R., Hermsen, W., & Schoenfelder, V. 1999, Astrophys. Lett. Commun., 39, 209

[254] Svrcek, P. 2006, arXiv:hep-th/0607086

[255] Svrcek, P., & Witten, E. 2006, JHEP, 06, 051

[256] Takhistov, V. 2020, PoS, ICRC2019, 803

[257] Tanabashi, M., et al. 2018, Phys. Rev. D, 98, 030001

[258] Taylor, B. E., Chambers, C. M., & Hiscock, W. A. 1998, Phys. Rev. D, 58, 044012

[259] Tisserand, P., Guillou, L. L., Afonso, C., et al. 2007, Astronomy &amp Astrophysics, 469, 387

[260] Valenzuela, O., & Klypin, A. 2003, Mon. Not. Roy. Astron. Soc., 345, 406

[261] Villanueva-Domingo, P., Mena, O., & Palomares-Ruiz, S. 2021, Frontiers in Astronomy and Space Sciences, 8, doi:10.3389/fspas.2021.681084

[262] Vincent, A. C., Martin, P., & Cline, J. M. 2012, JCAP, 04, 022

[263] Visser, M. 2007, The Kerr spacetime: A brief introduction, doi:10.48550/ARXIV.0706.0622

[264] Vladimirov, A. E., Digel, S. W., Jóhannesson, G., et al. 2011, Computer Physics Communications, 182, 1156

[265] Volonteri, M. 2010, The Astronomy and Astrophysics Review, 18, 279

[266] Weidenspointner, G. 2008, Nature, 451, 159

[267] Weidenspointner, G., et al. 2004, in 5th INTEGRAL Workshop: The INTEGRAL Universe

[268] Weidenspointner, G., et al. 2007, ESA Spec. Publ., 622, 25

[269] Weinberg, E. J. 1989, Phys. Rev. D, 40, 3950

[270] —. 1989, Phys. Rev. D, 40, 3950

[271] Weinberg, M. D., & Katz, N. 2002, Astrophys. J., 580, 627

[272] —. 2007, Mon. Not. Roy. Astron. Soc., 375, 460

[273] Wilkinson, R. J., Vincent, A. C., Bœhm, C., & McCabe, C. 2016, Phys. Rev. D, 94, 103525

[274] Woosley, S., & Heger, A. 2007, Physics Reports, 442, 269

[275] Woosley, S. E., & Heger, A. 2015, The Astrophysical Journal, 810, 34

[276] Xu, Y., Takahashi, K., Goriely, S., et al. 2013, Nucl. Phys. A, 918, 61

[277] Yoo, C.-M., Harada, T., Garriga, J., & Kohri, K. 2018, PTEP, 2018, 123E01

[278] —. 2018, PTEP, 2018, 123E01

[279] Young, S., & Byrnes, C. T. 2015, JCAP, 04, 034

[280] Zel'dovich, Y. B., & Novikov, I. D. 1967, Soviet Ast., 10, 602